SVERIGES GEOLOGISKA UNDERSÖKNING

Serie Ba ÖVERSIKTSKARTOR MED BESKRIVNINGAR Nr 30

J R MORTHORST H P ZECK P H LUNDEGÅRDH

THE PROTEROZOIC HYPERITES IN SOUTHERN VÄRMLAND WESTERN SWEDEN

UPPSALA 1983

SVERIGES GEOLOGISKA UNDERSÖKNING

Serie Ba ÖVERSIKTSKARTOR MED BESKRIVNINGAR Nr 30

J R MORTHORST H P ZECK P H LUNDEGÅRDH

THE PROTEROZOIC HYPERITES IN SOUTHERN VÄRMLAND WESTERN SWEDEN

WITH ONE MAP
INSIDE BACK COVER

UPPSALA 1983

ISBN 91-7158-284-3
ISSN 0373-2657

Kartorna godkända ur sekretessynpunkt för spridning.
Lantmäteriverket 1983-03-01.

ADDRESSES

J. R. Morthorst, Cryolite Company Øresund Ltd, Strandboulevarden 84, DK-2100 Copenhagen Ø, Denmark.

H. P. Zeck, Inst. of Petrology, Copenhagen University, Øster Voldgade 10, DK-1350 Copenhagen K, Denmark.

P. H. Lundegårdh, Geological Survey of Sweden, Box 670, S-751 28 Uppsala, Sweden.

CONTENTS

ABSTRACT

Large, doleritic-gabbroic, tholeiitic sills and dykes, collectively known as *Hyperites*, were intruded at c. 1 550 Ma ago in the gneiss basement of SW Sweden, which has given ages between 1 700 and 1 800 Ma. A detailed study has been made of a c. 60 km^2 large area around Ölme, on the N shore of Lake Vänern, between Karlstad and Kristinehamn. In this area the Hyperites are in the form of sills. The intrusive magma has followed to an important extent the pre-existing structures in the gneisses. Subsequently, the complex of gneisses and Hyperite intrusives went through two phases of folding, at least the latter of which seems to be of Grenvillian (Dalslandian) age (1 100–900 Ma ago). During the deformation and concomitant recrystallization, the intrusive doleritic-gabbroic rocks were replaced in part by amphibolites and hornblende metagabbros. The latter rocks lack the foliation shown in the amphibolites, but have the same mineralogy. The recrystallization of the doleritic-gabbroic rock is concentrated along the contact with the gneisses as well as along small internal faults and joints.

74 Hyperite samples, viz. 26 gabbroic rocks, 26 hornblende metagabbros and 22 amphibolites, have been analysed for major elements and 12 trace elements. A careful study was made of the metasomatic changes which have taken place in the basic rocks as a result of the recrystallization processes. The chemical comparisons between the original rock and its recrystallization products were made with the aid of two different types of orthogonal diagrams. The fixed pair diagrams plot on the abscissa and ordinate, respectively, a compositional aspect of pairs of gabbroic and amphibolitic rocks from the same locality. The relation of the resulting plot pattern to the 45° ordinate line brings out the metasomatic effect. The second type of diagram is of more general applicability, as it does not require a protolithic relation between the sample sets. It plots X/MgO (ordinate) against FeO*/MgO (abscissa), MgO and FeO*[1] being inert components. Special statistical tests were used to evaluate the plot patterns in both types of diagrams. These indicate that the recrystallization resulted in addition of (Mn,) Na, K, H_2O, Rb, (Ba,) (Zn,) Pb, Th and Cl to the basic rocks and an increase in Fe_2O_3/FeO, whereas S was taken away. For Si, Ti, Al, Fe*[2], Mg, Ca, P, Cu, Sr, Y, Zr, Ni, K/Rb and Mg/Ni no changes could be detected.

It is suggested that the element migration took place through the fluid phase assisting in the recrystallization. Presumably the elements added to the basic rocks were derived from the surrounding gneiss complex.

Morthorst, J.R., Zeck, H. P., and Lundegårdh, P. H., 1982-10-12: The Proterozoic Hyperites in southern Värmland, western Sweden. Sveriges geologiska undersökning, Ser. Ba, No. 30, pp. 1–104. Uppsala.

[1] FeO* stands for total iron computed as FeO (= FeO + 0.9 Fe_2O_3).

[2] Fe* means Fe^{2+} + Fe^{3+}.

INTRODUCTION

The area reported on in this study (Fig. 1, inside back cover) is situated in SE Värmland, on the N coast of Lake Vänern, between Karlstad in the W and Kristinehamn in the E (Fig. 2). It is located on the 1:50 000 topographical map sheet 10 D Karlstad NO, within the quadrangle with coordinates 1390(W)/1400(E) — 6575(S)/6590(N) on the Swedish national geographic grid *(Rikets nät)*. The c. 60 km² large area was mapped at a 1:10 000 scale, on a topographical basis provided by the *Ekonomisk karta över Sverige*, directly processed aerial photographs. The map sheets, viz. 5i Mårön, 5j Bonderud, 6i Ölme, 6j Nore, 7i Sikterud and 7j Skanum, were issued by *Rikets allmänna kartverk* in 1962. More detailed mapping (1:5 000 and 1:2 000) has been carried out at a number of selected localities, in order to bring out the detailed relations between the Hyperite bodies and the surrounding gneisses as well as between the various rock types within the Hyperite bodies.

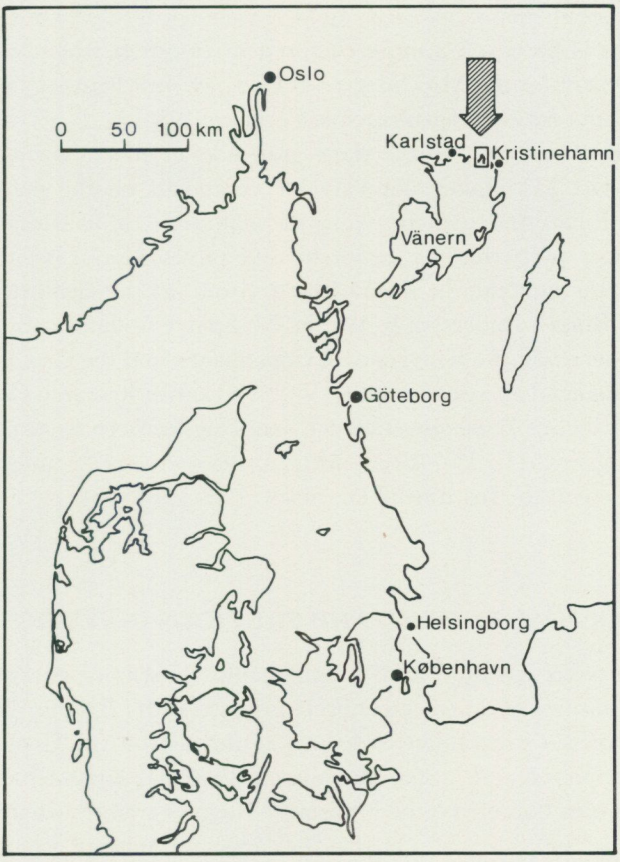

Fig. 2. Location of the area investigated.

The general degree of bedrock exposure in the area is not high. Relief is very low, relief energies are 40 m at a maximum. The landscape is dominated by large plains in which a few hundred metres to several kilometres long, rounded hills stand out. The plains are filled with Quaternary, mainly fluvioglacial, sand and clay, and are cultivated (usually wheat, barley and oats) or covered by large swamps. The underlying bedrock probably consists mainly of gneisses. The rounded hills are forested. The bedrock is much better exposed here and consists mainly of Hyperite. Such a geomorphology, with the gneisses predominantly underlying the plains and the Hyperites forming the shallow, rounded hills may be of glacial origin, reflecting the more erosion resistant character of the Hyperites compared to the gneisses.

The field work was done by one of us (J.R. Morthorst) as part of an M.Sc. degree study at the University of Copenhagen. The University financed his stay in the field for a period of three months, and made it possible for H.P. Zeck to visit the area several times. The mapping was started in 1975 and the last checks were made in 1977. All laboratory work was done in Copenhagen, at the Institute of Petrology, Copenhagen University, and the Geological Survey of Greenland. The present paper is based on a more comprehensive report which was accepted as partial fulfillment for the M.Sc. degree in Geology with Petrology and Geochemistry, at the University of Copenhagen in February 1980.

The authors wish to express their gratitude to the following persons and institutions: Dr. J.C. Bailey, for valuable comments on the manuscript, Gitte Sjørring and Lilian Andresen for typing the manuscript in its various versions and for meticulously preparing the comprehensive tables, Guta Lis for preparing the illustrations, the students in the Dalsland Group at the Institute of Petrology, especially P. Rubæk Andersen, B. Wallin, M. Sparre Andersen and C. Bülow, for pleasant cooperation, the University of Copenhagen and the Geological Survey of Sweden for financial and other support and the Danish Research Council (Statens Naturvidenskabelige Forskningsråd) for financing research work of H.P. Zeck in SW Sweden (J.nr. 511-7331, -8323, -881, -15495 and -15779) and supporting the XRF equipment at the Institute of Petrology (J.nr. 511-2825).

GEOLOGICAL SETTING AND PREVIOUS INVESTIGATIONS

The area between Karlstad and Kristinehamn consists of gneisses with large, elongated exposures of doleritic-gabbroic intrusives, the *Hyperites*. The rock complex is part of the Pregothian rock unit as defined on the Geological Map of Sweden (Magnusson *et al.*, 1958; Magnusson, 1960). At Kristinehamn the gneiss/Hyperite complex borders on the Filipstad—Hagfors granites which belong to the large, 1 600—1 700 Ma old, Småland—Värmland suite of granitic rocks and porphyries. W of Karlstad the gneiss/Hyperite complex borders on the Mylonite

Zone, a major tectonic boundary, separating two mega-units of different lithological character (Magnusson, 1937; Lindh, 1974). More recent investigations (Gorbatschev, 1971, 1975, 1980; Zeck and Malling, 1974; Lundegårdh, 1980; Lundegårdh *et al.*, 1982) have demonstrated several inconsistencies in the regional stratigraphy of Magnusson *et al.* (1958) and Magnusson (1960), and changes have been suggested (Fig. 3). A formal, improved classification has not come forward yet, although sketches are available (Gorbatschev, 1975, 1980; Zeck and Wallin, 1980). An outline of a comprehensive scheme for the petrogenetical and tectonical development of Central and SE Värmland has recently been given by Lundegårdh

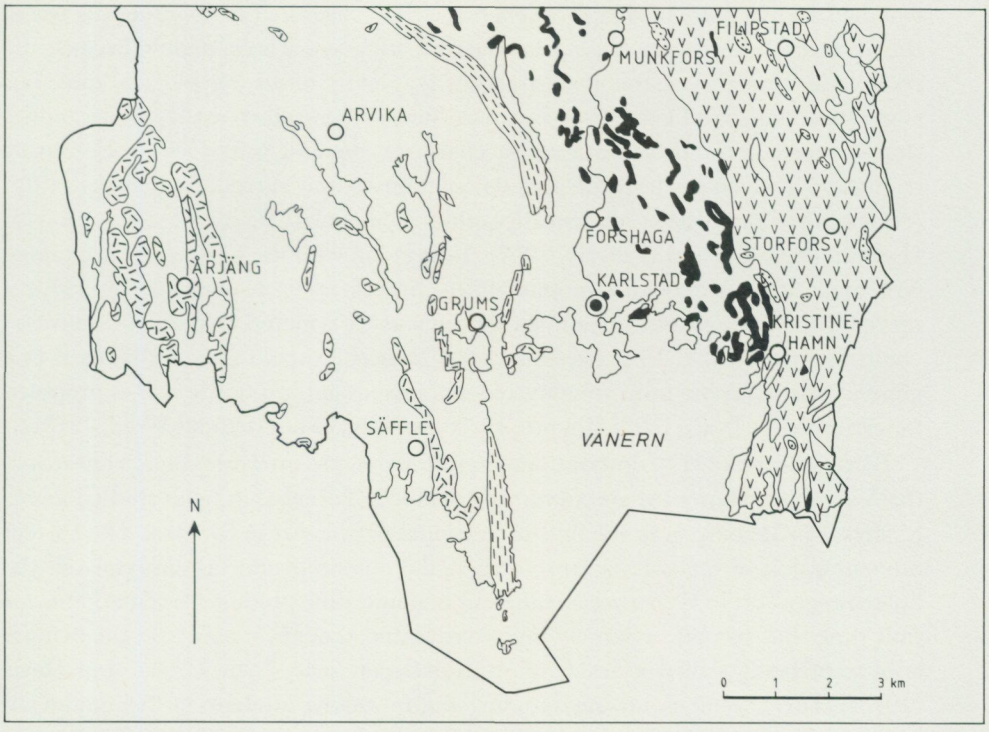

Mylonite, mylonite-gneiss and tectonic schists ("The Great Mylonite Zone")

Sveconorwegian ("Late Gothian" and Dalslandian) granites

Hyperite and, in the Värmland granitoids, dolerite

Värmland granitoids (granite, quartz-syenite, granodiorite, quartz-monzodiorite)

Gabbro, diorite, monzodiorite

Gneissic granites, gneisses, schists, metavolcanics ("Pregothian" and "Gothian")

Fig. 3. Simplified bedrock map of the S part of Värmland County, compiled by P.H. Lundegårdh (after Lundegårdh, *et al.*, 1982).

(1980), *inter alia* based on regional, structural evaluations and age determinations by Welin and Kähr (1980).

Geological investigations addressing the area between Karlstad and Kristinehamn begun in the middle of the 19th century when the Swedish Geological Survey started its work. A. Erdmann and J.H. af Forselles were among the first to study the area, and they introduced the term "Hyperite" for the voluminous intrusives of black doleritic gabbro in the Värmland gneiss basement (Törnebohm, 1877). The term was introduced as a general petrographic term for a granular rock composed mainly of labradorite and hypersthene (Erdmann, 1855). However, after more precise optical determination methods for hypersthene had become available, it was demonstrated that in many of these rocks hypersthene was lacking. In spite of this, Törnebohm (1877) suggested to continue the use of the agreeably short term *Hyperite* for the rock suite as a whole, mainly because the rock suite, though variable petrographically, clearly forms a geological unit. His suggestion has found general acceptance. Such a use of the term Hyperite implies that the term gets a lithostratigraphic character, defining as it does a rock unit by its lithological characteristics and its relation to the surrounding rock unit(s) (American Commission on Stratigraphic Nomenclature, 1970; compare also Hjelmqvist, 1950, and Gjelsvik, 1952). In keeping with the Code of Stratigraphic Nomenclature (American Commission on Stratigraphic Nomenclature, 1970) a more formal stratigraphic denomination such as "Värmland Hyperite Formation" could be introduced[1]. In present-day texts Hyperite should thus not be used as a general petrographic term roughly synonymous to gabbro-norite[2] (as is proposed for example by Teall, 1899; Holmes, 1920; and Gary, MacAfee and Wolff, 1972).

Törnebohm's (1877) descriptions and petrogenetic interpretations concerning the Värmland Hyperites are admirably detailed. Törnebohm, who studied under F. Zirkel in Leipzig, was the first professional petrologist in Sweden. The correct interpretation of the corona structures at the olivine/plagioclase interface in the doleritic-grabbroic Hyperites as inherent metamorphic products is remarkable for that time, but passed by largely unnoticed; later, though, it was paid the distinct tribute of being called a result of "a Norwegian school" by Griffin and Heier (1973). Törnebohm is an out-standing figure among students of Scandinavian geology. His contributions are manifold and cover a wide range of geological disciplines. He was foremost in recognizing large scale nappe structures in the Scandinavian Caledonides. His keen petrologic interest is illustrated by the habit of making his own thin sections — for example 500 for the 1877 paper — often before breakfast, as noted by Hamberg (1929) in his orbituary of Törnebohm.

Törnebohm distinguished two main rock types in the Hyperite bodies, viz. *hyperite* and *hyperite-diorite*. The first represents the gabbroic intrusive facies forming

[1] Note that this formation includes the Hyperites in Hedmark Fylke, E Norway, and the E part of Västergötland.

[2] Igneous rock classification and nomenclature in this paper is according to Streckeisen (1967, 1976).

the bulk of the formation. The second type represents the recrystallized equivalent in which the massive structure of the gabbroic parent rock has been preserved. The rock is composed mainly of oligoclase, quartz, hornblende and garnet. It corresponds to what we have called hornblende metagabbro (see pp. 15—25). Törnebohm (1877, p. 40) mentioned a third rock type which he called *dioritskiffer*. This rock was discribed as being of local character, developed in the strongly elongated Hyperite body Åstebyhöjden—Rattsjöberg—Kristinefors at the very contact with the gneisses. This *dioritskiffer*, which was not described further, represents what we have called amphibolite. The rock is much more wide-spread than suggested by Törnebohm.

The first detailed map over the investigated area is the map sheet "Väse", *Sveriges geologiska undersökning* (SGU), Ser. Aa, No. 151, scale 1:50 000, by Högbom (1922). The gneiss complex was recognized as part of the Värmlandic gneiss area wich again is part of the *järngneisregion* or *järngnejskomplex* (Iron gneiss area) of W Sweden. The gneisses were divided into three groups:

a — *red gneisses*, rather fine-grained rocks consisting mainly of quartz, potassic feldspar and plagioclase with only small amounts of mafic minerals,
b — *intermediate gneisses*, more coarse-grained than the red gneisses and with less quartz, more calcic plagioclase and a higher content in mafic minerals,
c — *grey gneisses*, with a still larger content in mafic minerals, and little if any potassic feldspar.

Not unlike Törnebohm (1877), Högbom (1922) divided the Hyperites into three rock types, *hyperite*, *hyperite-diorite* and *hyperite-amphibolite*, corresponding to what we in the present paper have called, respectively, gabbroic rock, hornblende metagabbro and amphibolite. Högbom reported that the fresh Hyperite was found only rarely, it being replaced by hornblende metagabbro and amphibolite. This is at variance with the results of our investigations which have shown that the magmatic, gabbroic rock is predominant in the Hyperite bodies. The Hyperites were claimed to be intrusive into the granites E of Kristinehamn. Later work by one of us (P.H. Lundegårdh, in Lundegårdh *et al.*, 1982) has revealed, however, that the basic intrusives — the Filipstad-Ullerud dolerites — upon which this conclusion was based, constitute a separate entity, much younger than the Hyperites.

A rather remarkable petrogenetic model for the area was put forward by Johansson (1927). This author claimed that both gneisses and Hyperites in the Värmland basement had been formed by *in situ* differentiation of one and the same parental magma. The present large scale structure in the basement complex, including the Hyperite/gneiss distribution, would have been formed during this event. Obviously, this hypothesis is at variance with some of the more fundamental and self-evident elements of the geology of the area. This was clearly pointed out by Magnusson (1928).

In 1929 and 1933, Magnusson published two bedrock map sheets, Nyed and Karlstad (scale 1:50 000), with descriptions. The subdivision of the gneisses into red, intermediate and grey types employed by Högbom (1922) was taken over, and also Högbom's subdivision of the Hyperites was followed. In a review of the Swedish Precambrian, Magnusson (1960) presented a further subdivision of the gneisses. Five types of gneisses were recognized: red salic, red semi-salic, intermediate, grey salic and grey basic gneisses. Supracrustal rocks were observed and grouped together in the Hammarö series (Magnusson, 1933). The Hyperites were subdivided as before. It is worth noting that Magnusson (1960) claimed that the Hyperites are younger than the surrounding rock material, but older than the regional gneissification, which was suggested also to have caused the recrystallization of the intrusive Hyperite facies to hornblende metagabbro and amphibolite.

A rather detailed description of the Hyperites, the surrounding gneisses and their contact relations was given by Wiman (1961) who mapped the Kristinehamn area on a scale of 1:100 000. This author recognized two types of gneisses, Väse gneiss and Ölme gneiss. The Väse gneiss, an aplitic, reddish gneiss was thought to be of sedimentary origin, being derived from an arkosic sediment.

Gorbatschev (1971), in his review of the geology of SW Sweden, noted that the Hyperites do not show much of the general granulation seen in the other "Pregothian" rocks, and also lack the strong foliation and extreme elongations shown by inclusions in the "Pregothian" metaplutonics. It was concluded that the Hyperites of central Värmland had generally escaped tectonization. Lundegårdh (1980), who has investigated the region in detail, reports that the Hyperite intrusives have been cross-folded and show boudinage structures.

Lundegårdh (1977) recognized three phases of deformation in the region. The oldest phase characterized by NNW-trending fold axes affected the Hammarö, Östmark, Hålsjö and Gräsmark supracrustals as well as the older granitic to granodioritic rocks (1 780 Ma, Welin and Kähr, 1980; cf. the 1 735 Ma age given by Welin and Gorbatschev, 1976, for "Pregothian" granitic rocks more to the S). The latter are intrusive into the supracrustals but predate the Hyperite intrusions (1 550 Ma; Priem *et al.*, 1968; Mulder, 1971; Welin *et al.*, 1980). The second phase of deformation is characterized by E—W trending axes, and is especially well developed on Hammarö, S of Karlstad. It postdates the emplacement of the Hyperites. The third phase is characterized by N(NW) trending axes and NNW striking thrust zones. In 1980, Lundegårdh presented additional evidence which confirms the model with three phases of deformation, but which claims that the second phase of deformation produced N(NW) trending axes (rather than E—W) and the third phase E—W axes (rather than N—S). It was further suggested that the Gräsmark Formation of metavolcanics was deposited at 1 100—1 200 Ma ago (Dalslandian) rather than between 1 600 and 1 700 Ma ago.

Hageskov (1980) reported results of investigations in Østfold, SW Norway, an area located 100—200 km more to the W. This author suggested three phases of

deformation in the area. The first with N—S axes (E—W compression), the second with E—W axes (probably N—S compression) and the third with N—S axes (E—W compression). This tectonic scheme is in agreement with the original one of Lundegårdh (1977). The last tectonic event was dated at 1 015 Ma by means of Rb/Sr whole rock determinations (Hageskov and Pedersen, 1981), which conforms well to the 1 030 ± 40 Ma of Skiöld (1976) for the metamorphism and deformation along N—S trending axes of the Dalslandian Group.

Lindh (in Lundegårdh *et al.*, 1982) has found E—W dislocations which offset the Great Mylonite Zone W of Karlstad (Fig. 3; compare also Lindh and Malmström, 1980). These faults coincide with dislocations of the Hyperites along the cross fold limbs described by Lundegårdh (1980 a, *ibid.* 1982) from the Hammarö Formation.

K-Ar determinations from the dislocated part of the Great Mylonite Zone have given ages between 878 and 968 Ma (Lindh and Kähr, 1977). The E—W dislocations of the Great Mylonite Zone and the E—W deformation of the Hammarö Formation have thus been interpreted as the final tectonic phase of the Sveconorwegian, or Dalslandian, in southern central Värmland (Lundegårdh *et al.*, 1982).

LITHOSTRATIGRAPHY OF THE KARLSTAD–KRISTINEHAMN AREA

The lithostratigraphical classification of the area comprises two main divisions: the *gneisses* and the intrusive gabbroic rocks and its metamorphic derivatives, the *Hyperites*.

GNEISSES

Several kinds of gneisses are present in the area. The various types may occur together within small areas. A precise, regional mapping of the variation within the gneisses is made difficult, if not impossible, by the low degree of exposure. Besides, such a detailed investigation of the gneisses is outside the scope of the present work, which is aimed at the Hyperites. Therefore, on the geological map (Fig. 1, inside back cover), the gneisses are not differentiated. A short description of some types of gneisses is given here.

Granitic to quartz-monzonitic biotite gneisses are wide-spread in the area and correspond roughly to the *"järngnejs"* of previous publications. The rocks comprise red to grey, fine- to medium-grained types and correspond to part of the gneissic granites, or gneiss-granites, described by Lundegårdh (1980 a). Two varieties occur, the first characterized by up to 1 cm long and 1—2 mm wide biotite aggregates which indicate the foliation of the rock, and a second type, more compact with less well-developed foliation and a lower biotite content. Both types are closely interrelated. In some areas, the biotite-rich variety dominates, the biotite-poor one forming layers in it. At other localities the relation is reversed. The biotite-rich variety consists in the main of an intergrowth of 0.5—5 mm large, anhedral crystals of plagioclase (~40%), microcline (~30%) and quartz (~15%); biotite and lesser amounts of hornblende crystals, ∅ = 0.2—3 mm, are mainly assembled in small aggregates parallel to the foliation. Magnetite (1%) is in up to 2 mm large, often euhedral crystals, usually isolated, in some cases associated with hornblende and biotite, as are the accessories zircon, apatite, titanite and orthite (metamict). Retrogressive influence is seen in the alteration of hornblende to fine-grained biotite (?), and more rarely by the formation of some chlorite at the expense of biotite as well as some sericite at the expense of plagioclase. The biotite-poor variety is similar to the biotite-rich one; it differs in that mafic minerals and accessories are present in smaller amounts, and that biotite and hornblende occur mostly in isolated crystals dispersed throughout the rock.

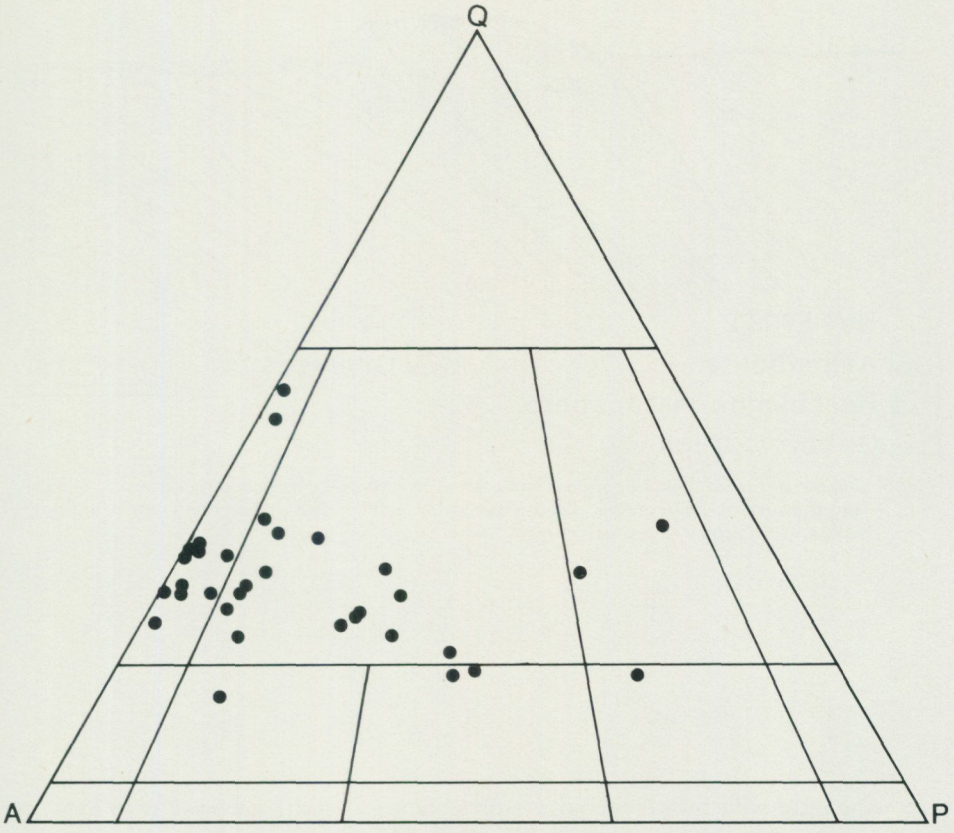

Fig. 4. Normative gneiss compositions (CIPW, see Table 1) plotted in a Niggli diagram. Normative Ab is distributed over A (alkali feldspar) and P (plagioclase) under the presumption that the magmatic plagioclase has a composition of An_{25}, a value that comes close to modal values. Field boundaries after Streckeisen (1967, 1976). The rocks plot mainly in the fields for alkali granite and granite. A few scatter in the fields of granodiorite, quartz-monzodiorite, quartz-monzonite and quartz-syenite. The data points do not define clearly separated populations, and thus do not give specific support to the notion that the gneiss basement is made up of several generations of granitic rocks.

Fine-grained biotite gneisses are rare in the area studied. These rocks are restricted to 1—2 m wide zones along the E—W running Hyperite contacts. The rock is grey, fine-grained and rather homogeneous. The foliation shows a variable character. In some rocks the biotite crystals occur in small aggregates and there the foliation is well developed. Quartz-rich schlieren up to 10 cm in length locally accentuate the foliation. The rocks consist mainly of plagioclase, quartz and microcline, usually

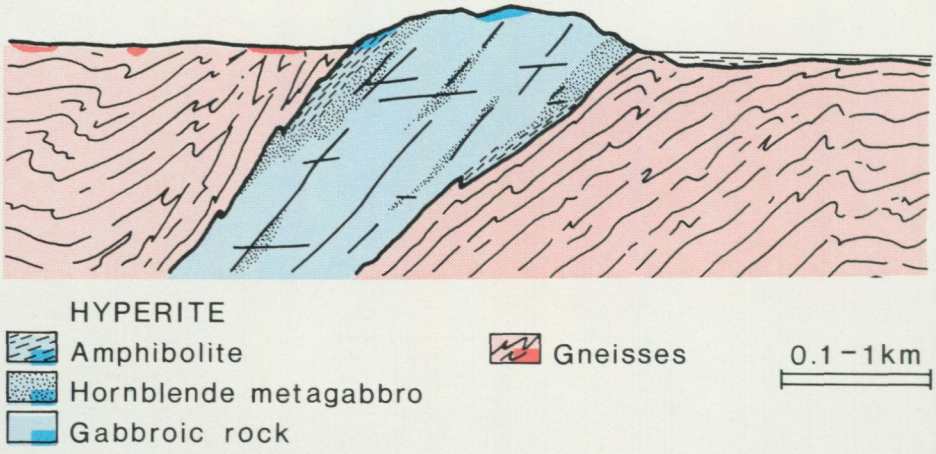

Fig. 5. *Schematical* profile illustrating the relation between a Hyperite body and its various rock types, and the surrounding gneisses. Legend valid also for Figs. 7–14, where the gneisses are given without structural indications.

showing granoblastic polygonal textures. Some isolated garnet and muscovite crystals may be present. Accessories are titanite, zircon, apatite and magnetite. Minor retrogressive influence is responsible for the formation of some sericite in plagioclase and some chlorite in biotite.

The contact between the gneisses and the Hyperite bodies is always sharp. The foliation in the gneisses is generally concordant to that in the amphibolites in the marginal parts of the Hyperite bodies. At a few E—W running contacts (Västkärr—Träfors, Mickelsrud, vicaridge of Sjöstad and Bråten) Hyperite material is intimately interfolded with the gneisses. The resulting rock consists of an alternation of 1—10 cm thick layers of amphibolite and gneiss. The amphibolite layers consist mainly of hornblende (~50%), plagioclase (~30%), quartz (~10%) and microline (~5%). The hornblende crystals are up to 3 mm in size and have often assembled to schlieric aggregates, the felsic minerals in intergrowths of anhedral crystals filling out the space between them. Accessories are apatite, titanite and magnetite. Retrogressive influence is indicated by strong saussuritization of plagioclase and probably also by the occurrence of larger discrete crystals of epidote. The gneiss layers consist mainly of plagioclase (~75%), quartz (~5%) and microcline (~5%). Hornblende and biotite are

present in roughly equal amounts, together 10—15% of the rock. Many of the larger felsic grains are supplied with an inconstant rim of small newly formed crystals. These crystals have probably been developed by a combination of deformation-induced recrystallization, and recrystallization of products of cataclasis. Biotite crystals are clearly deformed, "kinked". Epidote is a rather common mineral, forming independent crystals and saussurite replacing plagioclase. Accessories are apatite, titanite and zircon.

Chemical analyses of 33 gneiss samples have been made. The results are given in Table 1. The normative compositions (CIPW) are plotted in a Niggli diagram (Fig. 4). This illustrates that gneiss compositions range mainly from alkali granite to granite, with a few samples extending as far as quartz-syenite, quartz-monzonite, quartz-monzodiorite and granodiorite. The diagram does not give any indication for the existence of several generations of granitic rocks in the gneiss basement. However, the diagram should be interpreted with some care because it is meant for modal compositions, and because no effort was made to obtain a representative sample collection of the gneisses.

HYPERITES

Three main rock types can be distinguished within the Hyperite bodies (see Fig. 5). These will be descibed below.

1, *gabbroic rocks*, showing dark grey to black colours, with a brownish-violet tinge; grain sizes are from 0.2 to 4 cm. The rocks have a homogeneous appearance, a massive structure, without any foliation. They represent the original intrusive facies of the formation. In most Hyperite bodies in the present exposure surface, it is the dominating rock type (see Figs. 1 and 7—14). Locally the gabbroic Hyperite has been intruded by granitic and pegmatitic dykes and more irregular bodies up to several metres in thickness (Fig. 16). This intrusive material has not been foliated and is interpreted to represent a quartzo-feldspathic melt produced by melting of the country rock gneisses under the influence of the intrusive Hyperite magmatic mass (cf. Malmström, 1981).

2, *hornblende metagabbros*, which have a less homogeneous appearance than the gabbroic rocks. These rocks have the same massive structure, but the plagioclase crystals are white-grey and the material filling out the space between the plagio-

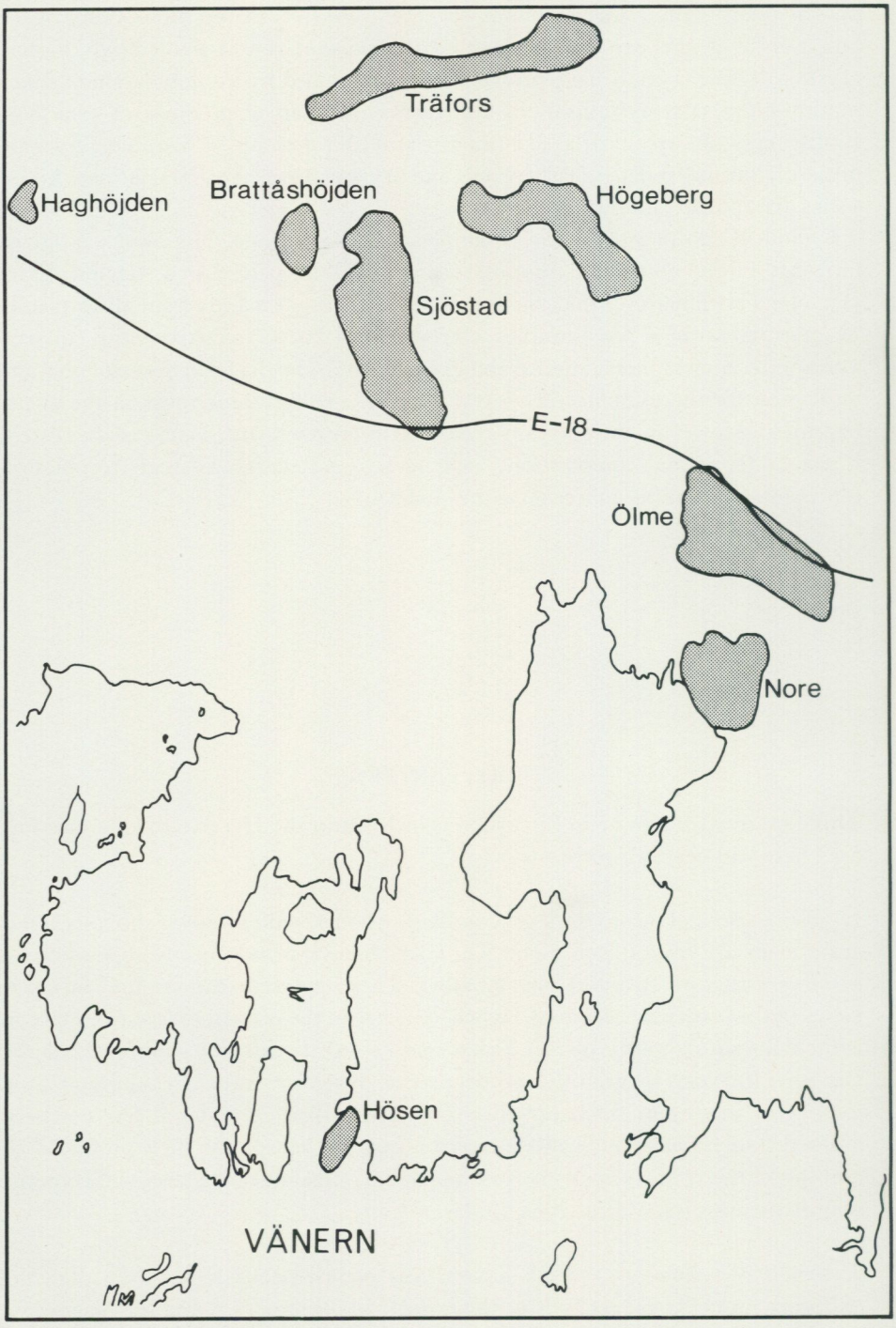

Fig. 6. Location of some well exposed Hyperite bodies which have been mapped in some detail (by J.R. Morthorst; see Figs. 7—14).

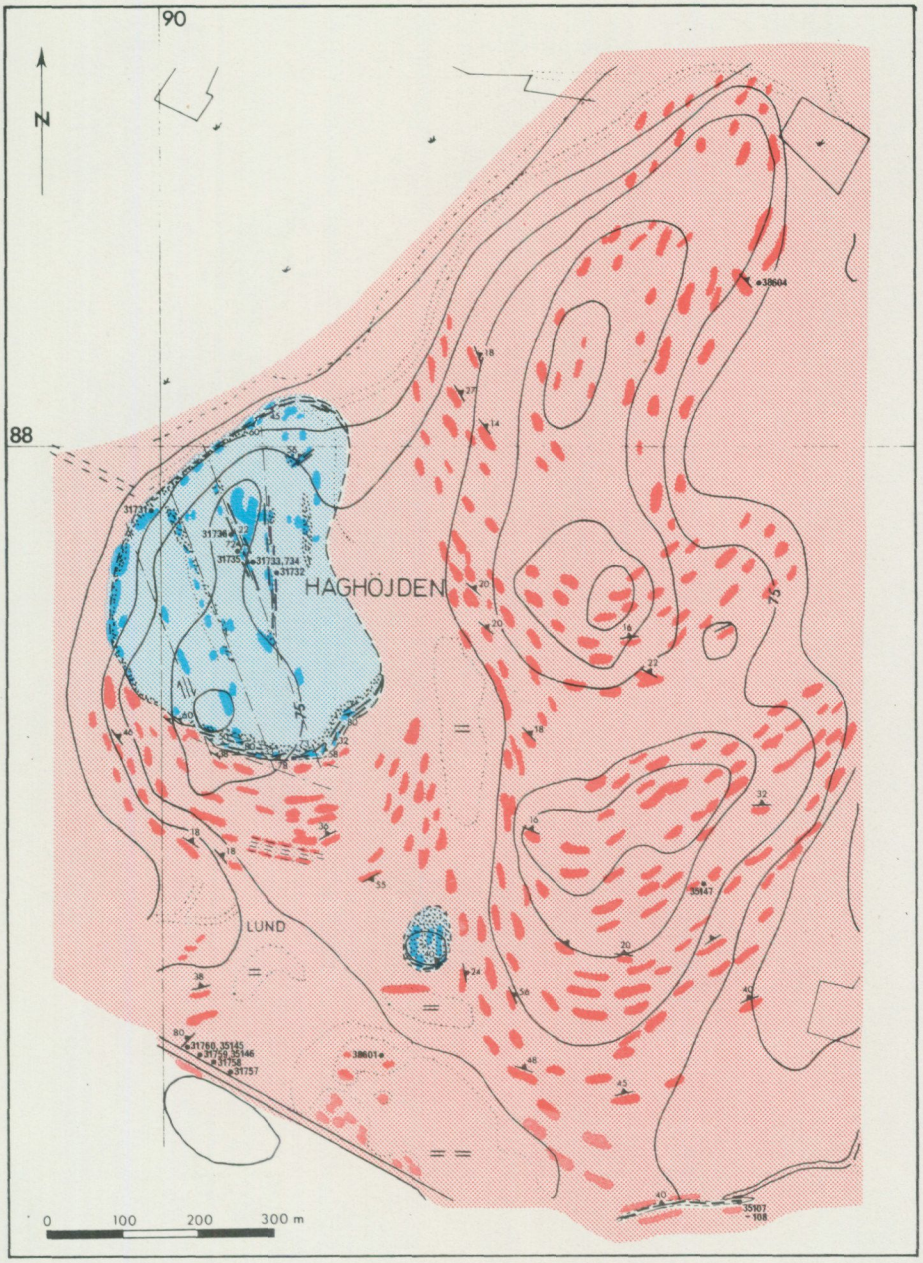

Fig. 7 . Haghöjden Hyperite body, approx. grid coordinates 1390/6588 (Figs. 6 and 1, legend in Fig. 5). A small body, c. 300 to 500 m in diameter, consisting mainly of gabbroic rock. The W contact shows well developed amphibolites and locally, towards the gneisses, a few metres of amphibolite. Haghöjden hill itself is situated a few hundred metres E of the Hyperite body, and is one of the few hills in the area that consists of gneiss and not of Hyperite.

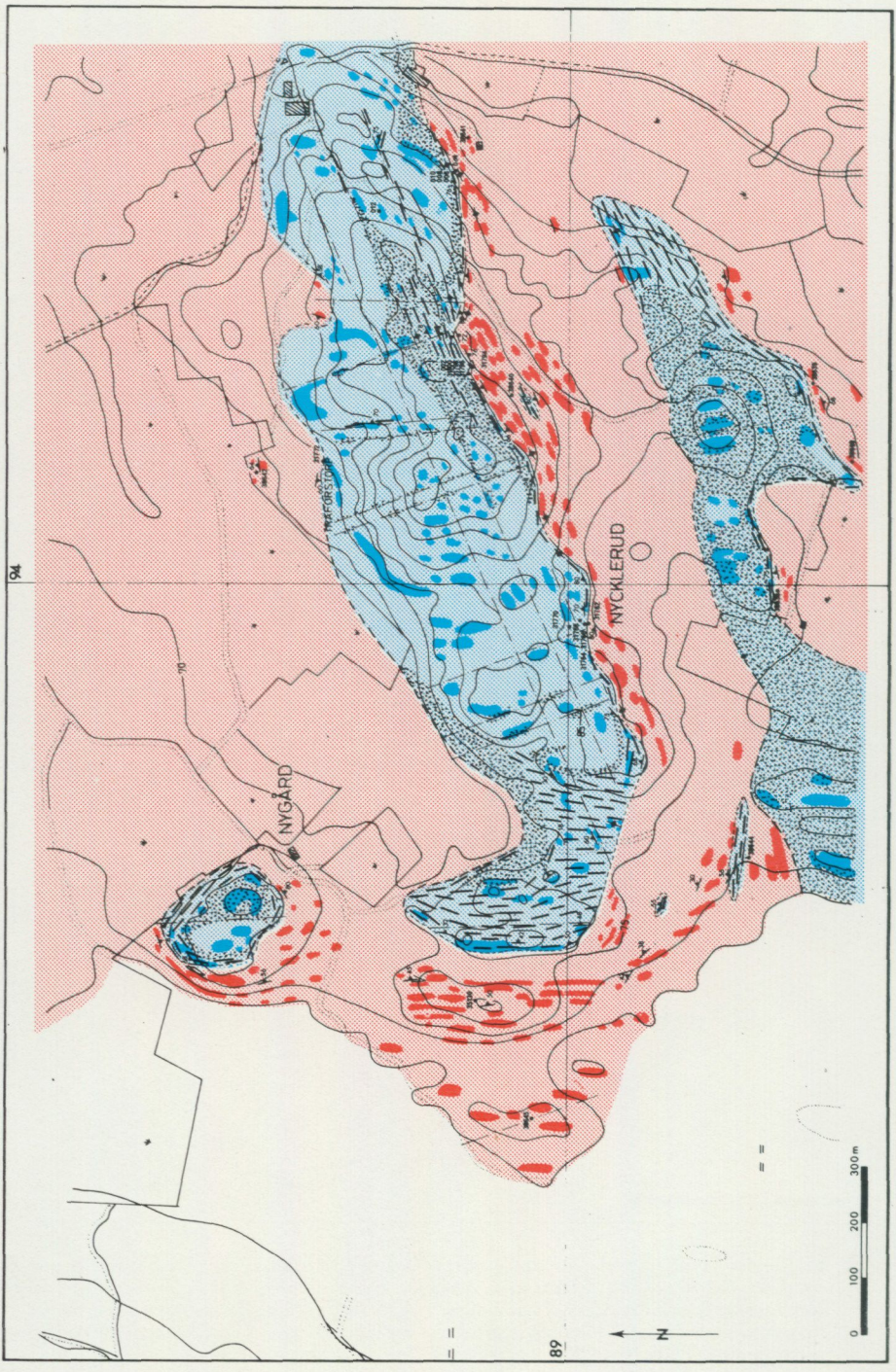
NYGÅRD
NYCKLERUD
94
89
N
0
100
200
300 m

clase skeleton is predominantly dark green to black, consisting mainly of amphibole and biotite. Usually some red garnet crystals are also present. This rock type has been developed by recrystallization of the gabbroic intrusive rock. In some Hyperite exposures it is the major rock type; however, in most Hyperite bodies it is a minor component (Figs. 1 and 7—14).

3, *amphibolites*, foliated rocks consisting mainly of a fine-scale alternation of lenses and schlieren rich in white plagioclase and black-green hornblende, respectively. Garnet and biotite are of regular occurrence. This rock type is less wide-spread than the hornblende metagabbro, usually occurring in close association with it. Zones of hornblende metagabbro are often found between the gabbroic rock and the amphibolites. Locally, in some Hyperite occurrences, at the amphibolite/gneiss contact, *biotite amphibolites* occur which have biotite as a major mineral. The rocks form bands to lenses ranging in width from a few decimetres to one metre. Locally the biotite content is very high and the rocks grade into biotite schists.

The transition between the different rock types within the Hyperite bodies is rather abrupt, taking place over a few decimetres, so that mapping out these rock types does not present technical problems. Mineral compositions and petrographical descriptions of the Hyperite rocks will be given on pp. 36—45. The geochemistry, in particular a chemical comparison between the three main rock types in the Hyperites, will be given on pp. 46—82.

Fig. 8. Träfors Hyperite body, approx. grid coordinates 1394/6589 (Figs. 6 and 1, legend in Fig. 5), Length 3—4 km. Only the W part is represented in this figure. In the Ölme area it is the best example of an ENE oriented body, contrasting with the majority of the Hyperites which trend NNW. It is well exposed. The contact with the gneisses is seen over large distances along the S contact. At the central and E part of the contact the gneisses are layered and show isoclinal folding with axial planes parallel to the Hyperite contact, which shows high dips, 70—90°. Within the Hyperite body gabbroic rocks dominate by far. Hornblende metagabbro has been developed rather sparsely, mainly SE of Träfors along joint systems and W of Träfors at the N contact. Amphibolite is abundant at the westernmost part of the exposure, and common at the S contact, S of Träfors. Along the S contact a several metres wide zone of anorthositic, plagioclase-rich cumulate rock has been found. It is dominated by 0.5—5 cm large plagioclase crystals. At the W part of the exposure this rock has been recrystallized and foliated, but the anorthositic parentage is always apparent.

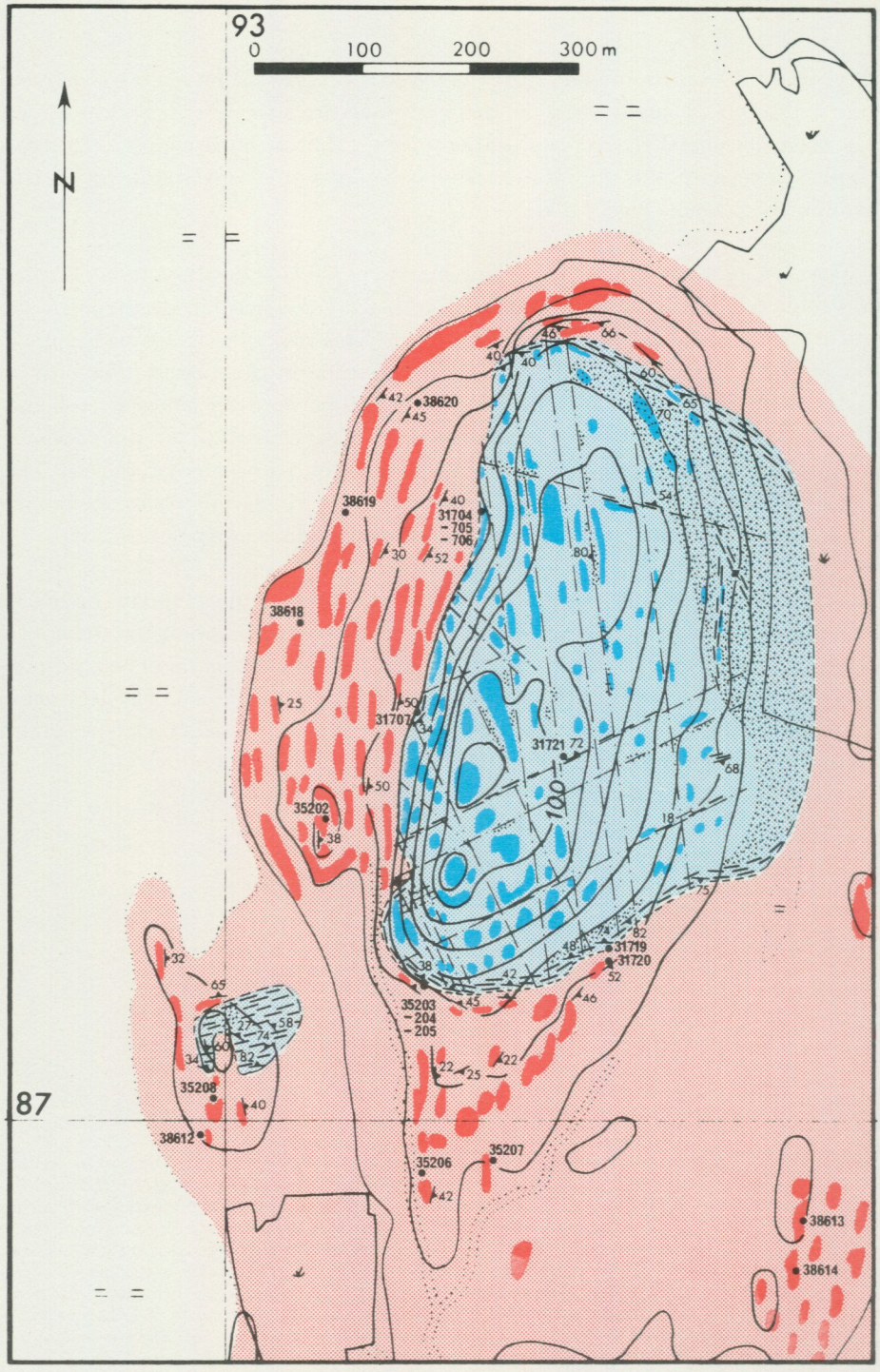

Fig. 9. Brattåshöjden Hyperite body, approx. grid coordinates 1393/6587 (Figs. 6 and 1, legend in Fig. 5), a rather small body, 300—600 m in diameter. Its W boundary is very well exposed, and is an example of a direct contact between the gabbroic rock and the gneisses. The gabbroic rock is fine-grained at the contact and increases in grain size inwards. It is suggested that this contact represents a nearly unaltered intrusion contact of the Hyperite. At the N contact the gneisses contain isoclinally interfolded Hyperite material.

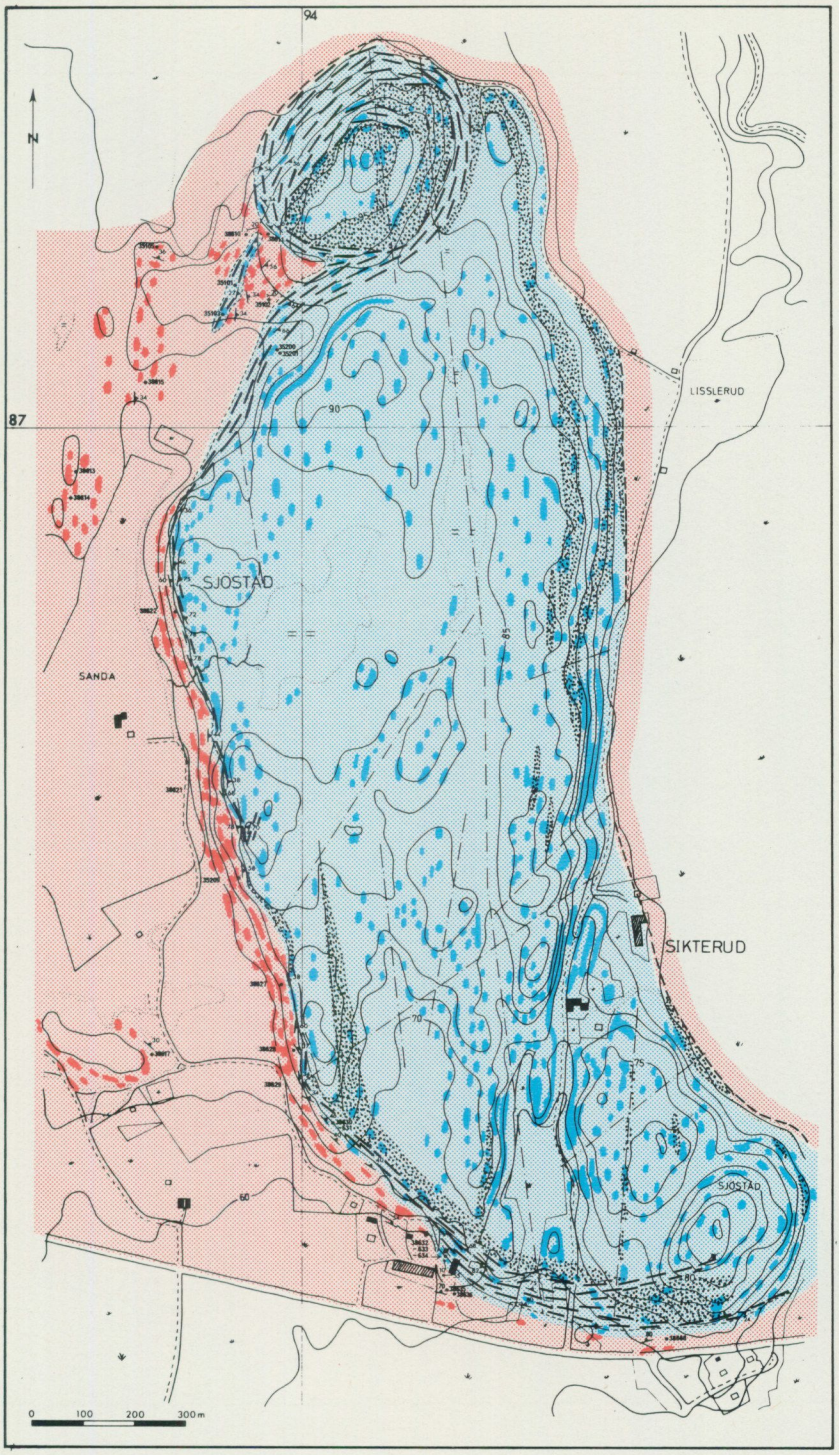

Fig. 10. Sjöstad Hyperite body, approx. grid coordinates 1394/6587 (Figs. 6 and 1, legend in Fig. 5), comparatively large and well exposed, length about 2.5 km, width 1 km. The contact with the gneisses can be studied in the S and W part of the body. Locally at the W boundary, fine-grained gabbroic rock is found immediately at the contact, probably representing the undisturbed margin of the intrusion. The gneisses at the S contact are interlayered with Hyperite material. These rocks show multiple fold patterns (Fig. 15 a).

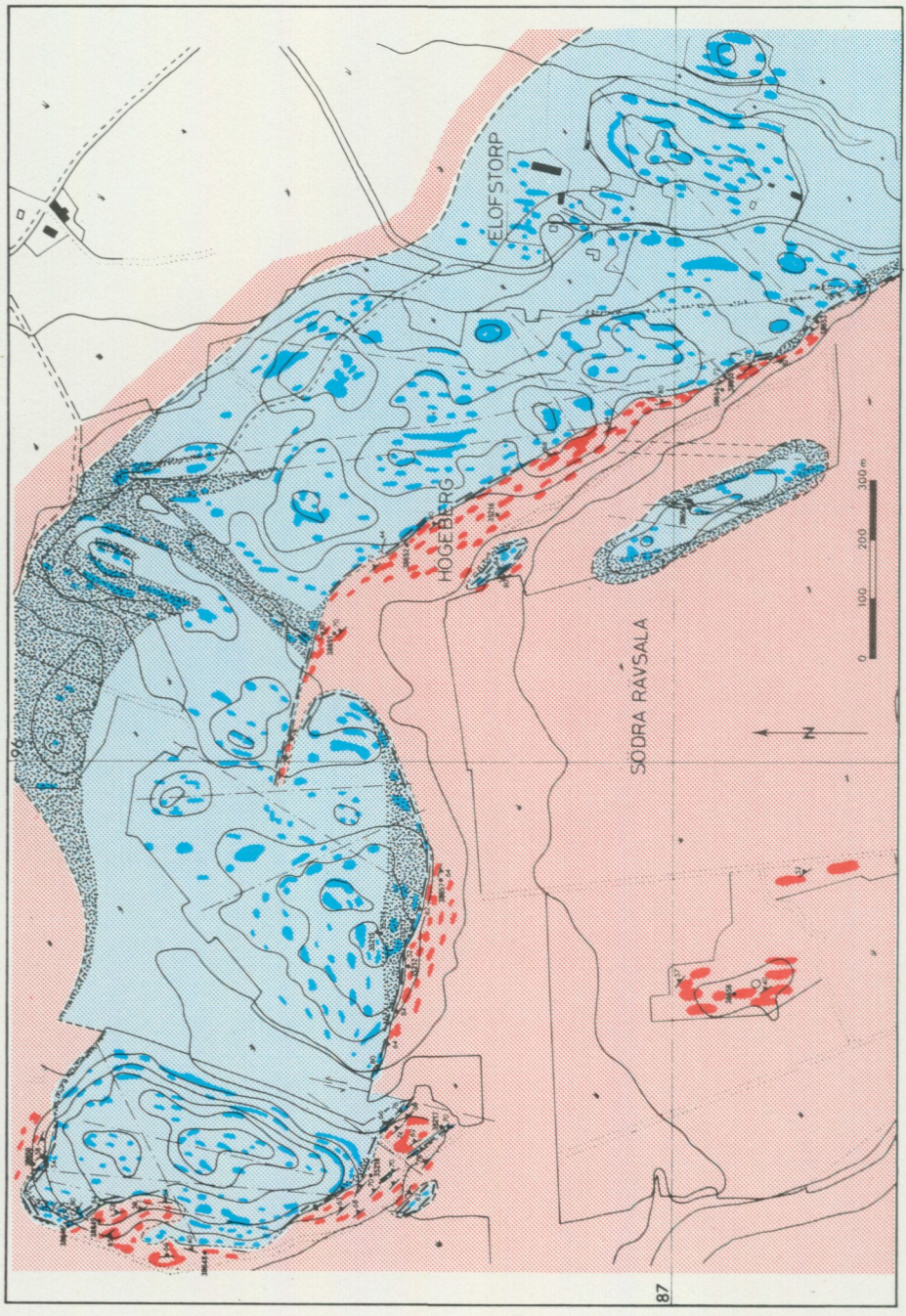
ELOFSTORP
HÖGEBERG
SÖDRA RÅVSALA
N
0
100
200
300 m
96
87

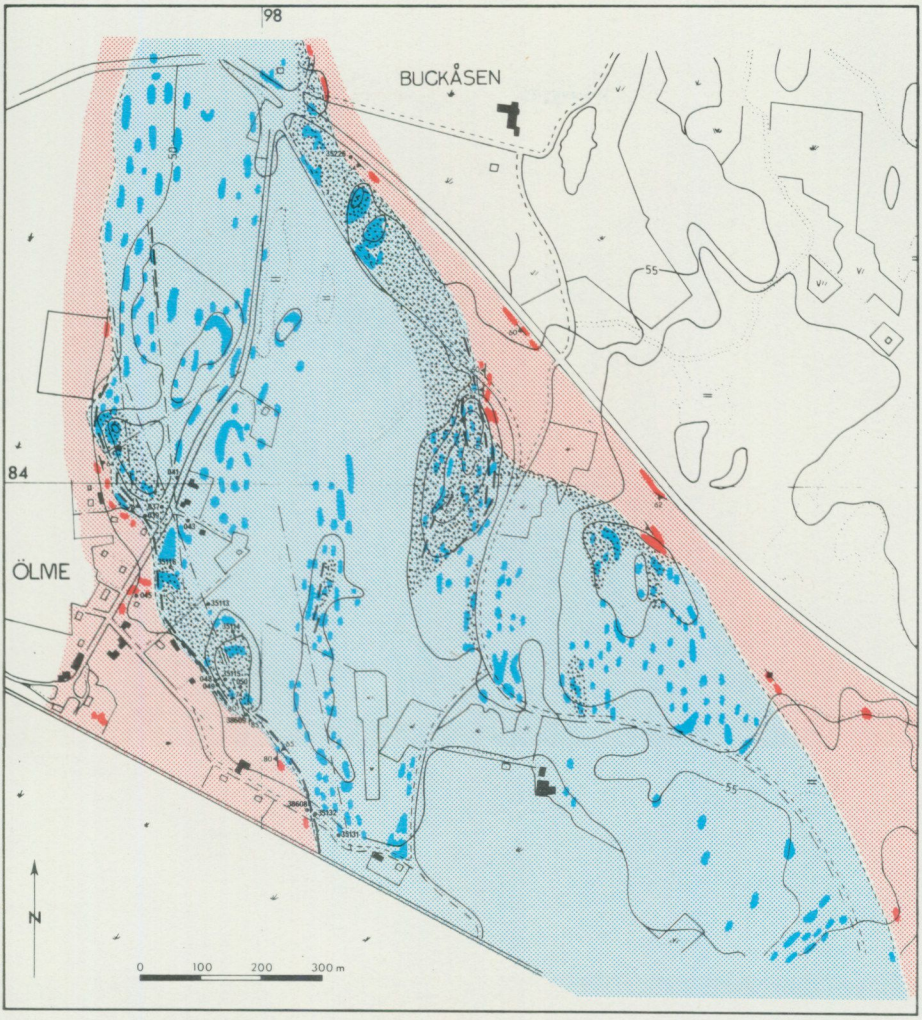

Fig. 12. The central part of the Ölme Hyperite body, viz. the part E and NE of Ölme railway station. A small sinistral strikeslip fault is seen a few hundred metres E of Ölme railway station. Legend in Fig. 5.

Fig. 11. N part of the Ölme Hyperite body. This is the largest body in the area; being semi-continuously exposed in a zone c. 8 km long and 0.5–1 km wide. The part shown in the figure has approximate grid coordinates 1396/6588 and is located near Högeberg (Figs. 6 and 1, legend in Fig. 5). The S and W boundaries are well defined with well exposed contacts towards the gneisses. The amphibolites at the E — W striking contact W of Högeberg show infolded gneissic material with multiple fold patterns (Fig. 15 b). The westernmost part of the body forms a hill — Tyskberget — separated from the rest of the body by a depression without exposures. The contact relations at the S part suggest that a small sinistral strike-slip fault might occur in the depression.

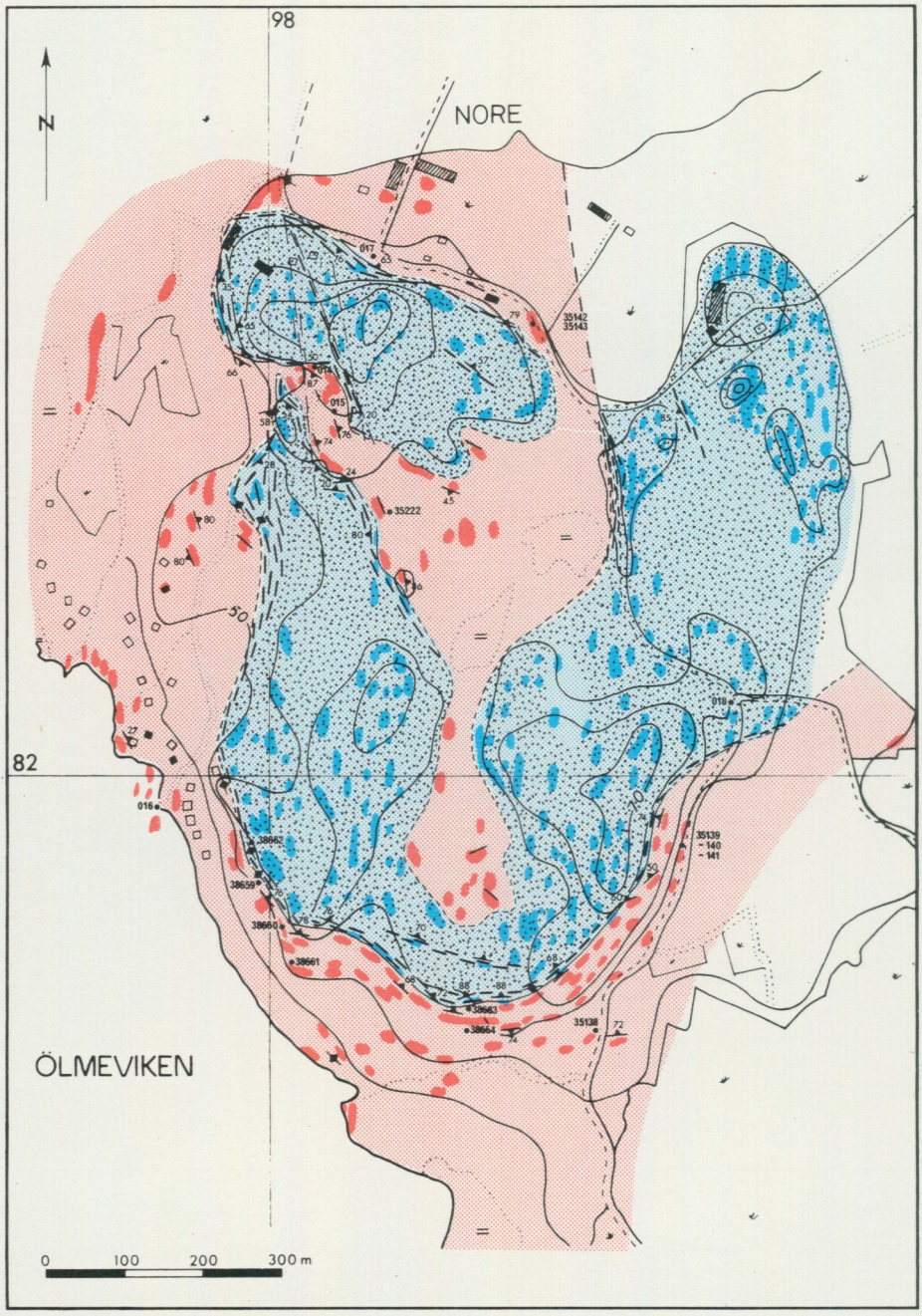

Fig. 13. The S part of the Ölme Hyperite body, around the farm Nore, approx. grid coordinates 1398/6582 (Figs. 6 and 1, legend in Fig. 5). The Hyperite exposure here consists predominantly of hornblende metagabbro. The magmatic gabbroic rock is only present as isolated relics. Amphibolites occur in rather thin zones along the gneiss contact. The exposure pattern might have been caused by multiple folding. The lack of exposures and relief, as well as the local character of the folding at the Hyperite/gneiss contact, preclude a reconstruction of the structure.

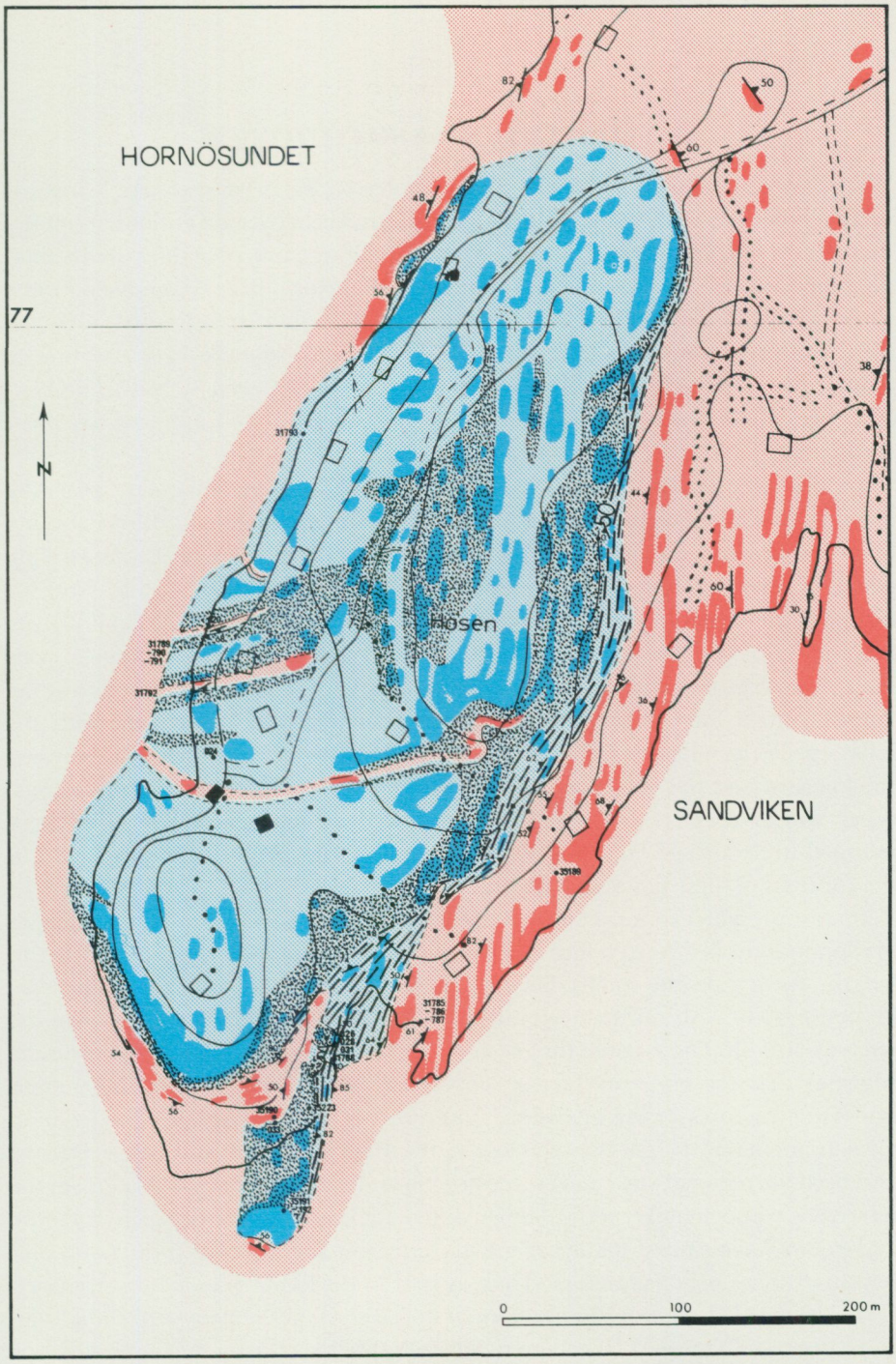

Fig. 14. Hösen Hyperite body, approx. grid coordinates 1393/6577 (Figs. 6 and 1, legend in Fig. 5). A small body, well exposed and showing contact relations with the surrounding quartzo-feldspathic rocks which are not seen in other Hyperite bodies in the area. Especially at the W part of the body on the Vänern shore, several metres wide dykes of granitic and pegmatitic material occur in the Hyperite (see Fig. 16). The pegmatitic material makes up the thinner dykes and veins and has a direct genetical relation to the granitic rock. The granite and pegmatite dykes are interpreted as back-veining phenomena: small intrusions of granitic magma produced by melting of the country rock under the influence of the intrusive mass of basic magma (contact anatexis).

FIELD RELATIONS AND TECTONICS

The regional structure of the basement complex on the N coast of lake Vänern is relatively well known. On the islands and peninsulas between Kattfjorden (immediately SW of Karlstad) and Kristinehamn, E—W trending structures predominate, especially in the Hammarö Formation (Högbom, 1922; Magnusson, 1933; Lundegårdh, 1977, 1980). The regional foliation pattern strikes E—W with low dips. Fold axes trend E—W to ENE—WSW with generally very low plunge values. More to the N these E—W orientations are superseded by N—S (NNW—SSE) directions which dominate the regional structure of the Värmland basement further N.

In the area studied here approximately N—S striking foliations, generally dipping 20—50°, mostly E, locally W, are by far the most common. E—W striking foliations are also met with, and usually occur in connection with E—W striking contacts between Hyperite and gneiss. (See the geological map, Fig. 1.) Note for example the structures at Träfors, Bråten and Nore (cf. Figs. 8, 9 and 13). As mentioned before, the foliations in the gneisses follow the Hyperite/gneiss contacts. Likewise, the foliations in the amphibolites within the Hyperite bodies at the gneiss contact follow the contact, and are thus generally concordant with the foliations in the adjacent gneisses. To bring out more clearly the relations between the gneisses and the Hyperite bodies, and the relations between the various rock types within these bodies, eight relatively well exposed Hyperite bodies were mapped in detail; see Figs. 6—14. More details on the field relations are given in the captions of these figures.

In the present exposure surface, the Hyperite bodies form elongated masses predominantly NNW trending and usually 0.2—1 km wide and up to 8 km in length. As a rule the gneiss foliation at the Hyperite contact dips under the Hyperite body with rather steep angles, usually 60—70°, much steeper than the gneisses are dipping outside the reach of the Hyperites. Such a foliation attitude suggests that the Hyperite bodies consistently fill out the cores of rather tight synform structures in the gneisses. However, it is doubtful whether the foliation measurements in the gneisses so close to the Hyperite bodies can be generalized and used for regional structural reconstructions. It seems possible that close to the relatively competent Hyperite bodies differential movements between Hyperite and gneiss have caused folding of greater intensity and different style, not representative of the regional picture. Thus, in spite of the local foliation measurements (Figs. 10 and 11) the exposure pattern of the large Hyperite body stretching from Nore through Ölme and Högeberg to Sikterud (see Fig. 1) may be interpreted as a large synform or antiform, in which the gneisses exposed in the centre of the structure and those around it represent opposite sides of the intrusive body.

Fig. 17 presents a large number of foliation and fold axis measurements in the

Fig. 15 a, b. Multiple fold patterns observed in interlayered gneisses and amphibolites at the Hyperite/gneiss contact, a (above) — from the S contact of the Sjöstad body (see Fig. 10), b (below) — from the Ölme body close to Högeberg (see Fig. 11).

gneisses, arranged in 40 sterographic plots, each representing a number of measurements taken within a selected area. In our interpretation the measurements indicate that two phases of folding have taken place after the formation of the foliation in the gneisses, one on approximately E—W trending axes and one on approximately N—S trending axes.

Close to the Hyperite contacts, especially at places where thin layers of Hyperite material are interlayered with the gneisses, *e.g.* at Hösen and Sjöstad, multiple fold patterns at a scale of a few centimetres to a few metres may be observed, see Fig. 15. These interference patterns suggest that structures with E—W axes were refolded on N—S axes.

In conclusion: measurements of foliation plane and fold axis attitude in a number of selected areas, as well as the regional exposure pattern of the Hyperite bodies (Fig. 1) and directly observed multiple fold patterns suggest that two phases of folding have been active after the formation of the foliation in the gneisses and the emplacement of the Hyperite bodies, viz. one with E—W trending axes, during the field work interpreted as older, and one with N—S trending axes, suggested to be younger.

The general concordance of the Hyperite/gneiss contacts with foliation planes both in the gneisses and in the amphibolites within the Hyperites might indicate that the Hyperite magma intruded the quartzo-feldspathic material at a time when it had not acquired its present foliation. Subsequently, Hyperite and quartzo-feldspathic country rock would have undergone a phase of deformation and recrystallization producing the present foliation planes. However, several observations argue against such a model. The most important is that the foliation and layering in the gneisses are very well developed, producing a truly pervasive structure. The foliation seen in the Hyperite bodies has a different character. It is only locally developed at the contacts with the gneisses and, very rarely, along small shear zones within the bodies. Such a striking and consistent difference indicates that the foliation in the gneisses and the amphibolites, respectively, were not formed simultaneously. The difference is so large that it can hardly be explained by the lithological difference between the two rock types, inducing them to act differently under the same deformation-recrystallization phase. Another observation in disagreement with the model is the slight discordance which locally can be seen between the layering/foliation in the gneisses and the Hyperite contact (cf. Magnusson, 1929). It thus seems that the general concordance of the Hyperite/gneiss contact with the foliation in gneiss and amphibolite has to be explained in another way.

For the area investigated we prefer a model according to which the Hyperite magma was intruded at a time when the country rock had already acquired (practically all of) its present foliation. The foliation in the gneisses may have been roughly horizontal, and the intruding basic magma is thought to have been intruded (mainly) to form large sills following, generally, the regional structure of the

Fig. 16 a, b. Granitic and pegmatitic material intrusive into the Hyperite body of Hösen. a (above) — A c. three metres wide, E — W striking dyke consisting of granitic material with irregularly distributed pegmatite. b (below) — A c. 75 cm wide, E — W striking dyke of unzoned granitic pegmatite.

rock complex. Very locally the structures in the gneisses were cut, which explains the rarely observed discordance between Hyperite contact and gneiss foliation. Subsequently the rock complex — gneisses and Hyperite bodies — underwent a phase of deformation (E—W axes?) and recrystallization which caused the formation of the amphibolites primarily at the gneiss contact and in small shear zones within the Hyperite bodies, places where differential movements were concentrated. During a final phase of deformation (N—S axes?) the complex was folded once more and additional recrystallization may have taken place.

As indicated in the text above, our work in the Ölme area seems to suggest that the phase of folding producing E—W axes predates the phase producing N—S axes, such in agreement with suggestions of Lundegårdh (1977). Observations by Lundegårdh (1980), Lindh and Malmström (1980), and Lundegårdh *et al.* (1982) have proved a reverse relation, visible, *inter alia*, in the Hyperites cutting the Hammarö Formation where the phase with N—S axes predates the phase with E—W axes. Our work in the Ölme area has been primarily directed at evaluating the metasomatic effect of the recrystallization processes within the Hyperites. A precise structural analysis of the area has not been the aim of our study. We therefore suggest that a more definite evaluation of the relative timing of the two phases of deformation awaits more detailed structural work in the area. Perhaps more than one folding around axes trending E—W has occurred in the bedrock of S Värmland.

No radiometric dating was attempted on the rocks in the area. Comparison with dating results from neighbouring areas may provide some age indications. The youngest deformation might represent the late Dalslandian phase which further W is dated at 1 030±40 Ma B.P. (Skjöld, 1976) and 1 015 Ma B.P. (Hageskov and Pedersen, 1981). The older phase might correspond to a N—S compressive phase proposed in Østfold and preliminarily dated as younger than 1 325 m.y. (Hageskov, 1980), and the older Dalslandian phases found in S Norway, dated at 1 170±50 Ma B.P. (O'Nions and Baadsgaard, 1971). The intrusion of the Hyperite magma was suggested to have taken place at ca. 1 550 Ma B.P. (Priem *et al.*, 1968; Mulder, 1971; Welin *et al.*, 1980). The dating of the formation of the foliation in the gneisses is more problematic. Gorbatschev (1980) claimed that the voluminous intrusions of the magmas of the Småland-Värmland granites and porphyries at 1 600—1 700 Ma B.P. (see *e.g.* Welin *et al.*, 1977; Lundegårdh, 1980) went together with a period of intense metamorphism. However, the precise relation between the extensive magmatism and the metamorphism is far from clear, and observations to support the claim were not given. It seems more probable that the foliation in the gneisses was formed earlier, 1 700—2 000 Ma B.P., possibly during the Svecokarelian orogeny. (Compare Lundegårdh,1980 a.)

Because of the glacial erosion, many *joints and small faults* in the area find their expression in the field as 1—20 m wide gullies and small escarpments. These joints and small faults are of common occurrence, though virtually restricted to the

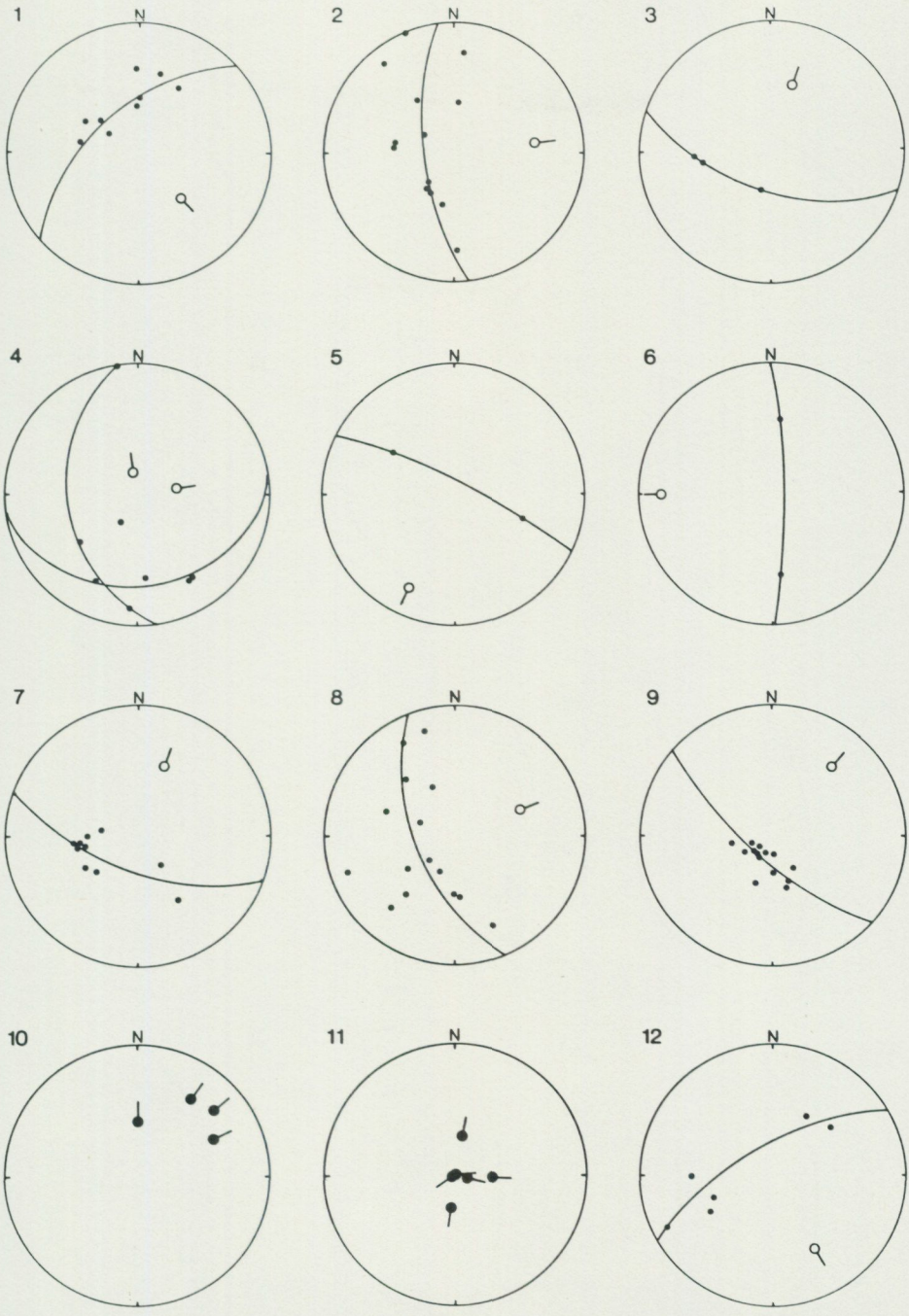

Fig. 17. Foliation and fold axis measurements in the gneisses from 40 selected areas presented in stereographic plots (lower hemisphere). Foliation plane poles are given as black dots. Constructed fold axes are indicated by small open circles with dip indications. Directly measured fold axes are indicated by larger black dots with dip indications. The 40 selected areas are given on p. 34.

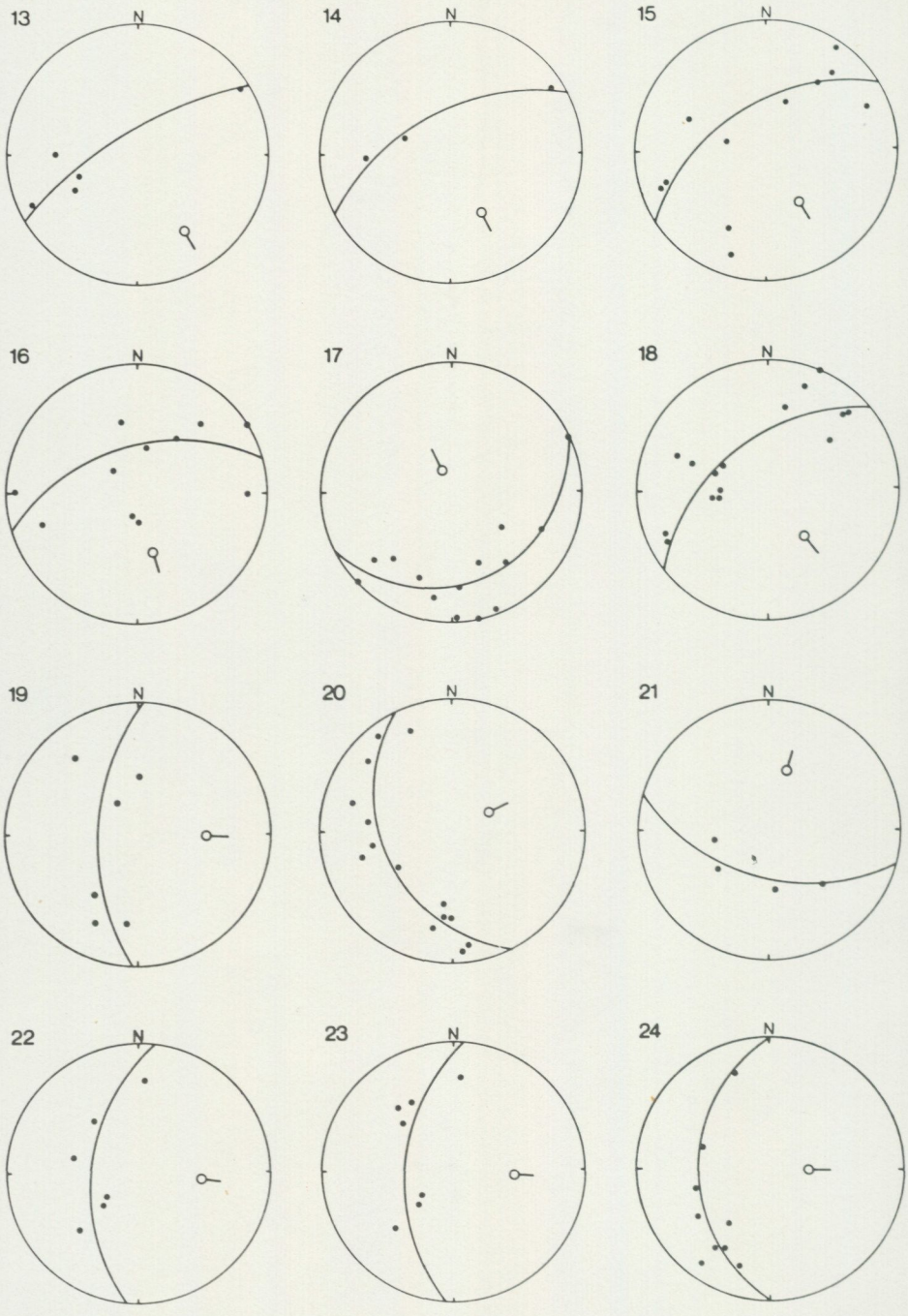

Fig. 17, continued.

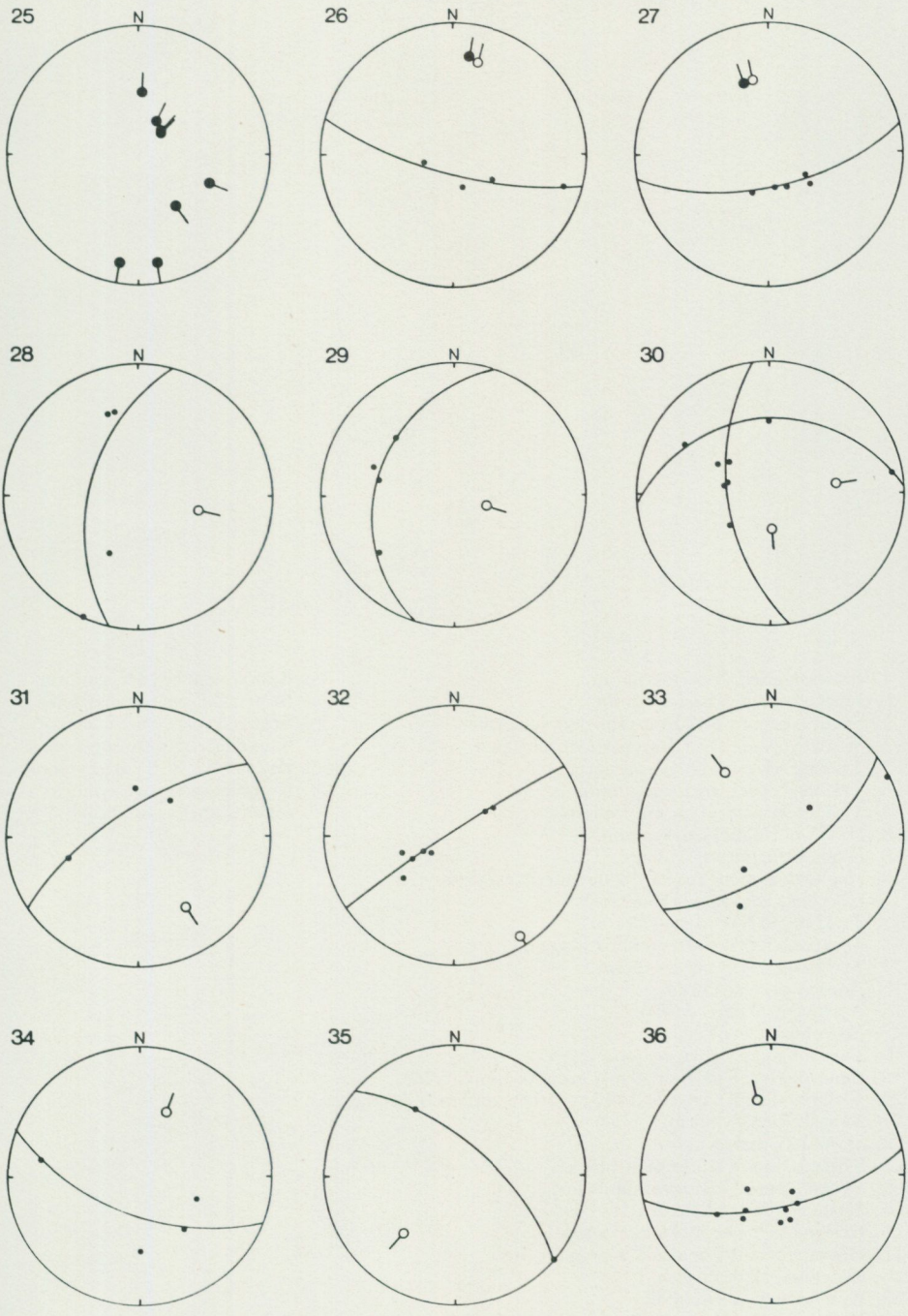

Fig. 17, continued.

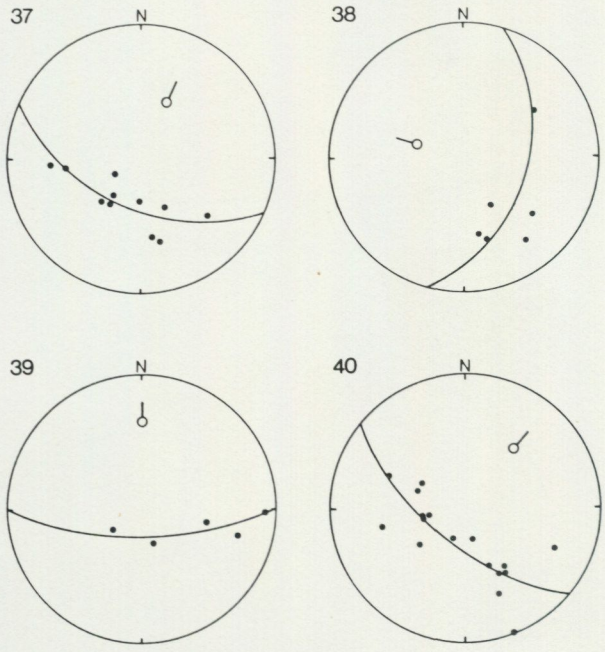

1. Brattåshöjden, N part, synform.
2. Brattåshöjden, S part, synform.
3. Small exposure W of Brattåshöjden, synform.
4. Small exposure W of Brattåshöjden, two axes.
5. Träfors, NE part, gneiss, antiform.
6. Träfors, N part, gneiss, antiform.
7. Träfors, W part, Hyperite, synform.
8. Hill W of Haghöjden, synform.
9. Haghöjden, gneiss, synform.
10. Haghöjden, along road E 18, measured fold axes.
11. Högeberg, fold axes of small folds.
12. Tyskberget, NW part, synform.
13. Tyskberget, NW part, antiform in gneiss.
14. Tyskberget, NW part, synform.
15. Nore, N part, synform.
16. Nore, central part, synform.
17. Nore, S part, synform.
18. Tånäshöjden, N part, synform.
19. Tånäshöjden, S part, small fold in garnet amphibolite.
20. Tånäshöjden, S part, small fold in garnet amphibolite and gneiss.
21. Tånäshöjden, synform.
22. Sjöstad, N part, synform.
23. Sjöstad, N part, antiform in gneiss.
24. Sjöstad, S part, folds in amphibolite.
25. Sjöstad, S part, fold axes at the contact.
26. Hösenudden, isoclinal fold in amphibolite.
27. Hösenudden, isoclinal fold in amphibolite.
28. Hösenudden, pegmatite.
29. Hösenudden, pegmatite.
30. Hösenudden, pegmatite.
31. Bråten, N part, gneiss, antiform.
32. Bråten, N part, synform.
33. Bråten, central part, gneiss, antiform.
34. Bråten, central part, synform.
35. Bråten, NE part, gneiss dome.
36. Bråten, E part, gneiss, antiform.
37. Kummelön, S part, synform.
38. Kummelön, SSE part, synform.
39. Kummelön, E part, synform.
40. Finnön, gneiss, antiform.

Fig. 17, continued.

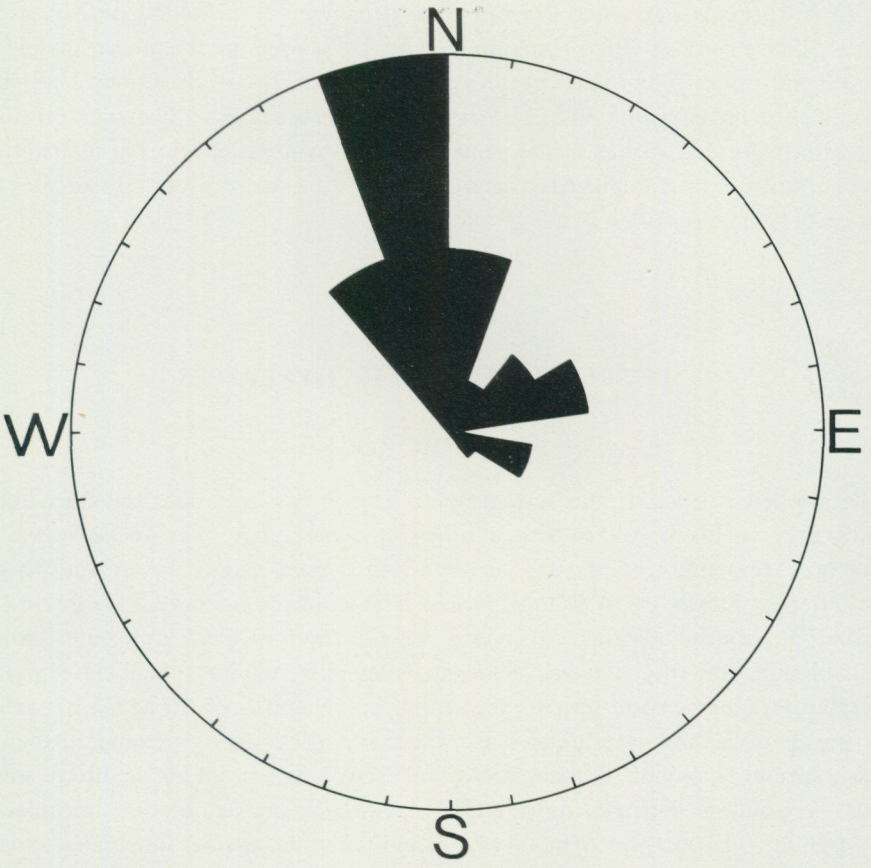

Fig. 18. Rose diagram of strike measurements on (sub-)vertical joint planes within the Hyperite bodies (Table 2); 117 measurements at 20° intervals. The maximum (N 0 — 20°W) represents 39 measurements.

Hyperite bodies. The attitude of the planes is (near-) perpendicular. In narrow zones along many of these planes the gabbroic rock has been replaced by hornblende metagabbro and, more rarely, amphibolite. The occurrence of amphibolite — with foliation parallel to the fault planes — characterizes the (small) faults, along which some shear movements have taken place. At a few places these small faults were seen to continue in the surrounding gneisses, and the off-set indicates sinistral strike slip components of up to 25 m. The joint planes, which are far more abundant than the faults and which may be lined with hornblende metagabbro, are restricted to the Hyperite bodies. The planes stop abruptly at the gneiss contact. This suggests that the joints were formed at least partly as a result of the lithological and rheological differences between Hyperite and gneiss.

Strike measurements of 117 joint planes are listed in Table 2 and plotted in Fig. 18. The measurements indicate two maxima, one at c. N 10°W and another at c.

N 75°E. It seems warranted to relate these directions to the folding activity in the area. The strong N 10°W maximum may be related to the phase of folding developed under maximum compression (σ_1) in an E—W direction. The joints would then have originated upon stress relief. The weak N 75°E maximum could have been formed earlier in the same phase of deformation, during intermittent stress built up, or it might have been formed during the pressure release after the phase of folding resulting in E—W axes.

PETROGRAPHY OF THE HYPERITES

GABBROIC ROCKS

The gabbroic rocks are medium-grained. They show a massive structure and a dark grey to black colour with a brownish violet tinge. The rocks appear as isotropic aggregates of platy, somewhat lath-shaped plagioclase crystals, a few millimetres, locally up to 40 mm, in size. The following minerals were found (see Table 3): apatite, biotite, carbonate, Ca-rich and Ca-poor pyroxene, garnet, hornblende, ilmenite, potassic feldspar, magnetite, olivine, plagioclase, pyrite, pyrrhotite, quartz, rutil, sericite, serpentine, spinel and zircon. The main magmatic paragenesis comprises plagioclase, Ca-rich and Ca-poor pyroxene, further, in lesser amounts, olivine, ilmenite and titaniferous magnetite. Late magmatic minerals — potassic feldspar, more sodic plagioclase, quartz, biotite, hornblende, Ca-rich and Ca-poor pyroxene — were found filling the angular interstices between the earlier magmatic crystals.

Plagioclase crystals, idiomorphic to hypidiomorphic, zoned in the range An_{70-40}, Ø = 0.2—40 mm, are clouded with opaque material (Fig. 19), cf. Poldervaart and Gilkey (1954). Locally, opaque material was found filling cracks in plagioclase crystals (Fig. 20). The crystals are in nesophitic to ophitic intergrowth with pyroxene crystals which are irregular in form, up to 2 cm in size and show a great variety of exsolutions.

The *Ca-rich pyroxene*, augite, shows very regular and thin, 1—2 μ, (001) exsolution lamellæ of Ca-poor pyroxene. Locally, very small amounts of light greenish augite occur in the late magmatic interstices. In most samples the main magmatic *Ca-poor pyroxene* crystallized as pigeonite and now consists of a hypersthene matrix containing blebs and lamellæ of augite in different orientations. Locally this exsolution process did not take place, preserving the homogeneous pyroxene phase (with the same bulk composition as matrix and exsolutions put together). In the more Mg-rich samples the magmatic phase is hypersthene instead of pigeonite. Very minor amounts of both early and late magmatic Ca-poor pyroxene are present.

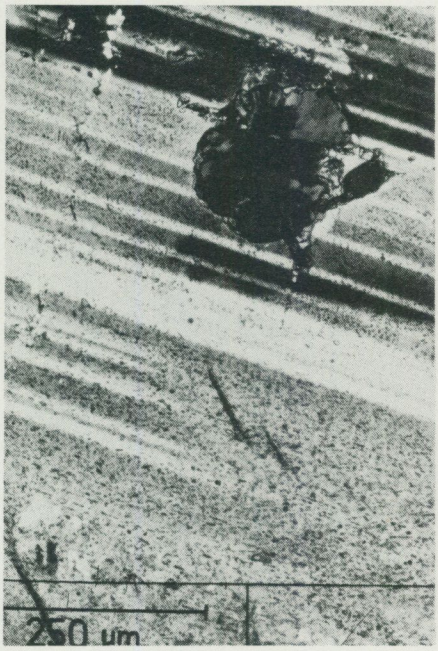

Fig. 19. Plagioclase containing finely dispersed opaque material (crossed polars); gabbroic Hyperite.

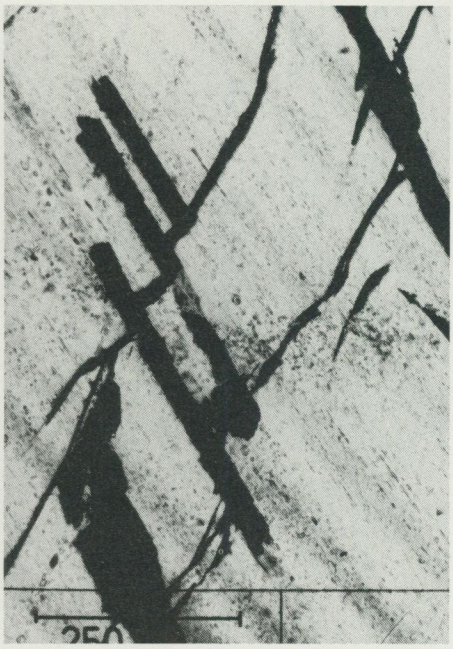

Fig. 20. Plagioclase showing cracks filled with opaque material (crossed polars); gabbroic Hyperite.

The magmatic *ilmenite* and *titaniferous magnetite* crystals (volume relation ilmenite/magnetite ≈ 4) are in a sub-ophitic type of intergrowth with the plagioclase crystals, or appear to be filling isolated interstices between the plagioclase crystals. Simple, magmatic intergrowths of ilmenite and titaniferous magnetite crystals do occur. The magnetite shows exsolutions of ilmenite sheets according to {111}, and spinel lenses according to {100}. The ilmenite shows exsolutions of spinel sheets oriented along (0001). Ilmenite and magnetite crystals have been marginally replaced by biotite and hornblende (plus some spinel).

Olivine crystals are present in only a few samples; they are rather large, Ø = 0.5—2 mm, locally in clusters of two or three crystals, and are supplied with two-tiered reaction rims along the olivine/plagioclase interface. An inner orthopyroxene rim, towards the olivine, is thus surrounded by an outer one of hornblende-spinel symplectite. Garnet has locally replaced the outer rim. In many samples where olivine is absent, these coronas indicate its former presence. Olivine is often replaced at a late stage by brown coloured material which might be bowlingite. Hypersthene-ilmenite (/magnetite) symplectites (Fig. 21) occur as irregular bod-

Fig. 21. Ilmenite (/magnetite)-hypersthene symplectite formed at the expense of olivine crystals during inherent metamorphism of gabbroic rock (Hyperite). Reflected light; the bright vermicular material is ilmenite (+ some magnetite ?), the dark material is hypersthene (cf. Zeck, Shenouda *et al.*, 1982).

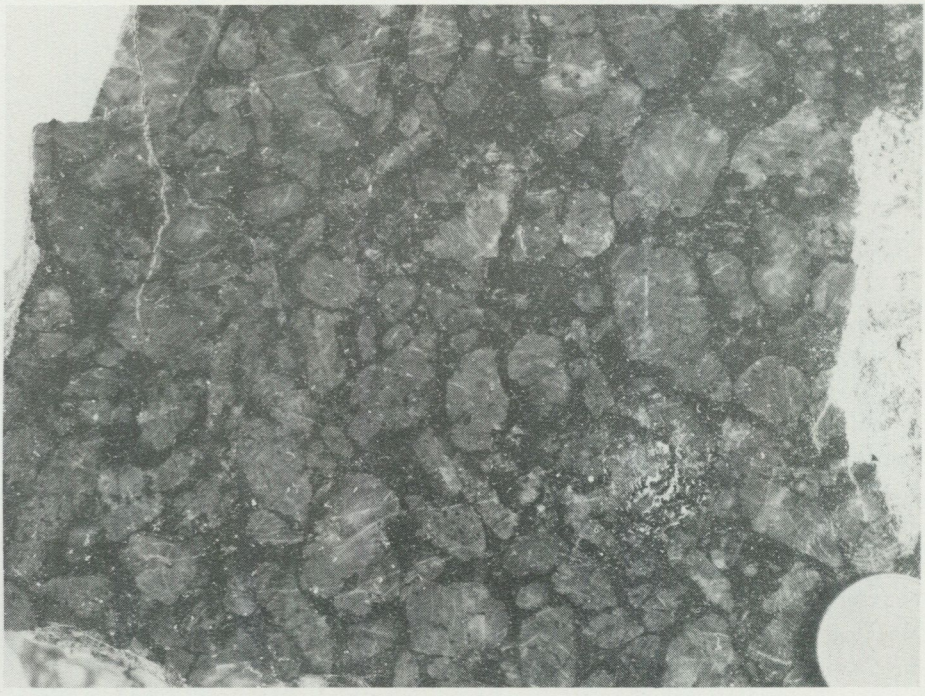

Fig. 22. Hand specimen of anorthosite-gabbro dominated by subhedral to euhedral plagioclase crystals. Scale 4:5

ies within olivine crystals. These intergrowths were formed as part of the inherent metamorphism of the gabbroic rock by replacement of olivine under the simultaneous replacement of adjacent magmatic ilmenite or magnetite crystals with hornblende and biotite, see Zeck, Shenouda *et al.* (1982). This publication gives some more details on the petrography and mineral chemistry of the gabbroic rocks.

In some Hyperite bodies, for example that at Träfors, a particular facies of gabbroic rock was found which differs from the main facies by the abundant occurrence of large euhedral to subhedral plagioclase crystals up to five centimetres in size (Figs. 22 and 23). The amount of these large plagioclase crystals is about 70—90 percent by volume, and the rock may be called anorthosite-gabbro. It usually occurs at the margin of the Hyperite bodies, and was apparently formed by concentration, presumably by gravitational means, of early, large plagioclase crystals in the Hyperite magma at the bottom of the intruded mass of magma. The transition towards the main gabbroic facies is rather sharp, taking place over a distance of a few decimetres. In a qualitative sense these rocks are not different from the main type of gabbros. Olivine is present, though often replaced by hypersthene-ilmenite (/magnetite) symplectites and (?) bowlingite.

Fig. 23. Coarse-grained anorthosite-gabbro consisting mainly of plagioclase. Left of centre an olivine crystal almost completely replaced by hypersthene-ilmenite (/magnetite) symplectite and surrounded by a two-tiered hypersthene-amphibole corona.

HORNBLENDE METAGABBROS

These rocks have the same massive structure as the preserved gabbroic rocks, but the magmatic crystals are largely replaced by metamorphic ones. The replacement has a clearly mimetic nature, magmatic relict structures are abundant, and the rocks thus show blasto-magmatic structures. The minerals found in the rocks are given in Table 3. The magmatic plagioclase crystals have lost the clouding with opaque material, and are more sodic in composition (An_{20-35}). Many crystals are rich in inclusions of epidote and biotite (Fig. 24). Other magmatic crystals have been replaced by aggregates of more sodic, polygonal plagioclase crystals. Furthermore, scapolite and garnet replace the magmatic plagioclase. The magmatic pyroxene has been altered to hornblende. The photomicrographs of Fig. 25 illustrate the sequence of replacement processes. The main stage is characterized by the formation of polycrystalline aggregates of hornblende and quartz. The hornblende then proceeds to form larger single crystals where the quartz crystals remain as poikiloblastic inclusions. The last stage, only developed incipiently in most rocks, is the removal of the quartz inclusions, apparently to form larger

Fig. 24. Hornblende metagabbro: a plagioclase crystal which has preserved its magmatic outline, but has become more sodic during the recrystallization and is filled with many euhedral inclusions consisting mainly of epidote, biotite and some apatite. The inclusions might in part have been formed by recrystallization of earlier replacement products.

quartz crystals elsewhere in the rock. In between the more obvious mimetic replacements of magmatic crystals, there is a finer grained matrix consisting mainly of plagioclase, biotite and garnet. Biotite often occurs around opaque material. Accessories are titanite and apatite. Retrogressive influence is indicated by sericitization of plagioclase, replacement of biotite by chlorite and formation of some carbonate.

Locally, recrystallization equivalents of the anorthosite-gabbro facies of the gabroic rock were found (see Figs. 26 and 27). The magmatic structure characterized by the large plagioclase crystals is clearly preserved. The plagoclase crystals have acquired a more sodic composition (An_{20-30}) and are partly replaced by smaller, polygonal, metamorphic crystals of plagioclase (and some garnet and scapolite). In the central parts they are filled with many euhedral epidote, muscovite and biotite crystals. The matrix between the large plagioclase crystals consists of plagioclase, hornblende, quartz, biotite, garnet, opaque material, titanite and apatite.

AMPHIBOLITES

The amphibolites are foliated, consisting of lenses and schlieren alternatingly rich in hornblende and plagioclase. The blasto-magmatic textures dominating the hornblende metagabbros have been replaced by purely metamorphic structures. Only very locally some equidimensional to roughly rectangular plagioclase aggregates can be seen, pseudomorphs after magmatic megacrystals (Fig. 28). The mineral composition of the rocks is given in Table 3. The plagioclase has a rather sodic composition (An_{20-30}). The plagioclase-rich schlieren frequently have a polygonal texture. Euhedral inclusions of epidote and biotite appear often parallel to the plagioclase cleavage. Discrete crystals of biotite and hornblende occur among the plagioclase crystals. The hornblende-rich schlieren consist mainly of subhedral hornblende and to a lesser extent biotite crystals, further plagioclase and garnet. The retrogressive influence in the rocks is demonstrated by the sericitization and saussuritization of the plagioclase, the formation of carbonate at the expense of plagioclase and by the alteration of biotite and garnet to chlorite, and perhaps also by the replacement of opaque material to titanite.

The biotite amphibolites have much in common with the amphibolites. The difference is that the biotite content is 40—50 %, and accordingly the foliation is much better developed (Fig. 29). Accessories are magnetite, apatite and zircon.

The three different rock types in the Hyperite bodies have been defined on structural and mineralogical features observed in hand specimens. These criteria were used to discriminate the rocks in the field during mapping. In order to check how this classification relates to the mineral compositions estimated in thin sections, we made a cluster analysis of the mineralogical information which is

a

b

c

d

e

f

Fig. 25. A sequence of photomicrographs illustrating the transition in the Hyperite from gabbroic rock to hornblende metagabbro with increasing recrystallization and formation of hornblende. a—Gabbroic rock: incipient formation of a 50–100 μm wide hornblende rim around magmatic augite crystals. b—Hornblende metagabbro: relict cores of augites preserved in replacive hornblende. Note the small quartz crystals in the hornblende which represent an additional product of the replacement (cf. Beach, 1973). c—Hornblende metagabbro: hornblende has replaced all augite. In the centre of the polycrystalline replacive aggregate the small quartz crystals are still preserved, at the margin a homogeneous, monocrystalline hornblende rim has been formed. d—Nearly identical area, photographed between crossed polars. e—Hornblende metagabbro: a monocrystalline hornblende crystal has been formed. The small quartz crystals are largely preserved. f—Amphibolite: new hornblende crystals have been formed. No quartz crystals are preserved. The smaller grain size might be due to paracrystalline deformation inducing recrystallization. The rock has been completely recrystallized. No traces remain of the original magmatic structure. Instead, the foliation developed during the metamorphism is the dominant structure of the rock.

Fig. 26. Hand specimen of recrystallized equivalent of anorthosite-gabbro from the bottom of the Hyperite body at Träfors. The magmatic structure has been largely preserved.

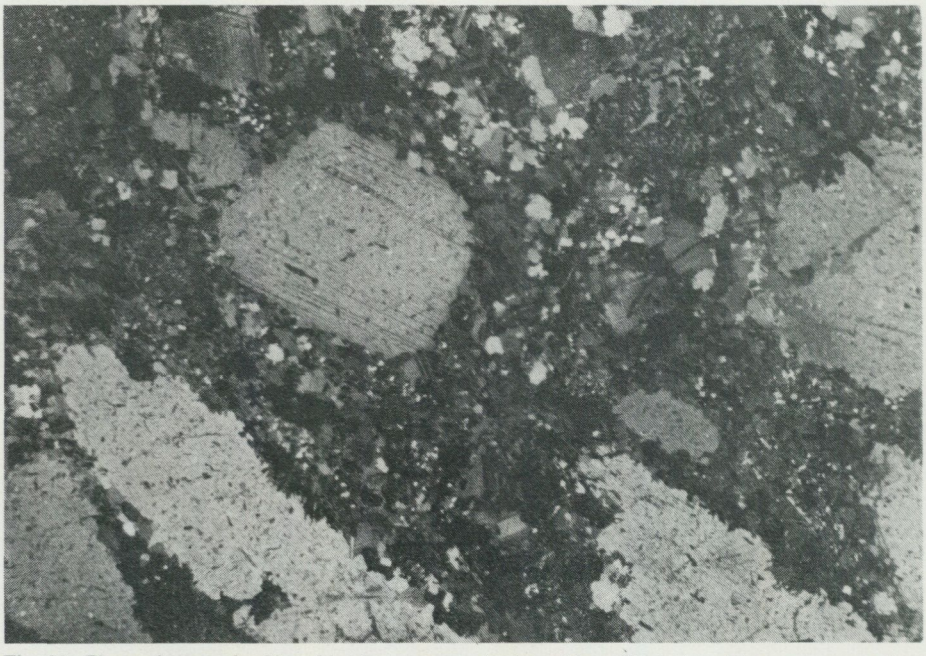

Fig. 27. Photomicrograph of hornblende meta-anorthosite-gabbro. Plagioclase blasto-megacrysts in a matrix of smaller hornblende, biotite, plagioclase and quartz crystals. Crossed polars.

Fig. 28. Amphibolite: a magmatic plagioclase crystal replaced by an aggregate of roughly equant, metamorphic plagioclase crystals.

Fig. 29. Biotite amphibolite. Biotite is a major mineral often assembled in schlieric aggregates.

summarized in Table 3. Fig. 30 shows a dendrogram constructed on the basis of an unweighted cluster analysis (Ujiie and Nagase, 1971) taking into account the following minerals: biotite, calcite, chlorite, orthopyroxene, clinopyroxene, epidote, hornblende, garnet, quartz, opaque material, plagioclase, titanite and scapolite. Minerals occurring in quantities lower than 1 % are scaled up to 1 %. At 70 % similarity, three well-defined groups occur. The rock type distribution in the three groups is as follows:

group 1, 9 amphibolites, 3 hornblende metagabbros,
group 2, 7 amphibolites, 12 hornblende metagabbros,
group 3, 1 hornblende metagabbro, 12 gabbroic rocks.

This distribution shows that the dendrogram classification based on the estimated total mineralogy reproduces rather well the classification based on field observations. The separation of the amphibolites and the hornblende metagabbros between group 1 and 2 is not too well expressed. This reflects that their main difference is a structural one which was not considered in the dendrogram classification.

GEOCHEMISTRY OF THE HYPERITES

SAMPLING PROCEDURE AND SAMPLE PREPARATION FOR CHEMICAL ANALYSIS

The Hyperite samples have been taken from localities where gabbroic rock, hornblende metagabbro and amphibolite occur close to each other, usually within a distance of 10—20 m, this to maximize the chance that a close protolithic relation exists between the samples. Where possible, the distance from the sample points to the Hyperite/gneiss contact has been measured.

The samples used for chemical analysis had a weight of c. 5 kg. In the field weathering surfaces were cleaned off by hammer chipping. The samples were broken into fragments with a maximum size of c. 5 cm and packed in plastic bags. In the laboratory these pre-treated samples were fed directly into a jaw crusher (Fritsch, WC) where they were crushed in several steps to a maximum grain size of 1 cm. Further crushing was done in two portions. The one for major element analysis was crushed in WC (Siebtechnik ring mill), and the one for trace element analysis was crushed mainly in agate (Fritsch ball mill) to minimize contamination effects.

ANALYTICAL METHODS

Major element analyses of the rocks were performed by the chemical laboratories of the Geological Survey of Greenland, under the direction of I. Sørensen and J. Kystol Christensen. SiO_2, TiO_2, Al_2O_3, FeO*, MnO, CaO, K_2O and P_2O_5 were determined with a Siemens SRS XRF-spectrometer using methods outlined by Sørensen (1975, 1976). Ferrous/ferric iron was obtained wet chemically. Na_2O and MgO were determined by atomic absorption spectrometry, H_2O by means of the Penfield method.

The trace elements Rb, Sr, Ba, Zr, Y, Ni, Cu, Zn, Pb, Th, S and Cl were analysed by one of the authors (J.R. Morthorst) with the Philips PW 1410/20 semi-automatic XRF spectrometer at the Institute of Petrology, Copenhagen University, under the supervision of Dr. J.C. Bailey, using general methods outlined by Norrish and Chappell (1967), and Bailey and Sørensen (1976). The measurements were carried out on 4 g powder tablets. Each tablet was measured twice to check the precision of the analyses. For S and Cl, new tablets were made shortly before the measurements, as these elements are very sensitive to atmospheric contamination. For calibration, the following international standards were used: G-1, G-2, GA, GR, GSP-1, AGV-1, BCR-1, W-1, PCC-1, BR, DR-N, as well as two home-made S standards. For each run, four or five of these standards were measured (cf. Flanagan, 1973, 1974). The accuracy decreases (depending on the element) from a few per cent for elements present in concentrations of a few hundred ppm, to 10—30 per cent for elements such as Pb and Th which occur in very low concentrations.

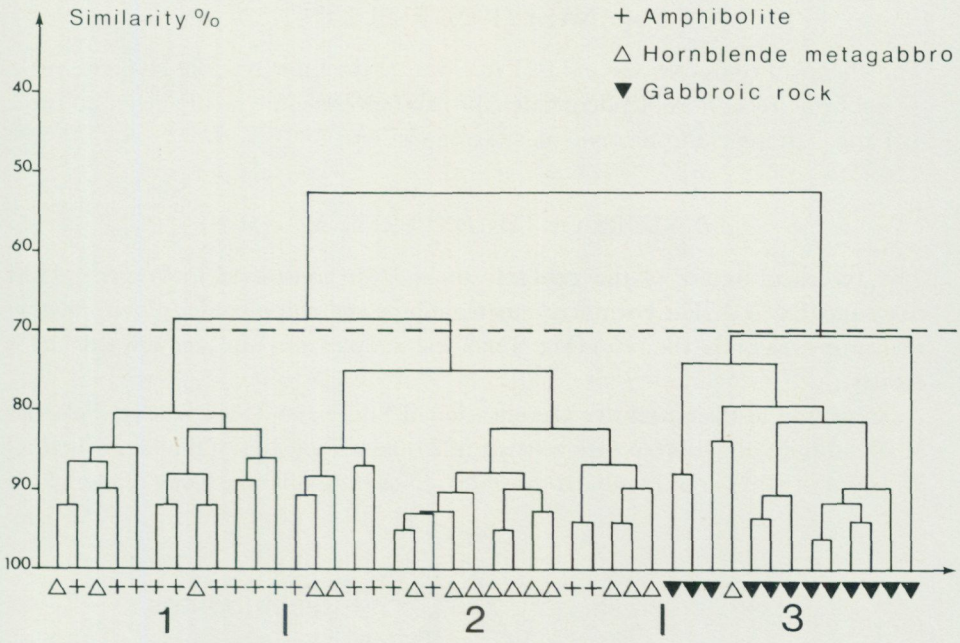

Fig. 30. Dendogram constructed on the basis of an unweighted cluster analysis of the estimated mineral contents of the same samples forming the base of Table 3. Three groups come out at 70 % similarity (dotted line).

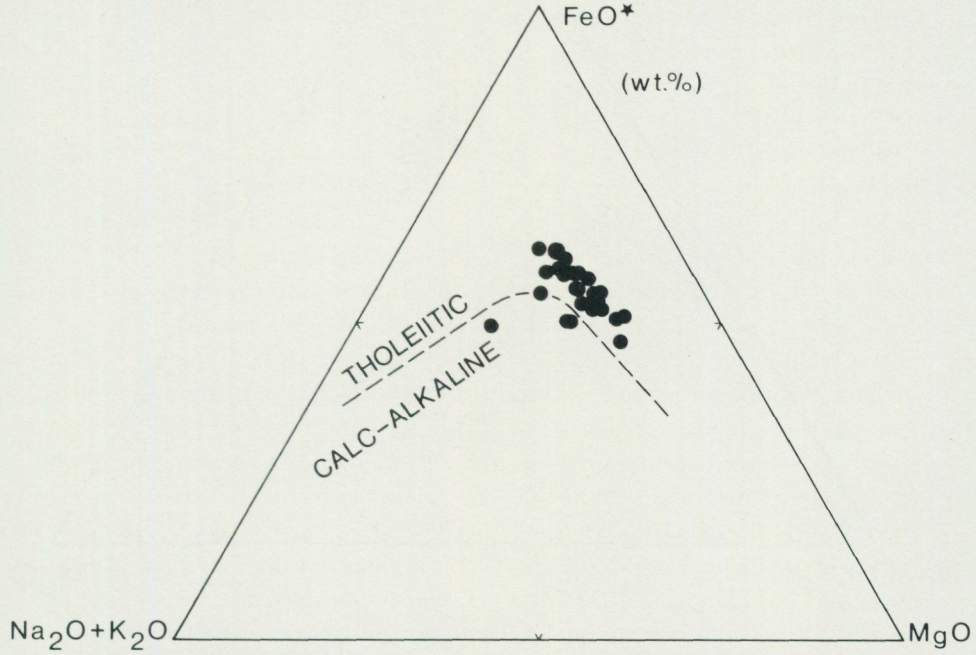

Fig. 31. AFM diagram showing the tholeiitic character of the gabbroic Hyperite rocks. Dividing line after Irvine and Baragar (1971).

ANALYTICAL RESULTS

The chemical compositions and CIPW norms of the three types of Hyperite rocks — gabbroic rock, hornblende metagabbro and amphibolite — are given in Table 4. Table 5 presents the average (mean) compositions.

NATURE OF THE HYPERITE MAGMA

The tholeiitic nature of the gabbroic rocks is demonstrated in Wager's AFM diagram (Fig. 31). The hornblende metagabbros and amphibolites plot in roughly the same area of the diagram (Fig. 32); a few samples are displaced towards the A corner.

According to the normative classification of Yoder and Tilley (1962), the series of 26 samples of gabbroic rock consists of 2 quartz-tholeiites, 5 tholeiites (both Q < 1 and ol < 1) and 19 olivine-tholeiites. (Norm calculations were made with a

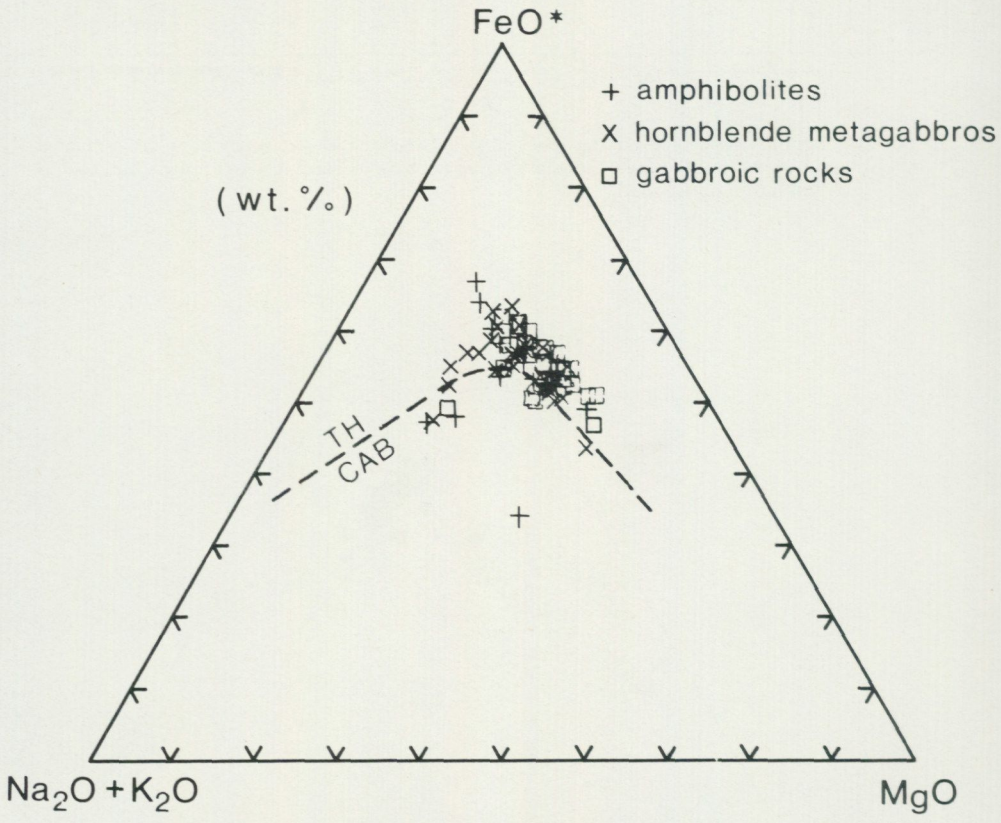

Fig. 32. AFM diagram (computer plot) featuring all three Hyperite rock types: gabbroic rocks, hornblende metagabbros and amphibolites. Compared to the gabbroic rocks (see also Fig. 31), a few amphibolites and hornblende metagabbros are displaced towards higher F and A values. Dividing line after Irvine and Baragar (1971).

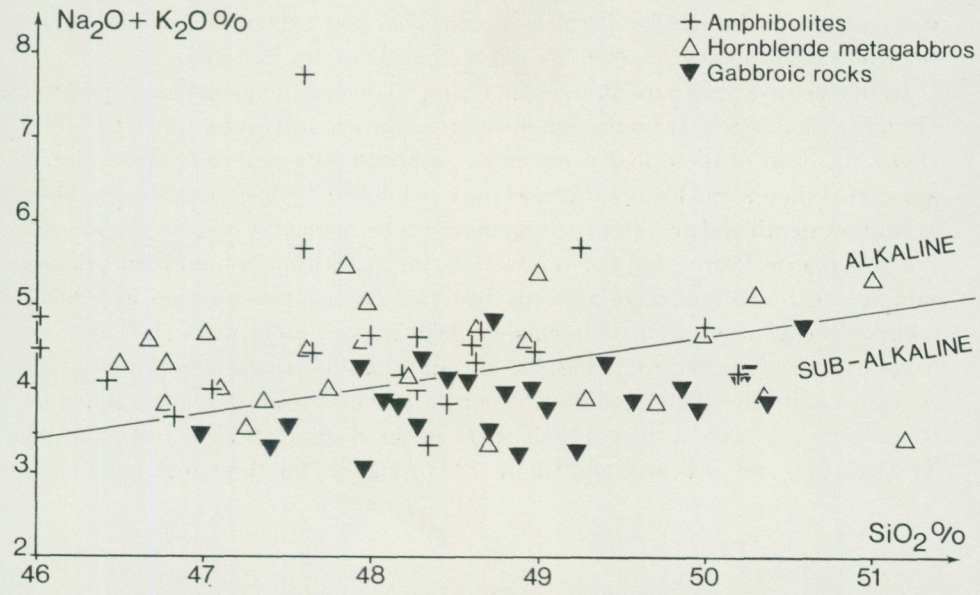

Fig. 33. Alkali-SiO_2 diagram showing the distribution of the three Hyperite rock types. Dividing line after Irvine and Baragar (1971). The gabbroic rocks plot close to the alkaline/sub-alkaline field boundary, predominantly in the sub-alkaline field. The hornblende metagabbros, and even more so the amphibolites, plot predominantly in the alkaline field.

program made by cand. scient. Tom S. Petersen, Danmarks Geologiske Undersøgelse.) The hornblende metagabbros (26 samples) consist of 4 quartz-tholeiites, 5 tholeiites, 14 olivine-tholeiites, 1 olivine-basalt (both hy $<$ 1 and ne $<$ 1) and 2 alkali basalts. The 22 amphibolites come out as 2 quartz-tholeiites, 5 tholeiites, 12 olivine-tholeiites, 2 olivine-basalts and 1 alkali basalt.

The alkali-SiO_2 diagram (Fig. 33) demonstrates the sub-alkaline nature of the gabbroic rocks. All but three samples plot in the sub-alkaline field. The three samples plotting in the alkaline field represent occurrences of anorthosite-gabbro or rocks closely associated therewith, suggesting that the location of these rocks in the alkaline field might be due to a local, shallow level differentiation process. The sub-alkaline character of the Hyperite magma as a whole thus becomes even more pronounced than suggested by Fig. 33. The hornblende metagabbros and the amphibolites are clearly displaced to higher ($Na_2O + K_2O$) values compared to the gabbroic rocks, and plot predominantly in the alkaline field.

In the An-Or-Ab' diagram of Irvine and Baragar (1971), Fig. 34, the gabbroic rocks plot on the boundary between the fields for common basalts and basalts rich in potassium. Notably some amphibolites deviate from this picture, being displaced towards the Or corner.

The discrimination diagram of Floyd and Winchester (1975) seems to suggest an ocean tholeiitic character for the gabbroic rocks (Fig. 35). The hornblende

metagabbros and amphibolites show a somewhat larger distribution field, but on the whole conform rather well to the gabbroic rocks in this diagram.

In the Ti-Zr-Y diagram (Pearce and Cann, 1973) only four samples of gabbroic Hyperite plot in field D (within-plate basalts), the rest are concentrated in field B (Fig. 36). Two of these four samples are of anorthosite-gabbro or rocks closely associated therewith. These rocks may have originated by differentiation processes at shallow depth and are apt to give an incorrect picture of the magma (see above). For this reason Pearce and Cann (1973) excluded such rocks from their primary sample set. So in fact there are only two *bona fide* samples plotting in field D, making the concentration of points in field B even more distinct. This field harbours mainly ocean ridge basalts, but also volcanic arc basalts (low potassic tholeiites and calc-alkali basalts). The hornblende metagabbros and amphibolites conform rather well to the gabbroic rocks in the diagram (Fig. 37). Also in the Ti-Zr-Sr diagram of Pearce and Cann (1973), Fig. 38, the three rock types show

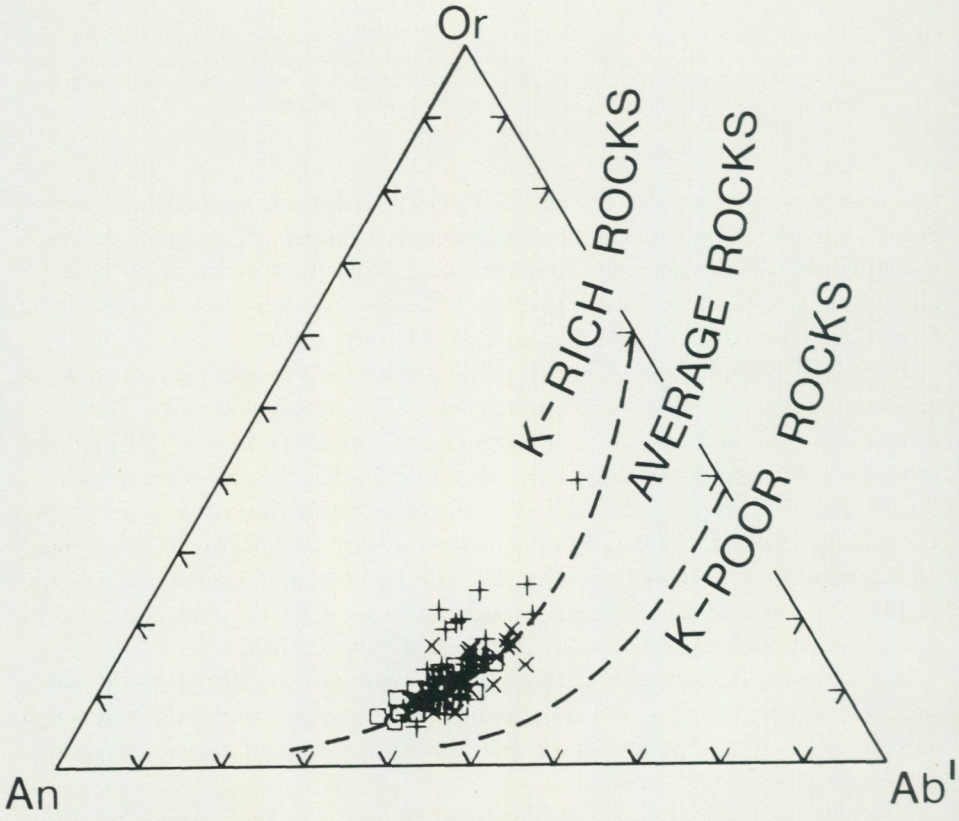

Fig. 34. An-Ab-Or diagram used to distinguish K-poor, average and K-rich rocks. Field boundaries after Irvine and Baragar (1971). Signatures as in Fig. 32.

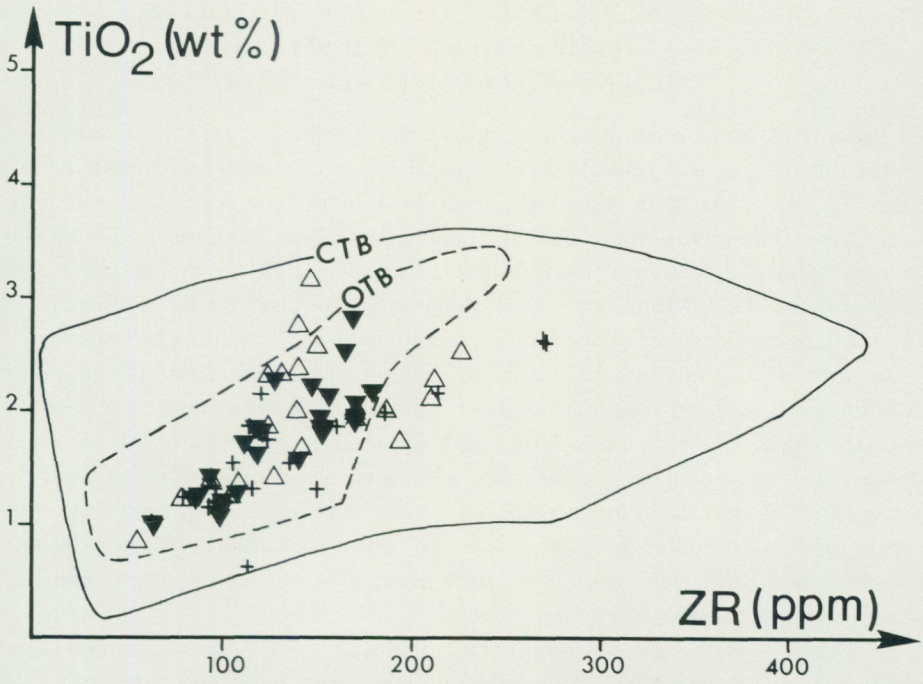

Fig. 35. Discrimination diagram efter Floyd and Winchester (1975). CTB: continental tholeiite basalt; OTB: oceanic tholeiite basalt. Signatures as in Fig. 33. All gabbroic Hyperite rocks plot in the field for oceanic tholeiite basalt. Hornblende metagabbros and amphibolites show a slightly larger distribution field.

very similar distribution patterns. This diagram confirms that the rocks could have originated in an ocean ridge environment.

In view of the clear-cut continental setting of the gabbroic intrusive rocks the ocean floor assignment appears not readily acceptable. It seems rather that the Ti-Zr and Ti-Zr-Y diagrams are unable to discriminate systematically between continental tholeiites and ocean ridge basalts. In a recent paper by Zeck and Morthorst (1982) this problem is discussed in more detail. The mentioned paper presents the Ti-Zr-Y plots for other basic igneous rock suites, viz. Karroo province, S Africa, Columbia River Group, Northwestern U.S.A., and the Early Mesozoic dyke suite in the coastal region of NE America. It is concluded that tholeiitic magmas which break through continental crust and which are arrested as dykes, sills or effusive lavas, may show Ti/Zr/Y ratios that are similar to those shown in ocean ridge basalts. This impairs the use of Ti-Zr-Y and related discrimination diagrams as a general means of assigning a geological setting to the formation of (the igneous progenitors of meta-)basic rocks.

METASOMATIC EFFECT OF THE AMPHIBOLITE FACIES METAMORPHISM PRESENTATION AND EVALUATION

In several of the discrimination diagrams the gabbroic rocks, the hornblende metagabbros and the amphibolites, respectively, plot somewhat differently (cf. Figs. 32–35). Also their range of normative mineral composition is different, suggesting that metasomatic changes have taken place in connection with the metamorphism that altered the gabbroic rocks to hornblende metagabbros and amphibolites. This demonstrates that discrimination diagrams based on magmatic standard rocks cannot be used indiscriminately for metamorphic rock series.

In order to demonstrate the chemical differences between the gabbroic rocks and the recrystallized rocks, two cluster analyses have been made, one dealing with the major elements and another with the trace elements. The two resulting dendograms are given in Fig. 39. They are based on the procedure outlined by Ujiie and Nagase (1971) for unweighted cluster analysis, and are prepared with the help of a computer program made by cand.scient. Bjarne Wallin (Atomforsøgsstation Risø, Denmark). The imput material consisted of the raw chemical data; no elements were scaled up or down.

In the major element dendrogram (Fig. 39 a) at a 95–96 % similarity two large clusters may be recognized alongside an unassorted rest. The three types of Hyperite rocks are not systematically divided among these three "clusters". For the samples taken together, the measure of similarity is quite high, about 90 %. This suggests that the major element metasomatism connected to the recrystallization within the Hyperites may be of minor importance, and further that the original intrusive gabbroic rocks represented a rather homogeneous magmatic suite showing only limited differentiation. A study of the distribution of Ca and Ni

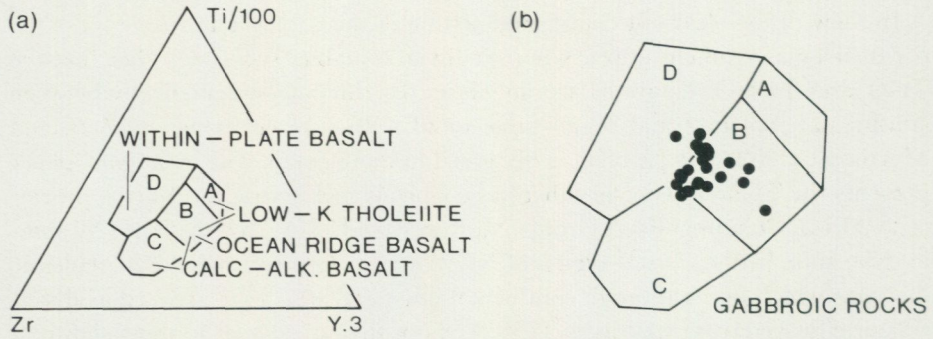

Fig. 36. a — Ti-Zr-Y discrimination diagram (Pearce and Cann, 1973) explained. b — 25 samples of gabbroic Hyperite rock plotted in the Ti-Zr-Y diagram. Only three samples plot in field D (within-plate basalts), the rest are concentrated in field B, claimed to be indicative of mainly ocean ridge basalts, but also volcanic arc basalts (low-K tholeiites and calc-alkali basalts).

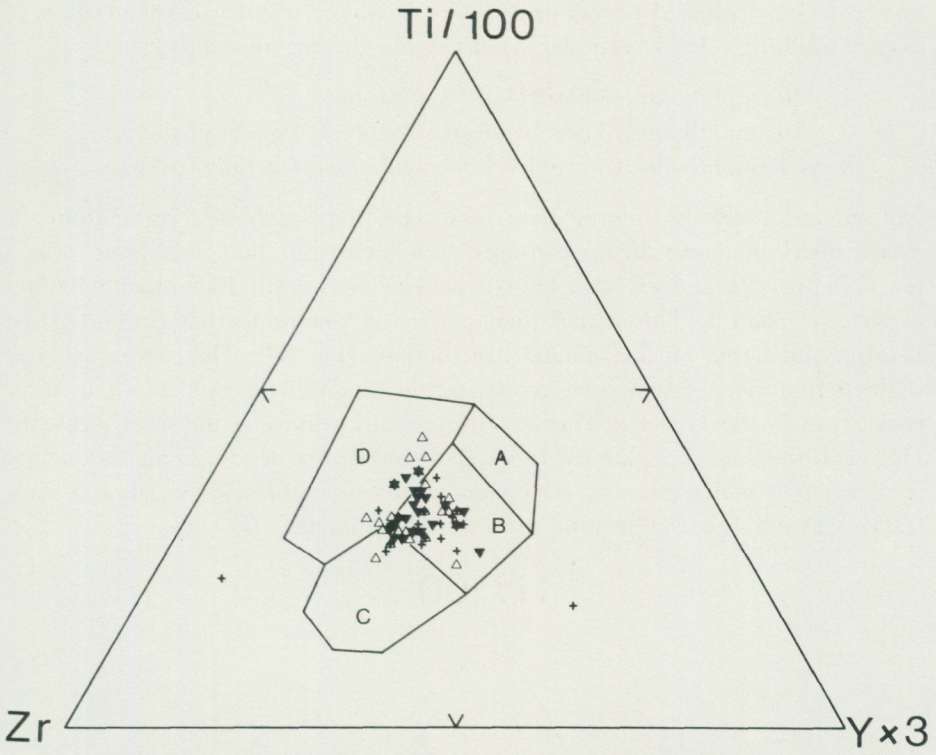

Fig. 37. All three types of Hyperite rocks plotted in the Ti-Zr-Y diagram. Signatures as in Fig. 33. The distribution fields for hornblende metagabbros and amphibolites conform rather well to that of the gabbroic rocks.

within the gabbroic rocks of the Hyperite bodies seems to confirm the latter suggestion. If a marked differentiation had taken place, it might have occurred within the intrusive bodies resulting in a systematic internal distribution of differentiation affected elements. Fig. 40 indicates that there is no systematic decrease in Ca and Ni in the gabbroic rocks as a function of the distance to the contact with the country rock, thus arguing against any pronounced form of differentiation within the magmatic bodies. In only a few Hyperite bodies, for example the one at Träfors (Norra Hålerud), are signs of a magmatic differentiation present in the form of a special marginal rock facies consisting of anorthosite-gabbro, probably formed by gravitational differentiation (see p. 39). In many geochemical diagrams (see, *e.g.*, Fig. 45, p. 71 ff), the four samples from the Träfors locality plot in a rather isolated position. The major element dendrogram (Fig. 39 a) brings out clearly the unique nature of these four samples. They plot most to the right, clearly separated from the rest of the samples.

The trace element dendrogram (Fig. 39 b) shows a much lower measure of overall similarity. At 75 % similarity, three main clusters come forward:

1, 10 amphibolites, 8 hornblende metagabbros,
2, 6 amphibolites, 8 hornblende metagabbros, 7 gabbroic rocks,
3, 1 amphibolite, 8 hornblende metagabbros, 18 gabbroic rocks.

Not unexpectedly the intermediate rock type, the hornblende metagabbro, is evenly distributed over the three groups. A clear concentration of gabbroic rocks is found in group 3, and a weaker but still convincing concentration of amphibolites occurs in group 1. This distribution pattern is similar to that read from the dendrogram based on the mineral distributions (Fig. 30). The cluster analyses indicate that there may be some systematic chemical differences between the three rock types in the Hyperite Formation, especially regarding the trace elements. However, the differences are not very well defined in the dendrograms and are not specified as to which elements are the major discriminators. Besides, no statistical tests are available to evaluate the outcome of the analyses.

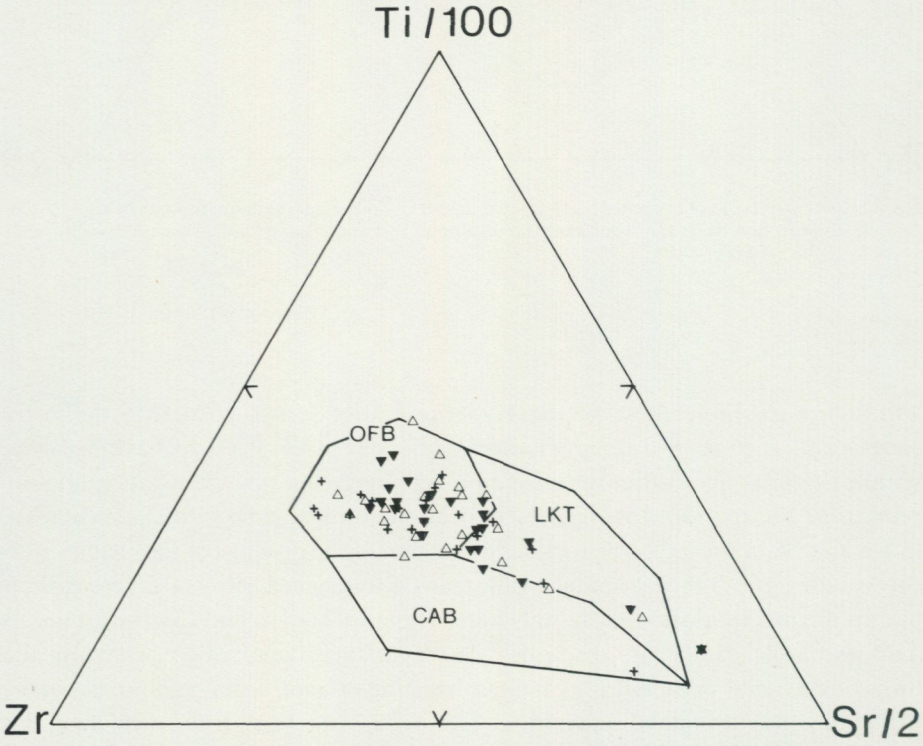

Fig. 38. All three types of Hyperite rocks plotted in the Ti-Zr-Sr diagram (Pearce and Cann, 1973). OFB: ocean-floor basalt; LKT: low-K tholeiite; CAB: calc-alkali basalt. Signatures as in Fig. 33. If anything, the diagram favours an ocean ridge basalt characterization for the gabbroic rocks — 18 out of 26 samples plot in field OFB. The hornblende metagabbros and amphibolites show distributions very similar to that of the gabbroic rocks.

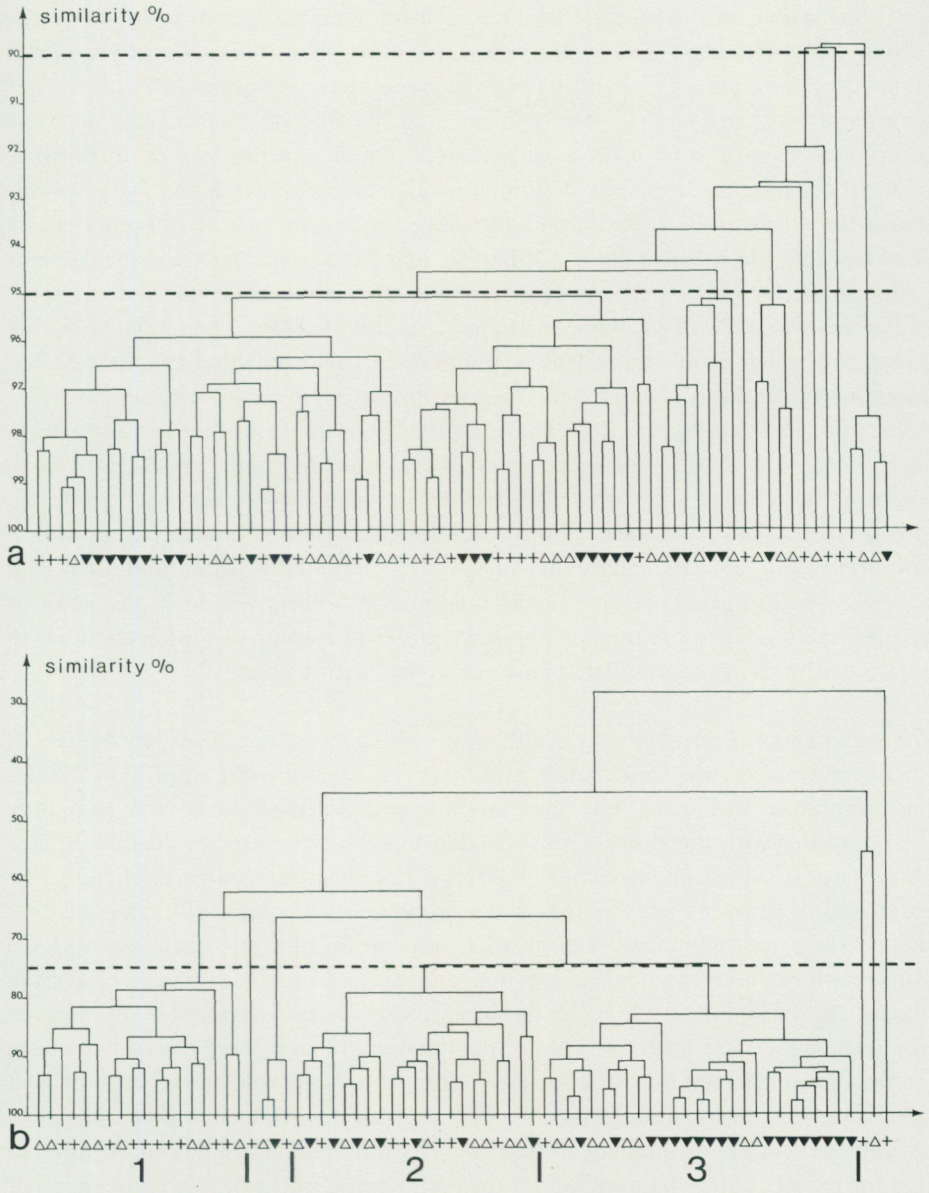

Fig. 39. Dendrograms based on unweighted cluster analysis (Ujiie & Nagasa, 1971) of the chemical composition of the Hyperite rocks, a — major elements, b — trace elements. Signatures as in Fig. 33.

Information on the metasomatic effect of the metamorphic transitions can be obtained by making a geochemical traverse in an exposure where the three rock types occur together. The results of such an analysis are given in Fig. 41. Four samples were analysed — one gabbro, one hornblende metagabbro and two amphibolites — and their compositions were plotted as a function of the distance from the gneiss contact. The diagrams in Fig. 41 suggest that the metamorphic transition from gabbro to amphibolite involves an increase in the contents of Fe_2O_3, K_2O, H_2O, MnO, P_2O_5, Cl, Ba, Zn, and Rb, and a decrease in the contents of CaO, MgO, TiO_2, Sr, Ni and Y. However, the interpretation of these apparent differences is not without complications. It is, for example, not so that a higher element content in the amphibolites automatically indicates that this element has been added to the rock during the metamorphism. (See below and compare, *e.g.*, Gresens, 1967, and Skala, 1979.) Besides, the longer these profiles are, the greater is the risk that the metamorphic effects are compunded with (small) differences existing in the original intrusive rock facies. We have noted before (pp. 52–53, Fig. 40) that marked magmatic differentiation within the Hyperite bodies is not apparent, but smaller magmatic variations could easily occur and therewith interfere with our evaluations of the metasomatic effects which in part may be rather subtle. Therefore, in this paper we prefer to employ two other methods to evaluate the metasomatic effect of the metamorphic transition.

1. *The first method* employs a type of diagram which we will call *fixed pair diagram*. It has been used earlier, for example by Elliott (1972), and Field and Elliott (1974). It is explained in Fig. 42. The data handling and plotting have been done mainly by computer with the aid of a program developed by cand. scient. Morten Sparre Andersen (Greenland Geological Survey). The diagram compares directly the chemical compositions of samples of the Hyperite rock types of the same locality, taken close to each other. In the plots the hornblende metagabbros and the amphibolites have been taken together and plotted on the ordinate, under the name "amphibolitic rock". The gabbroic rocks are on the abcissa. A separate diagram is given for each chemical component analysed. If there is no difference in composition between the amphibolitic rocks and the gabbroic rocks, all points will plot on the 45° slope line dividing the 90° angle of the orthogonal diagram. If the gabbroic rocks have a higher concentration the data points will be concentrated in the lower part of the diagram, and if the amphibolitic rocks have a higher content the data points will be concentrated in the upper part of the diagram.

However, many of the plots so produced (Fig. 43, p. 61 ff, the left hand diagrams marked with "a") are not very conclusive. The difference in point configuration and point density on both sides of the division line are too subtle to be evaluated by more visual inspection. A more rational way of deciding the differences is called for. Following suggestions by Zeck and Kalsbeek (1981) certain statistical tests can be applied to the diagrams (see Fig. 42). In the testing applied here the

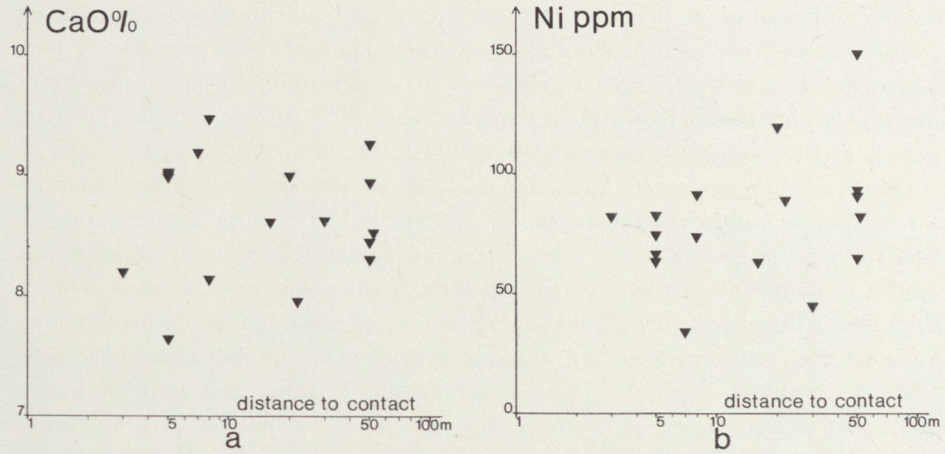

Fig. 40. Diagrams illustrating the areal distribution of CaO (a) and Ni (b) contents of gabbroic rocks within Hyperite bodies. The CaO and Ni contents of 17 samples of gabbroic rocks from different localities in different Hyperite bodies are plotted as a function of the distance to the contact with the surrounding quartzo-feldspathic rocks. No correlation is apparent in the two diagrams.

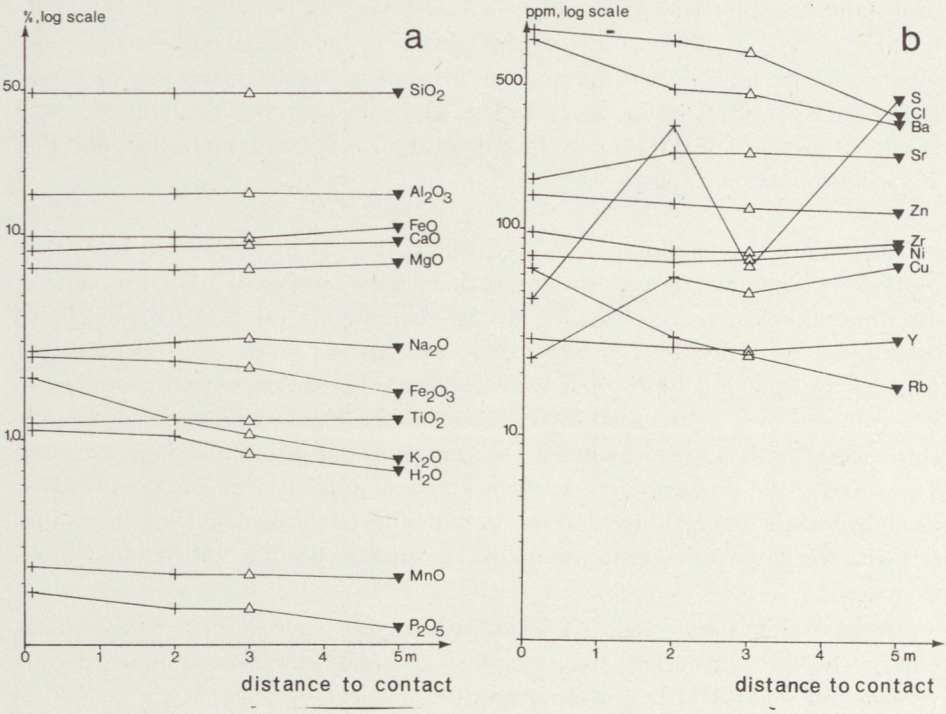

Fig. 41. Major element (a) and trace element (b) contents in a series of four samples from a sample traverse across a Hyperite/gneiss contact. The chemical composition of the samples have been plotted against the distance from the contact. Signatures as in Fig. 33.

distance of each point (locality) to the 1:1 dividing line is measured and given a positive or negative sign depending on whether it lies over or under the 1:1 line. The row of figures so obtained is then tested for significant bias of either positive or negative values by the t-test (Haber and Runyon, 1973, p. 255) and the Wilcoxon matched-pairs signed-rank test (*op. cit.*, p. 302).

However, if the tests were applied in this way, we would not allow for the closed array character of the chemical components. The influence of this internal correlation factor is best explained by considering an element migration in which, say, 2 weight % of a single element is removed without any compensating influx of other elements. This means that all the other elements present, majors and traces, will increase their concentration by a factor 100/98. This implies that differences observed between the two data samples might be caused not only by active migration of the elements involved, but also by these passive, arithmetically induced changes. This problem can be overcome by relating the element contents to a component (or set of components) remaining immobile during the process studied. (See, *e.g.*, Gresens, 1967, and Pearce, 1968, for a full discussion of this topic.) This leads to employing a new set of diagrams figuring element ratios in which the denominator is an immobile element (oxide). In the present paper we have chosen MgO as such an immobile component. MgO plots comparing gabbroic and amphibolitic rocks (Fig. 43,8 and Fig. 45,7) indicate its immobile behaviour. The X/MgO — FeO*/MgO plots (to be introduced below) for elements such as Ti, P, Y and Zr confirm this conclusion. The fixed pair diagrams based on X/MgO ratios are given in Fig. 43, in the right hand column (b). The results of the statistical testing in these diagrams as explained above (see also Fig. 42) will be found in Table 6.

2. *The second method* employs FeO*/MgO diagrams. The three Hyperite rock types plotted in these diagrams, one for each element analysed, have overlapping distribution fields, as seen from Fig. 45, left hand figures (a). As for the fixed pair diagrams, the differences between these plot patterns can only be evaluated properly by applying appropriate statistical tests. The differences are too subtle to be evaluated by a mere visual inspection of the FeO*/MgO diagrams or a crude comparison of average element (oxide) concentration values and their standard deviations. Note that also here, in the evaluation of the diagrams that will follow, the hornblende metagabbros and the amphibolites are pooled and will be compared with the gabbroic rocks as a combined group which will be called "amphibolitic rocks".

The statistical significance of the small differences between the two populations can be checked obviously by means of the t-test and the Wilcoxon matched-pairs signed-rank test (Haber and Runyon, 1973) *directly* applied to the analytical results. However, as was the case for the fixed pair diagrams explained above, the interpretation of the results of such tests on the raw analytical data is not without

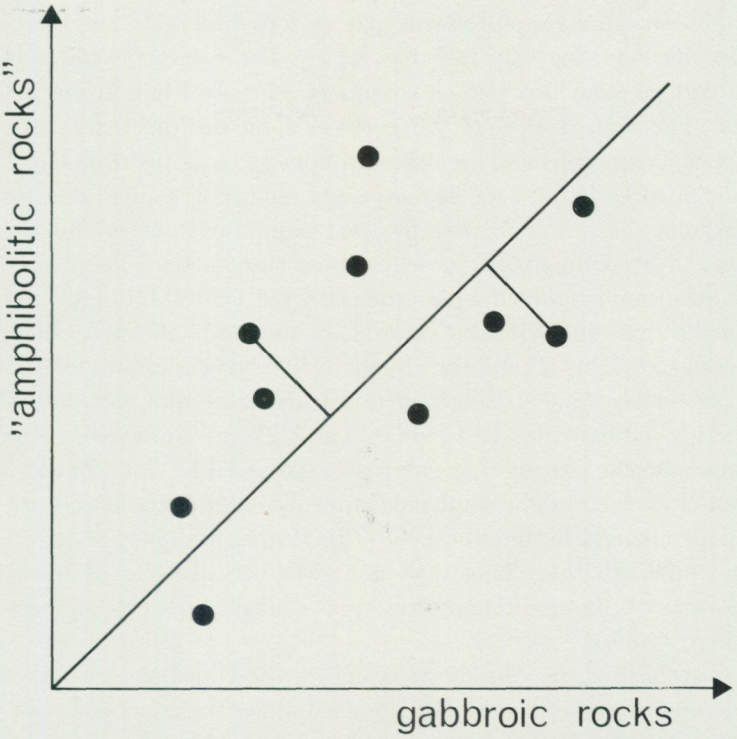

Fig. 42. Fixed pair diagram explained. For each element analysed a separate diagram will be given. Each point represents a locality where one or a few samples of "amphibolitic rock" (comprising both hornblende metagabbro and amphibolite) and gabbroic rock have been taken. The element (oxide) content of the gabbroic rock (in the case of two or more samples their average value) is given on the abcissa, and the content of the amphibolitic rock (or the average value, if more than one sample) on the ordinate. In case there is no difference between the gabbroic rock value and the amphibolitic rock value, the point for the location will plot on the 45° line dividing the 90° angle of the orthogonal diagram. If the concentration in the amphibolitic rock(s) is higher the points will plot above that line, and *vice versa*. To allow for a statistical evaluation of the plot pattern, residual values for each point (locality) *vis-a-vis* the 45° slope line have been computed (see text for further explanation).

complications. Two problem are to be considered. The first is explained in Fig. 44 a, illustrating a statistically significant difference between the two populations (ordinate values only) which needs not reflect the metamorphic effect, the aim of our study, but might be due merely to a difference in degree and range of magmatic differentiation between the gabbroic rocks and the actual gabbroic progenitors of the amphibolitic rocks. In order to reduce this effect we have collected our samples of gabbroic and amphibolitic rocks as close to each other as the degree of exposure permitted, but our procedure might not have been entirely successful. The second problem is explained in Fig. 44 b which shows a real difference between the two populations, but it will possibly be labelled as non-significant by the tests applied.

Both these interpretation problems may be solved by performing the statistical testing in the following way (see Fig. 44 c). The magmatic variation of each element/oxide is modelled by a least square regression line in the FeO*/MgO diagrams. The statistical tests are performed on the differences between the measured concentrations and the concentrations given by the regression line. Two conditions must be fulfilled for this improved method of statistical testing to give proper results. The first is that the magmatic variation in the FeO*/MgO diagrams can be reasonably represented by a straight line. The diagrams show that this condition is fulfilled within the restricted FeO*/MgO range considered. The second is that the FeO*/MgO ratio is not affected by the metasomatic process here investigated. This is confirmed by the FeO*/MgO diagrams for TiO_2, MgO, Zr and Ni, which show strikingly identical magmatic and metamorphic trends interpreted to indicate that TiO_2, FeO*, MgO, Zr and Ni have not been affected by the metamorphic process. The alternative is that TiO_2, MgO, Zr and Ni should have been influenced by the same type of metasomatism, simultaneously causing metasomatic changes in the ratio FeO*/MgO, so as to duplicate the effect of the magmatic differentiation. That does not seem very feasible. If it nevertheless would be realized, the resulting metamorphic changes would go undetected by the method here outlined.

A final problem to be considered is that of the closed array character of the chemical composition of a rock. As explained above in connection with the fixed pair diagrams, we will remedy this problem by working with element ratios. In agreement with arguments given above we selected MgO as divisor, which resulted in a series of X/MgO–FeO*/MgO diagrams, one for each element analysed, as shown in Fig. 45, right hand figures (b). The results of the statistical testing are given in Table 6.

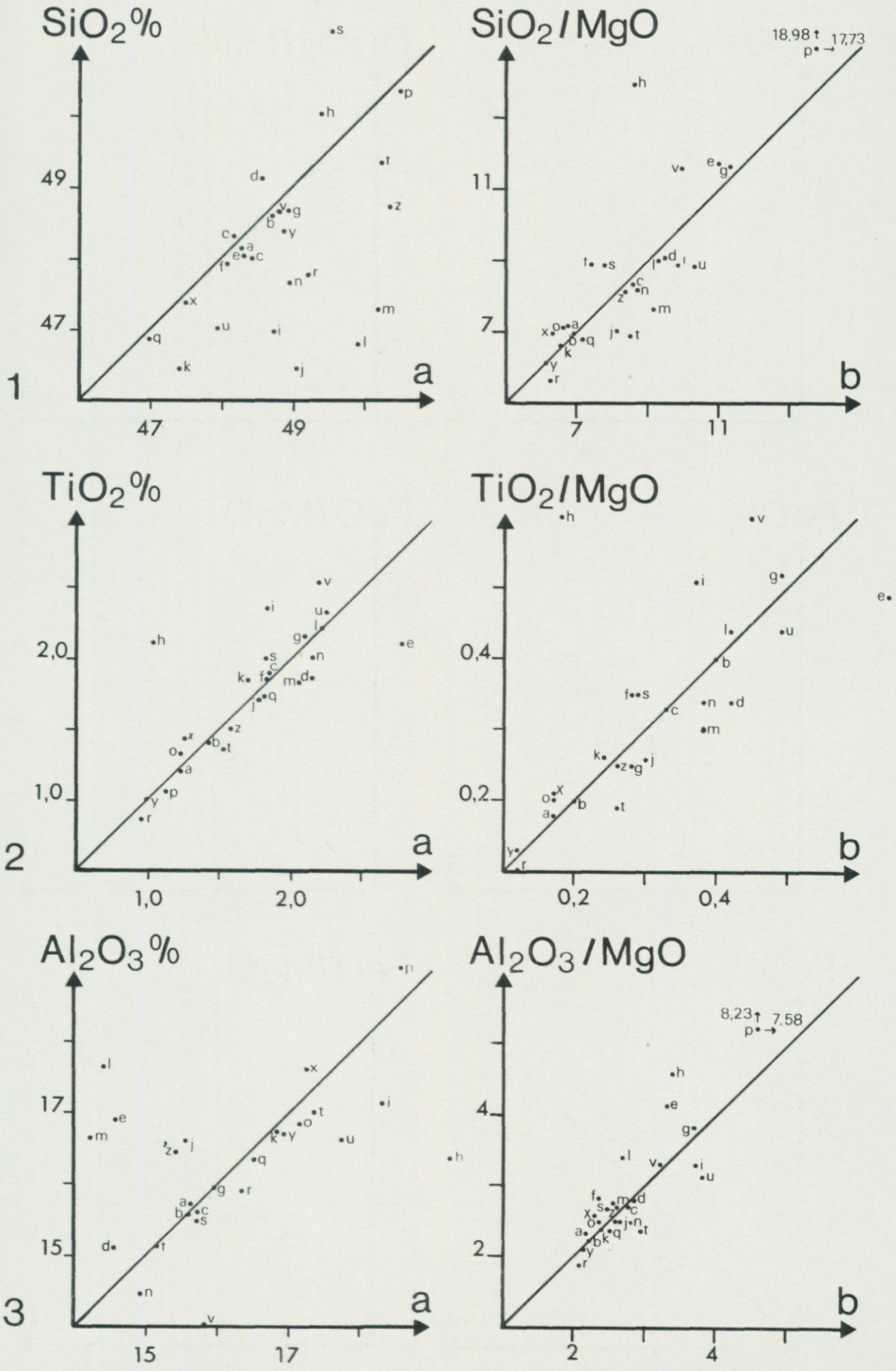

Fig. 43. Fixed pair diagrams as explained in Fig. 42. For each element (oxide) two diagrams are given: one for the direct analytical results (a) and one for the analytical values divided by MgO (b). 25 localities have been sampled. Each locality can be identified in the diagrams by a letter. Nos. 26 a, b differ slightly from the orthers, figuring K/Rb and Mg/Ni, respectively. The 25 localities are given on p. 69.

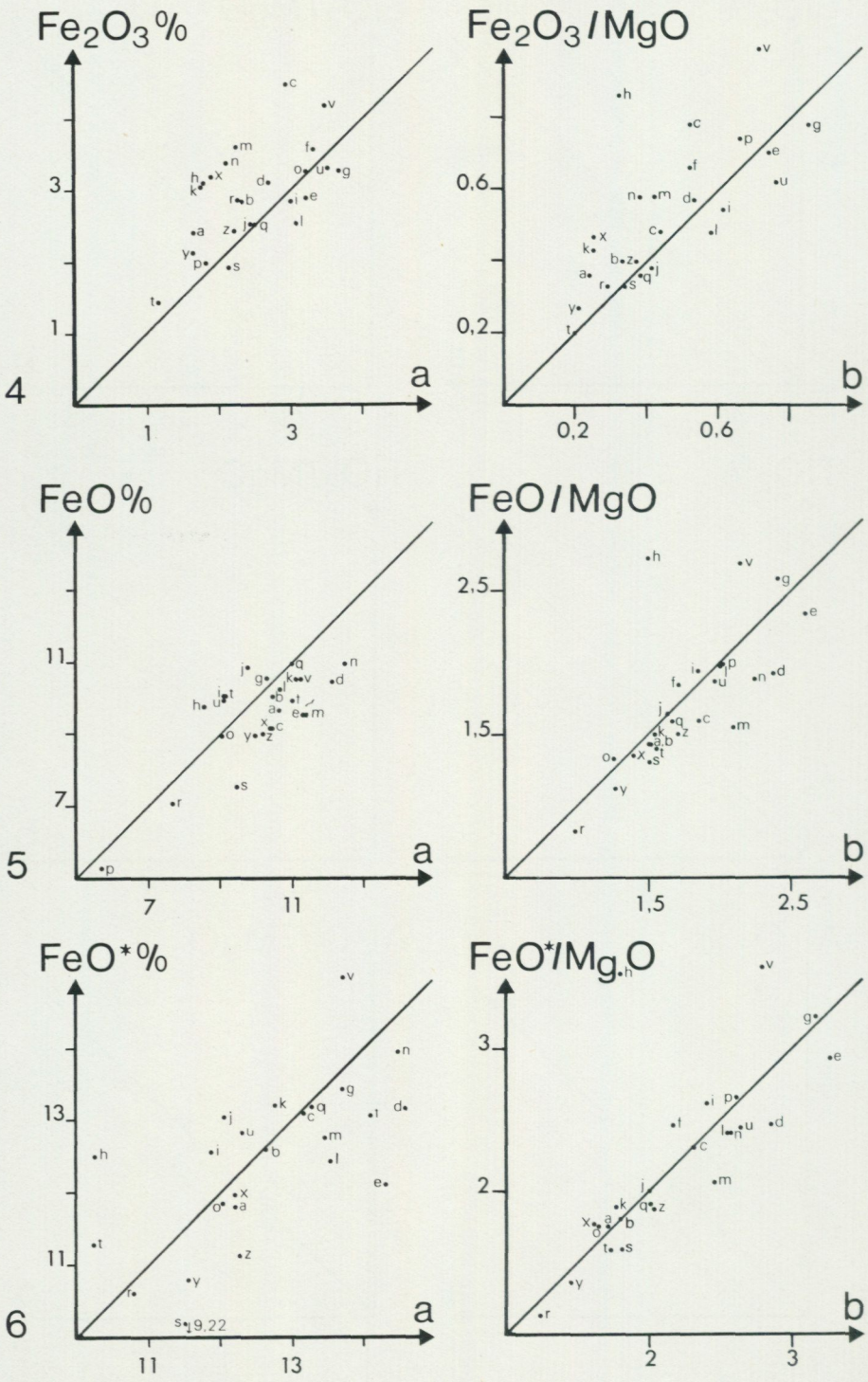

Fig. 43, continued.

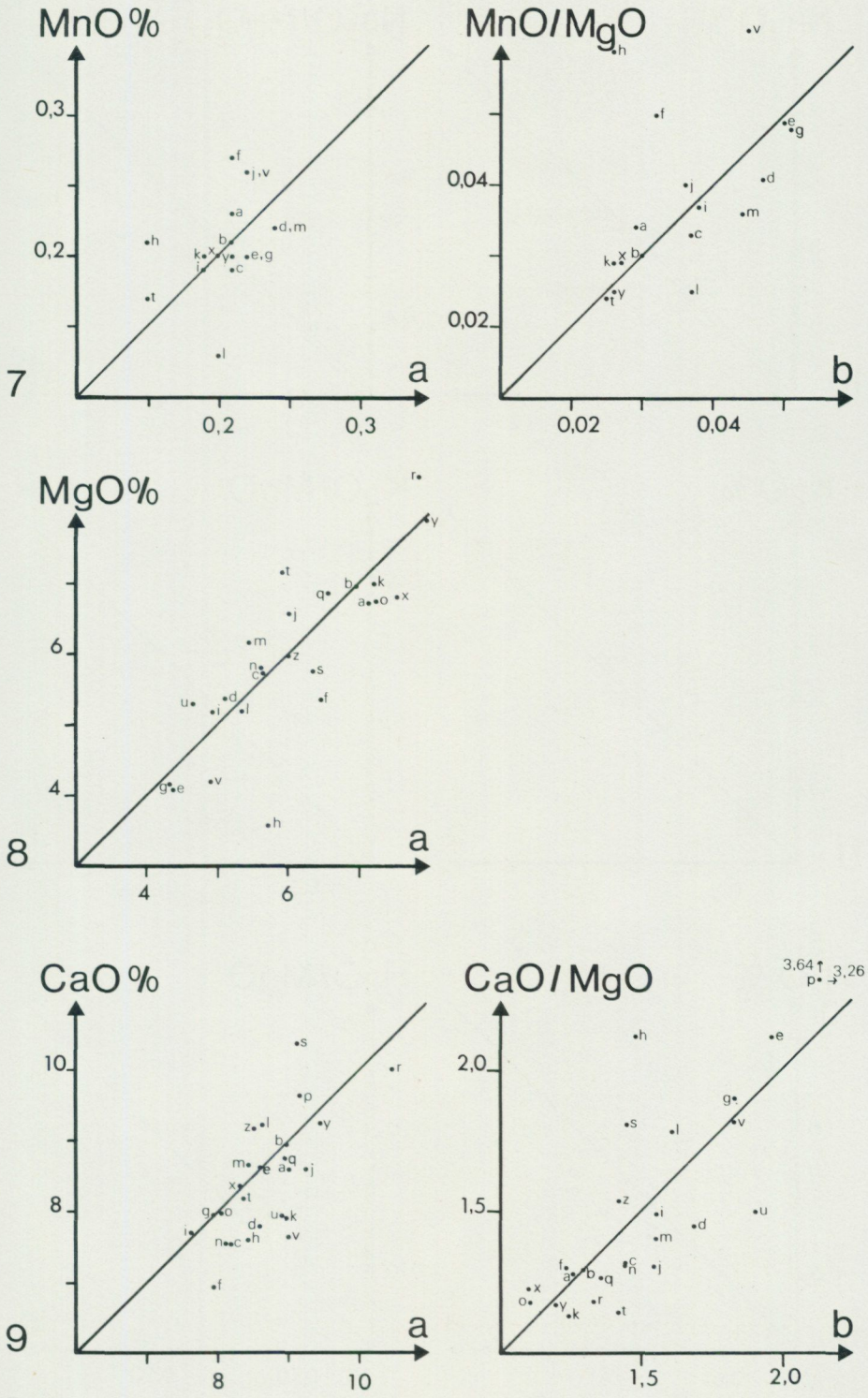

Fig. 43, continued.

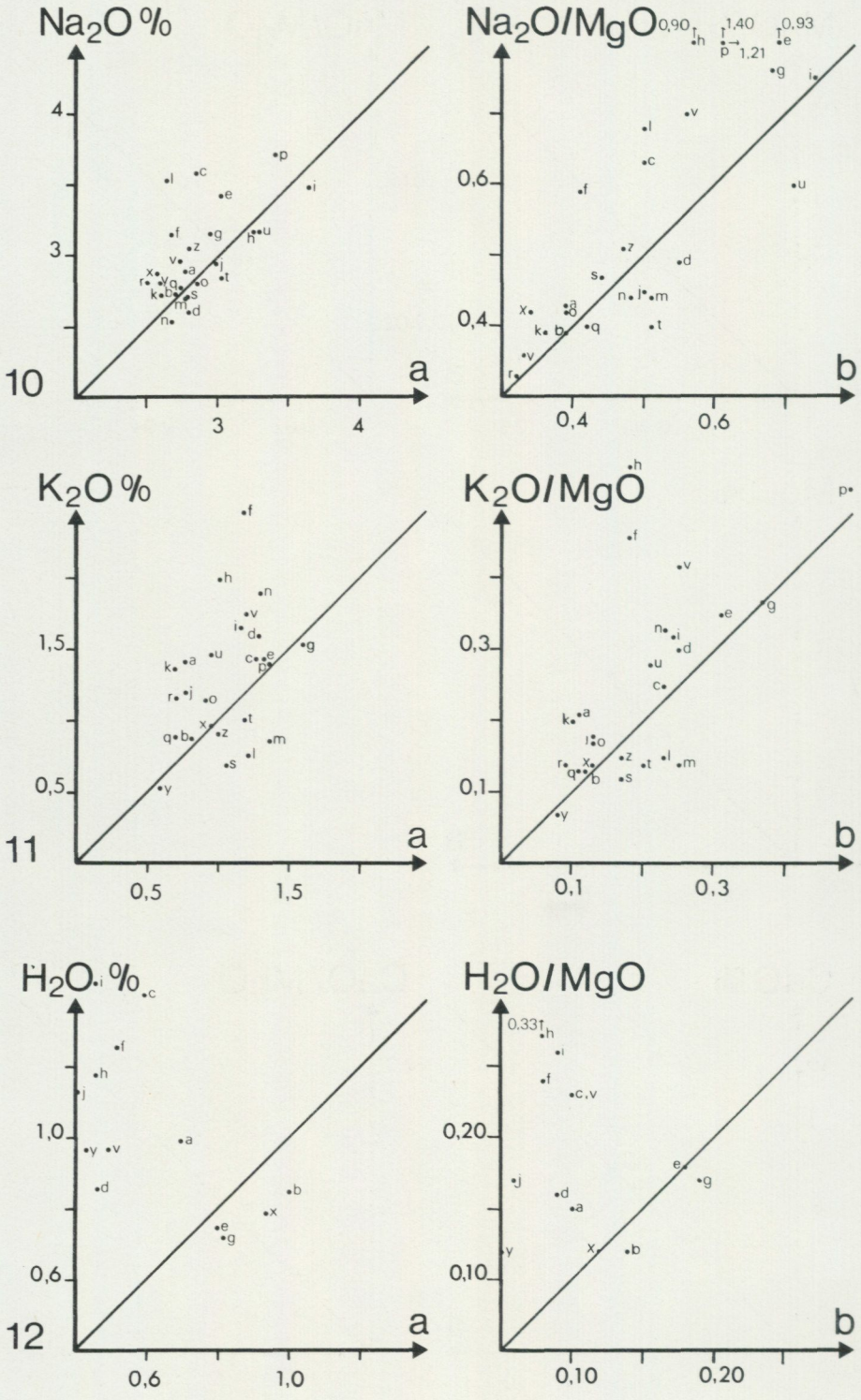

Fig. 43, continued.

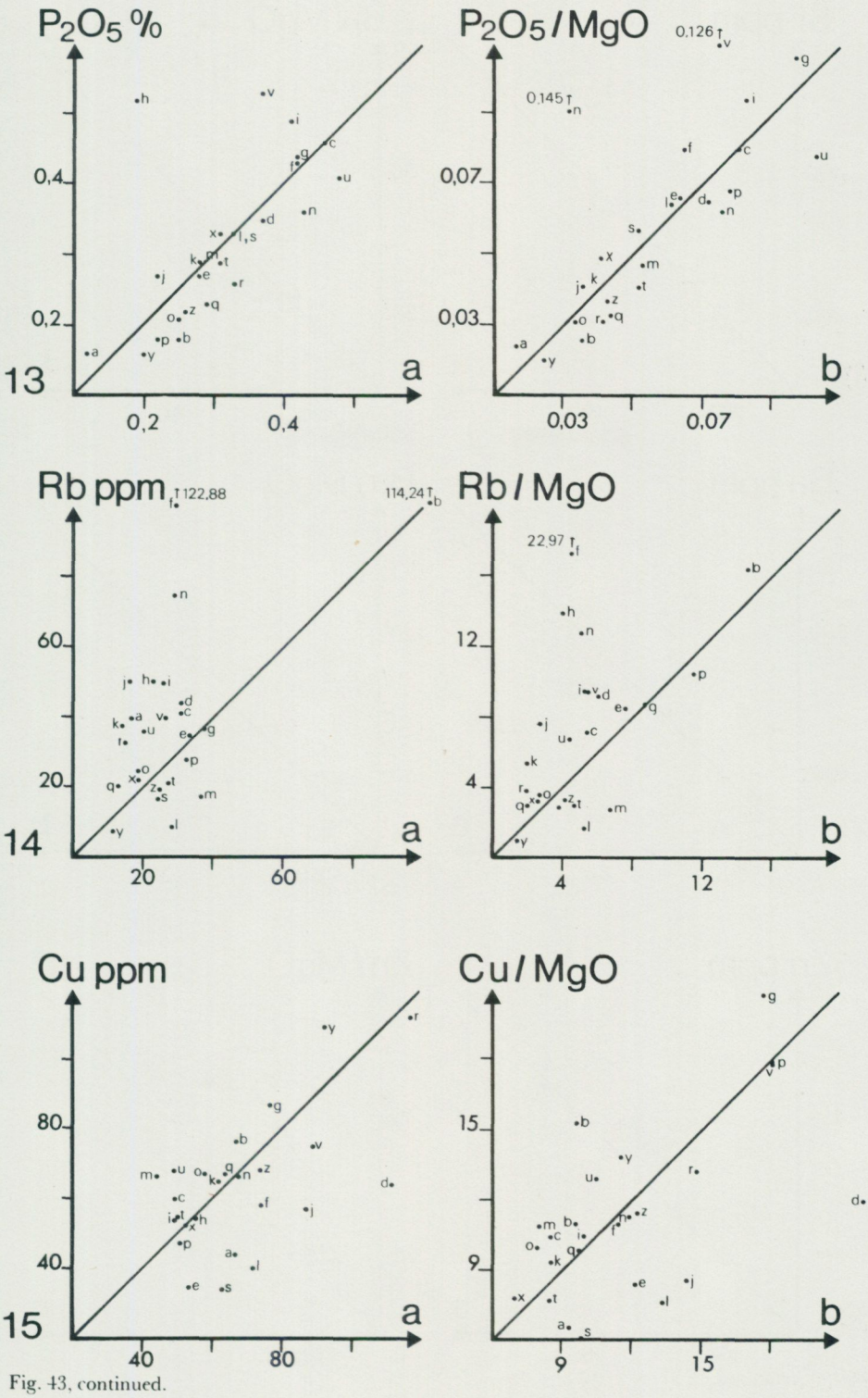

Fig. 43, continued.

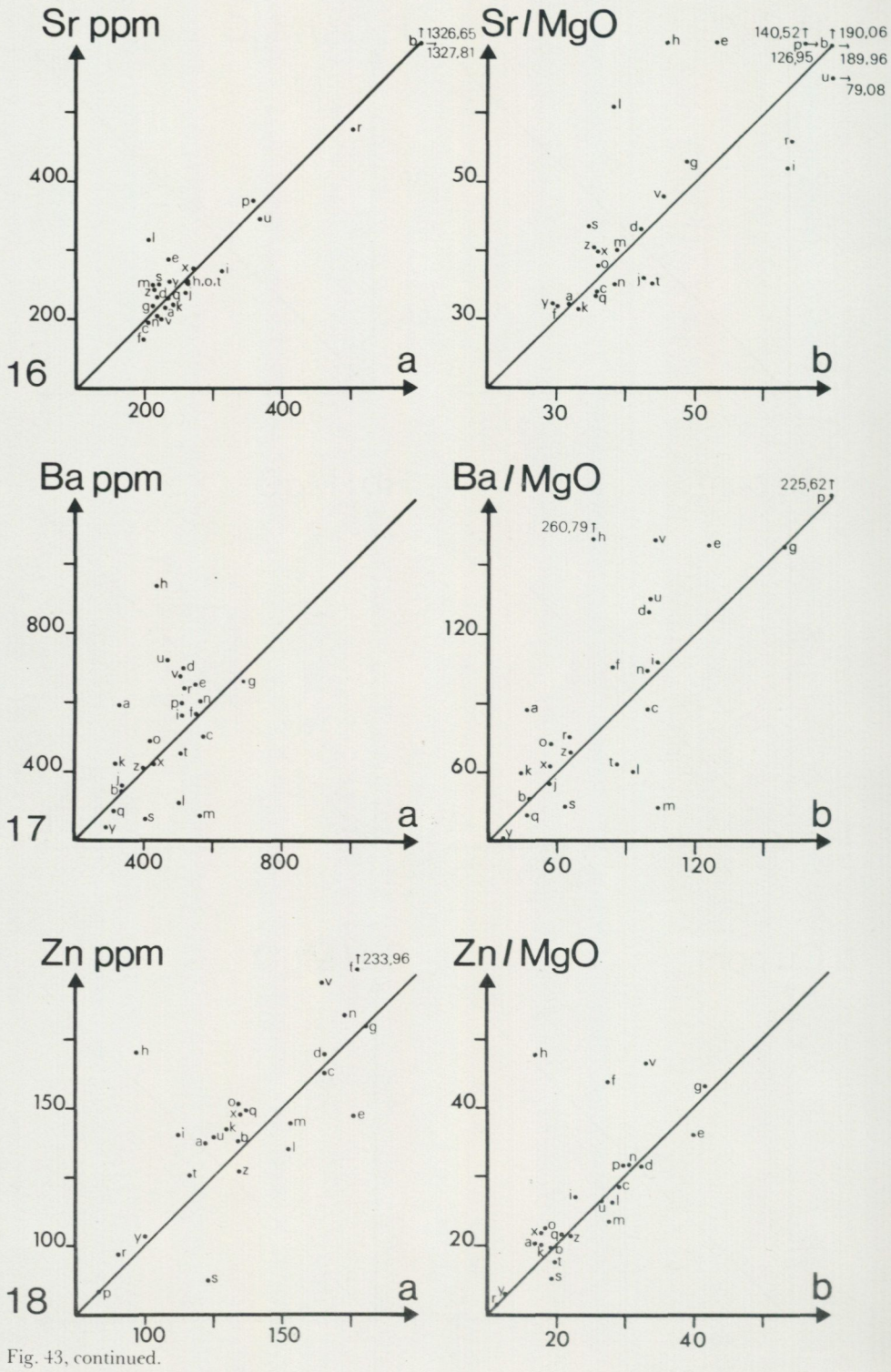

Fig. 43, continued.

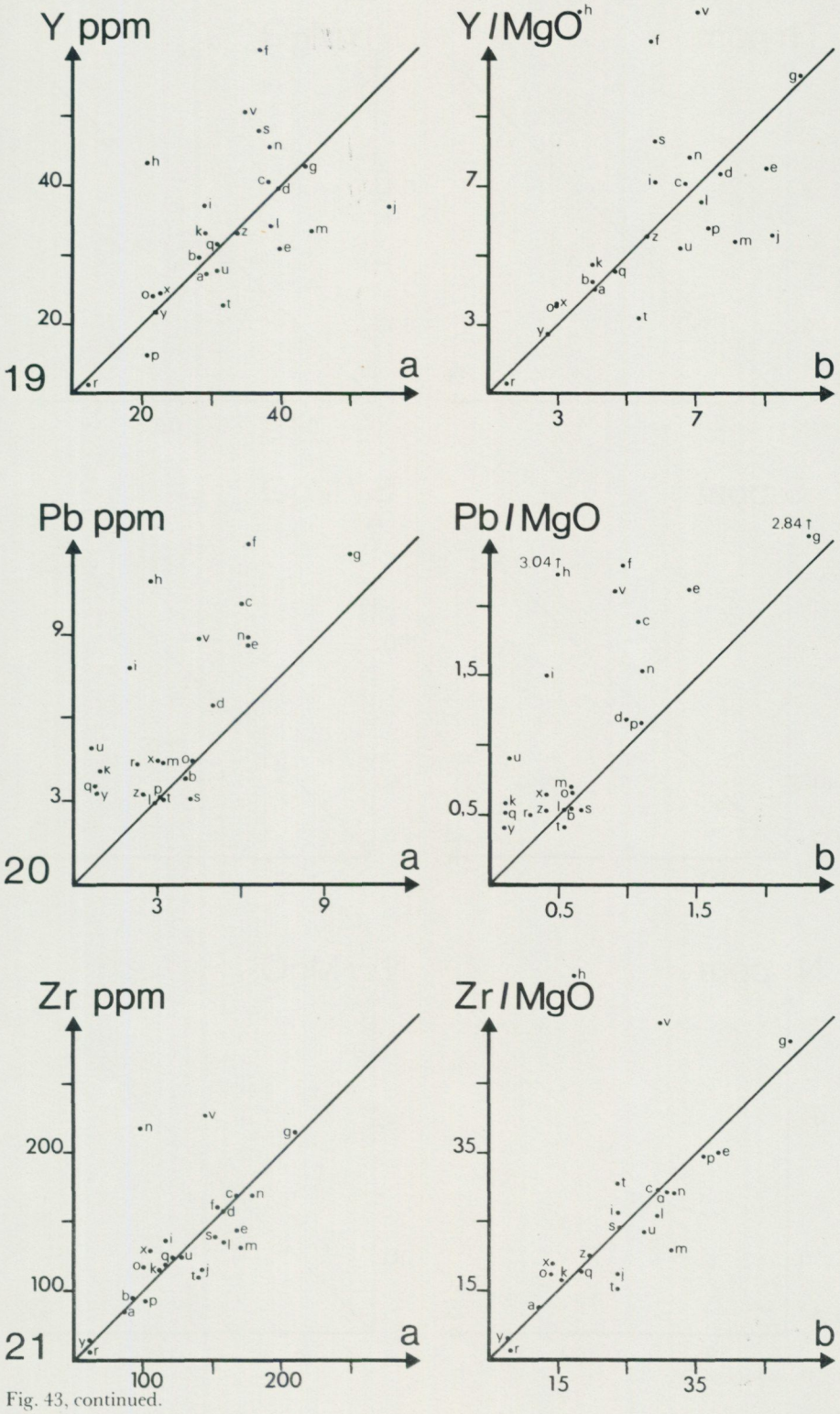

Fig. 43, continued.

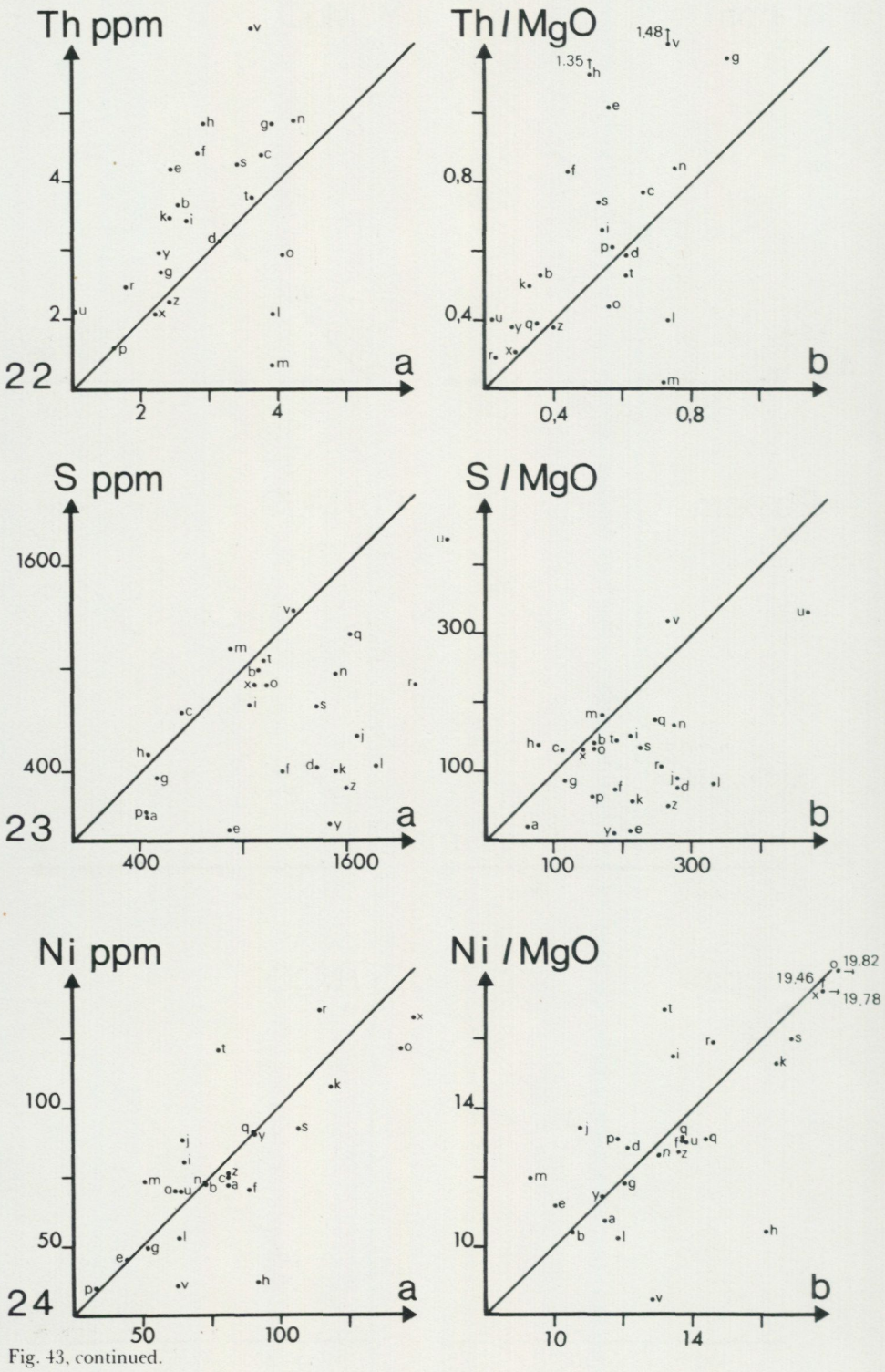

Fig. 43, continued.

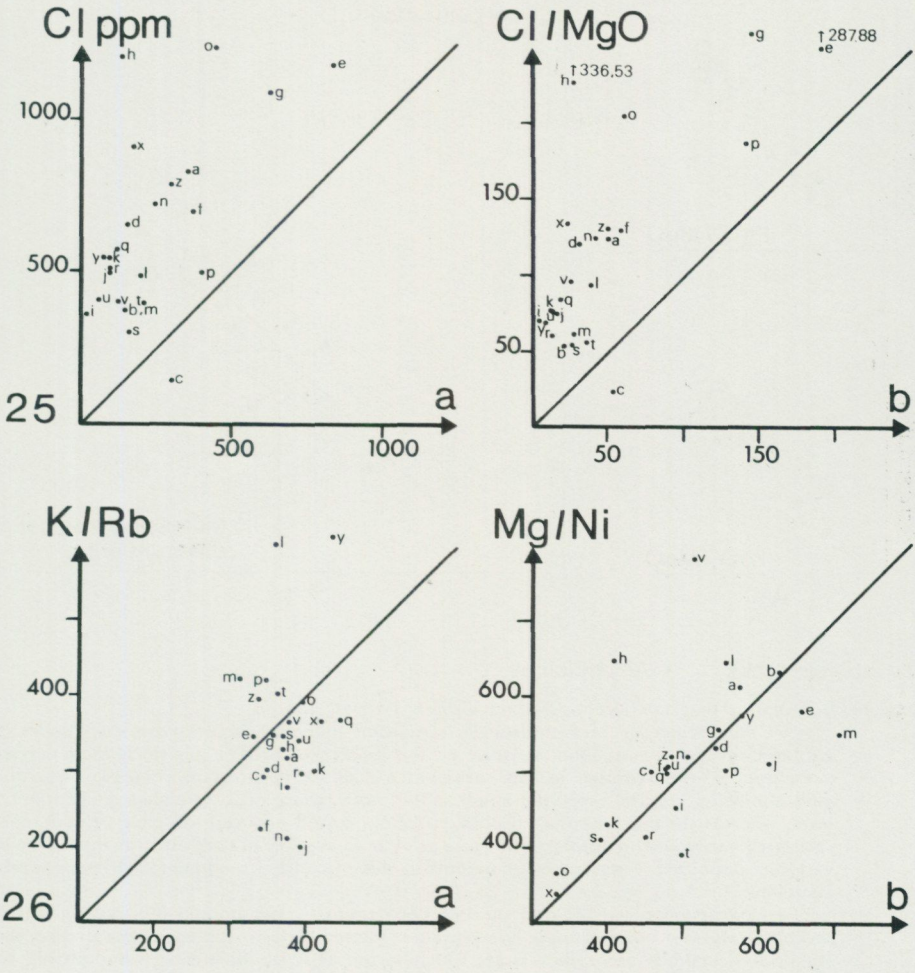

a. Brattåshöjden.
b. Brattåshöjden.
c. Haghöjden.
d. Haghöjden.
e. Träfors.
f. Haghöjden.
g. Träfors.
h. Träfors.
i. Hösenudden.
j. Ölme station.
k. Buckåsen.
l. Ölme station.
m. Ölme station.
n. Norra Hult.
o. Tållerud.
p. N Hållerud.
q. Ölme station.
r. Ö Fågelvik.
s. Kummelön.
t. Bråten.
u. Hösenudden.
v. Haghöjden (S of E 18).
x. Sjöstad.
y. Brattåshöjden.
z. Högeberg.

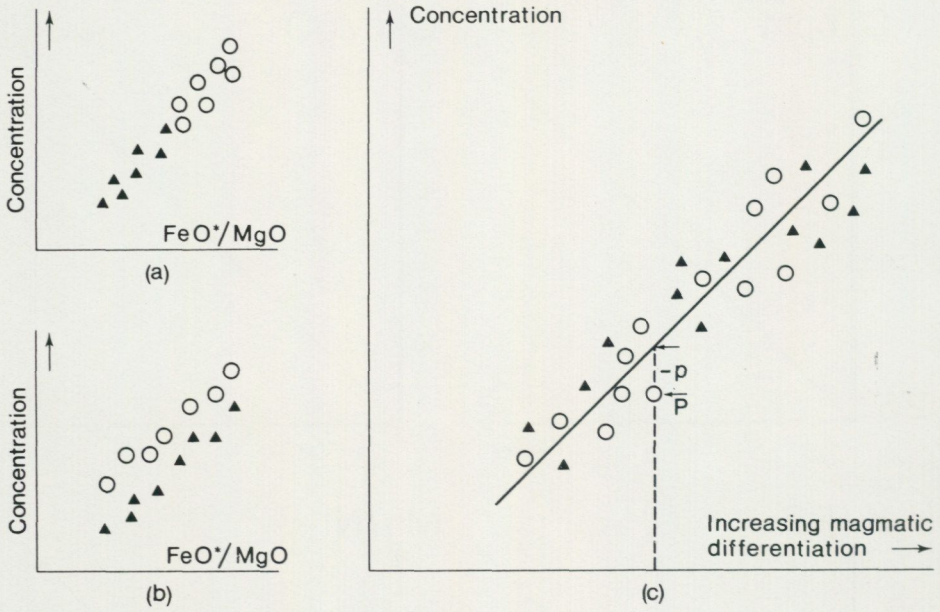

Fig. 44. Schematical diagram (after Zeck and Kalsbeek, 1981) illustrating

a — the occurrence of a statistically significant difference between two rock series of gabbroic rocks and amphibolites. However, this difference might be due solely to an overrepresentation — maximized in this cartoon-like diagram to stress its principle — in the gabbroic rocks (circles) *versus* the amphibolitic rocks (triangles) of a higher differentiation level, whereas the metamorphic effect might be non-significant. Our sampling procedure — collecting gabbroic and amphibolitic rocks as close as possible to each other as the degree of exposure permitted — was aimed at minimizing this effect, but it might not have been entirely successful.

b — a real difference between the two populations — the amphibolites having higher ordinate values — but due to the large variation caused by the magmatic differentiation, the standard deviations are rather large, which means that the difference will probably be classified as non-significant when the tests are applied directly on the analytical results (the ordinate values in the diagram).

c — the method employed here for the statistical evaluation of the difference between the sample population of the gabbroic rocks and that of the amphibolites. Each data point (P) is compared with the regression line modelling the magmatic evolution, and the differences thus found (-p) are compared statistically.

Fig. 45. A series of X–FeO*/MgO diagrams (left hand figures, a) and X/MgO–FeO*/MgO diagrams (right hand figures, b). Symbols: □ = gabbroic rocks, × = hornblende metagabbros, + = amphibolites.

The four samples ringed in the diagrams 1 b, 2 a, 3 a, 3 b, 5 a, 7, 8 b, 9 b, 15 b, 18 a, 20 a and 23 a come from the contact zone of the Hyperite body at Träfors (norra Hållerud). This contact zone consists of anorthosite-gabbro (gravitationally) enriched in large plagioclase crystals (see p. 39). These four samples are not included in the statistical evaluation of the plots.

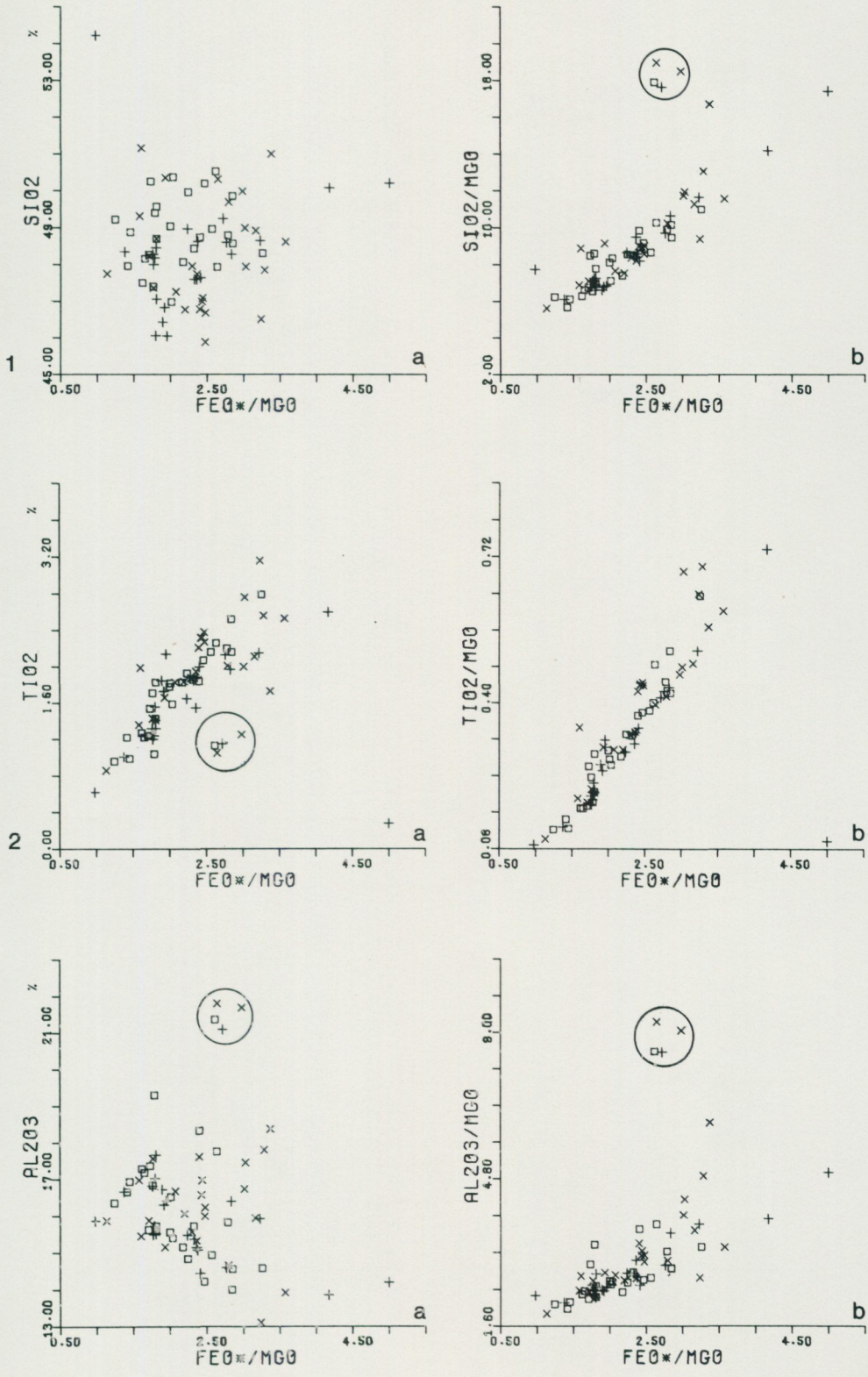
1
SI02
%
53.00
49.00
45.00
0.50
2.50
4.50
FE0*/MG0
a
SI02/MG0
18.00
10.00
2.00
b
2
TI02
3.20
1.60
0.00
TI02/MG0
0.72
0.40
0.08
AL203
21.00
17.00
13.00
AL203/MG0
8.00
4.80
1.60

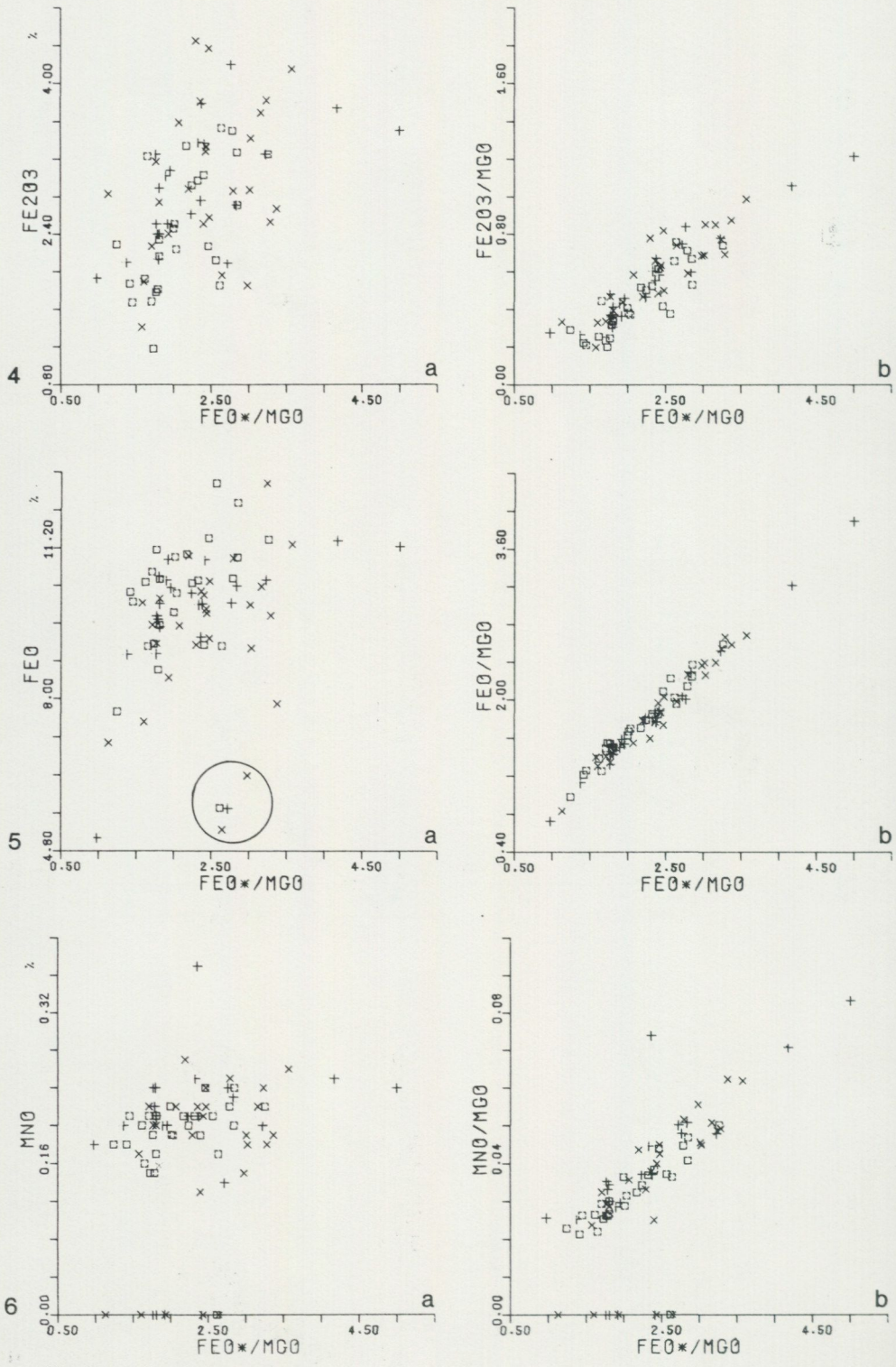

Fig. 45, continued.

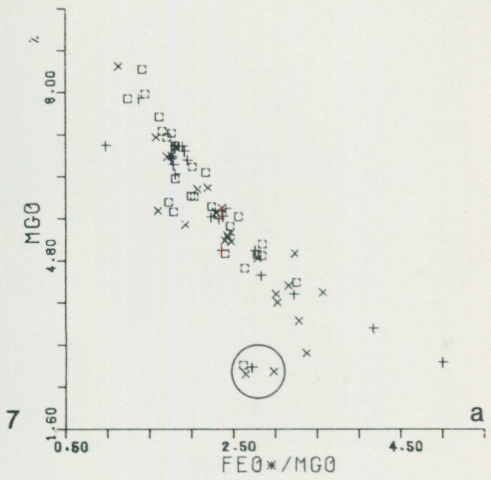

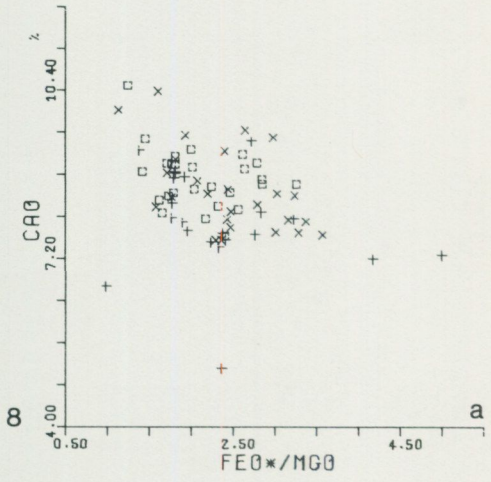

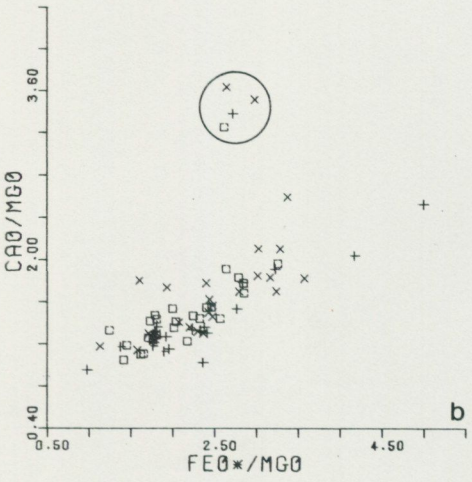

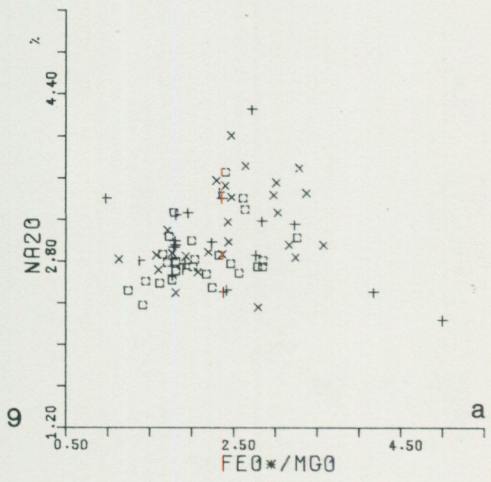

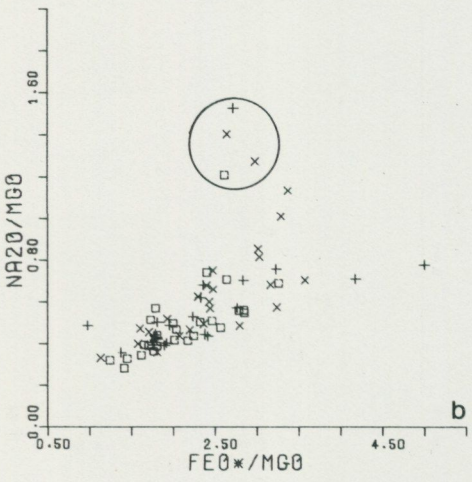

Fig. 45, continued.

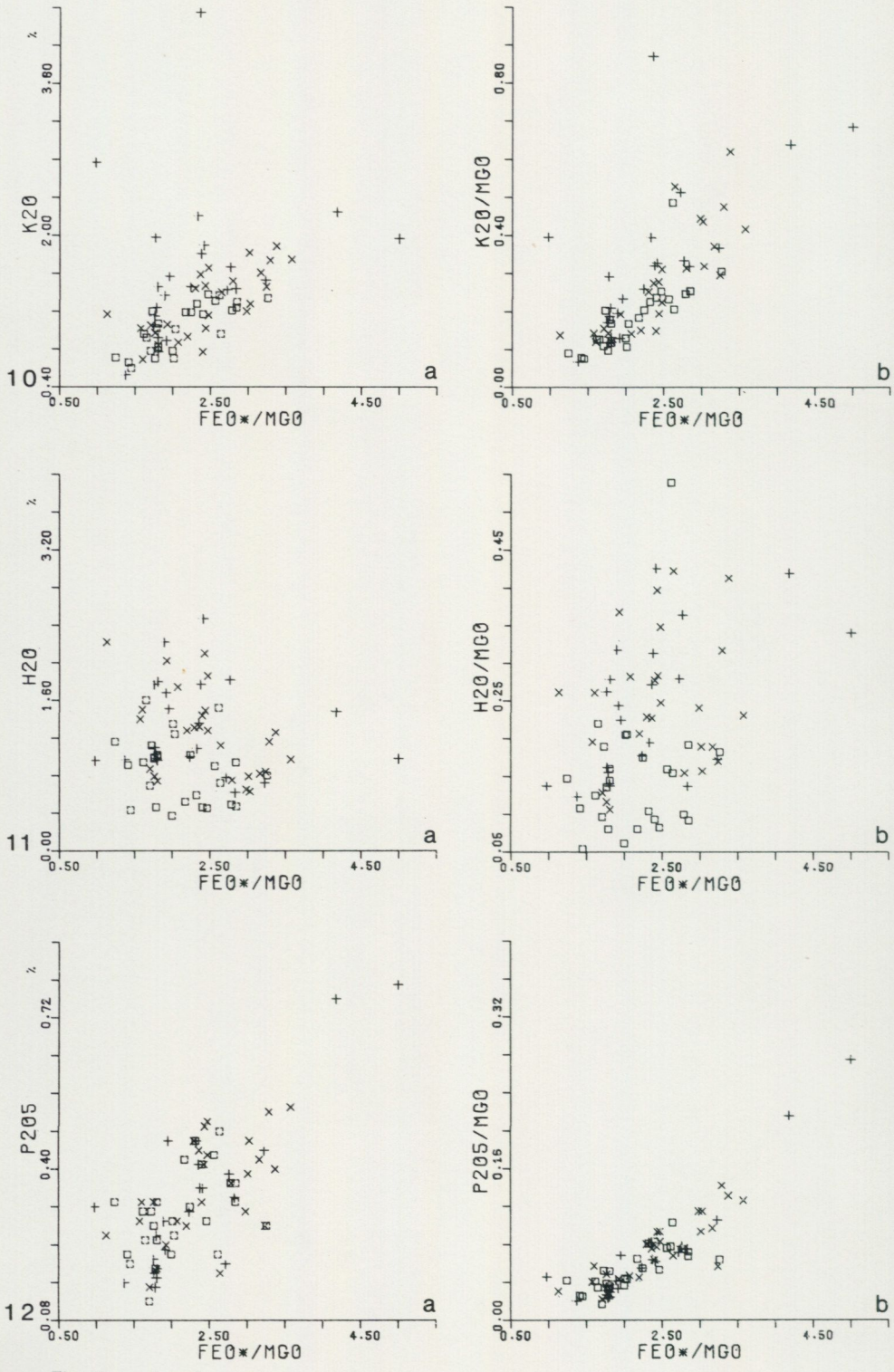

Fig. 45, continued.

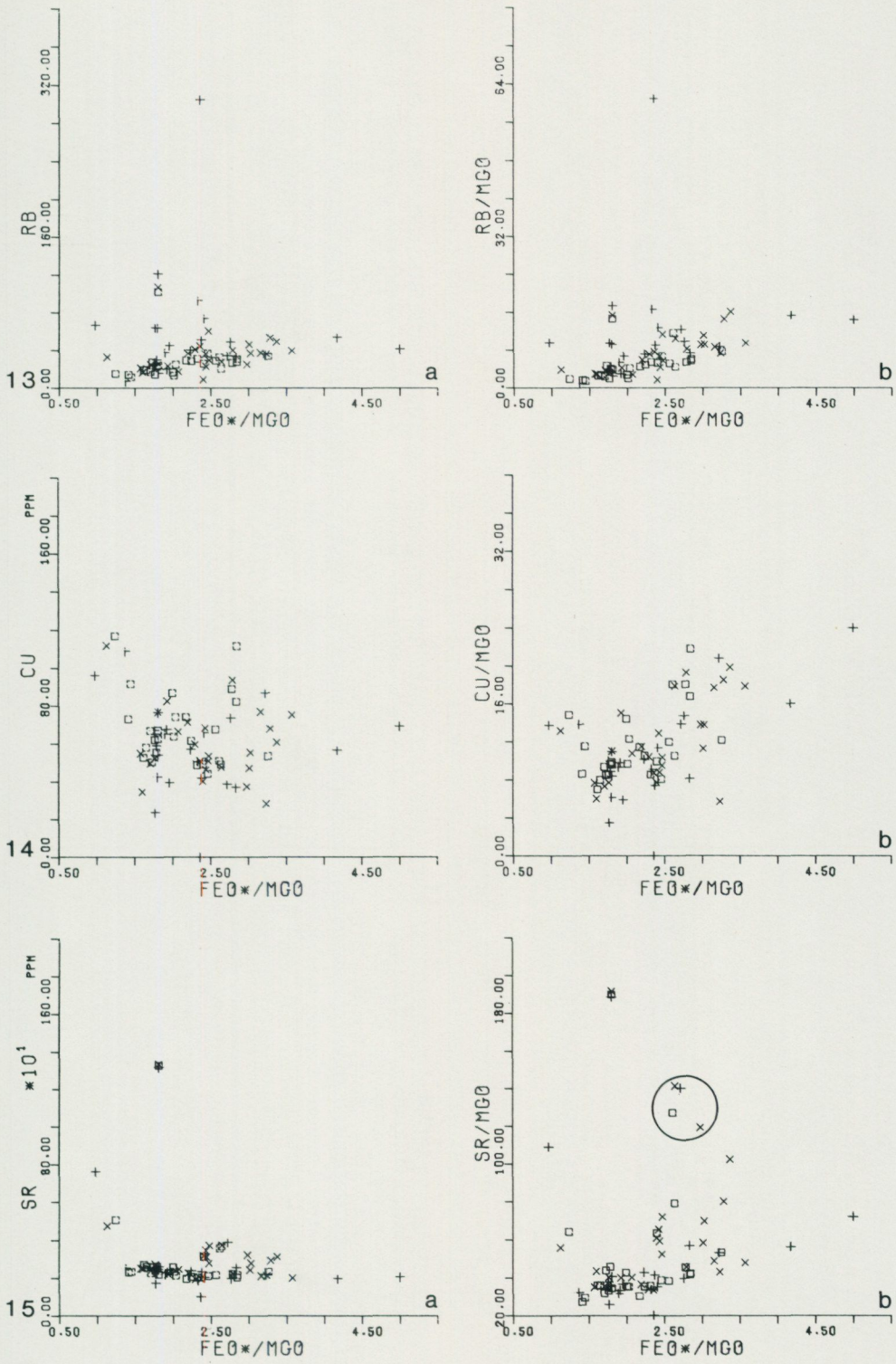

Fig. 45, continued.

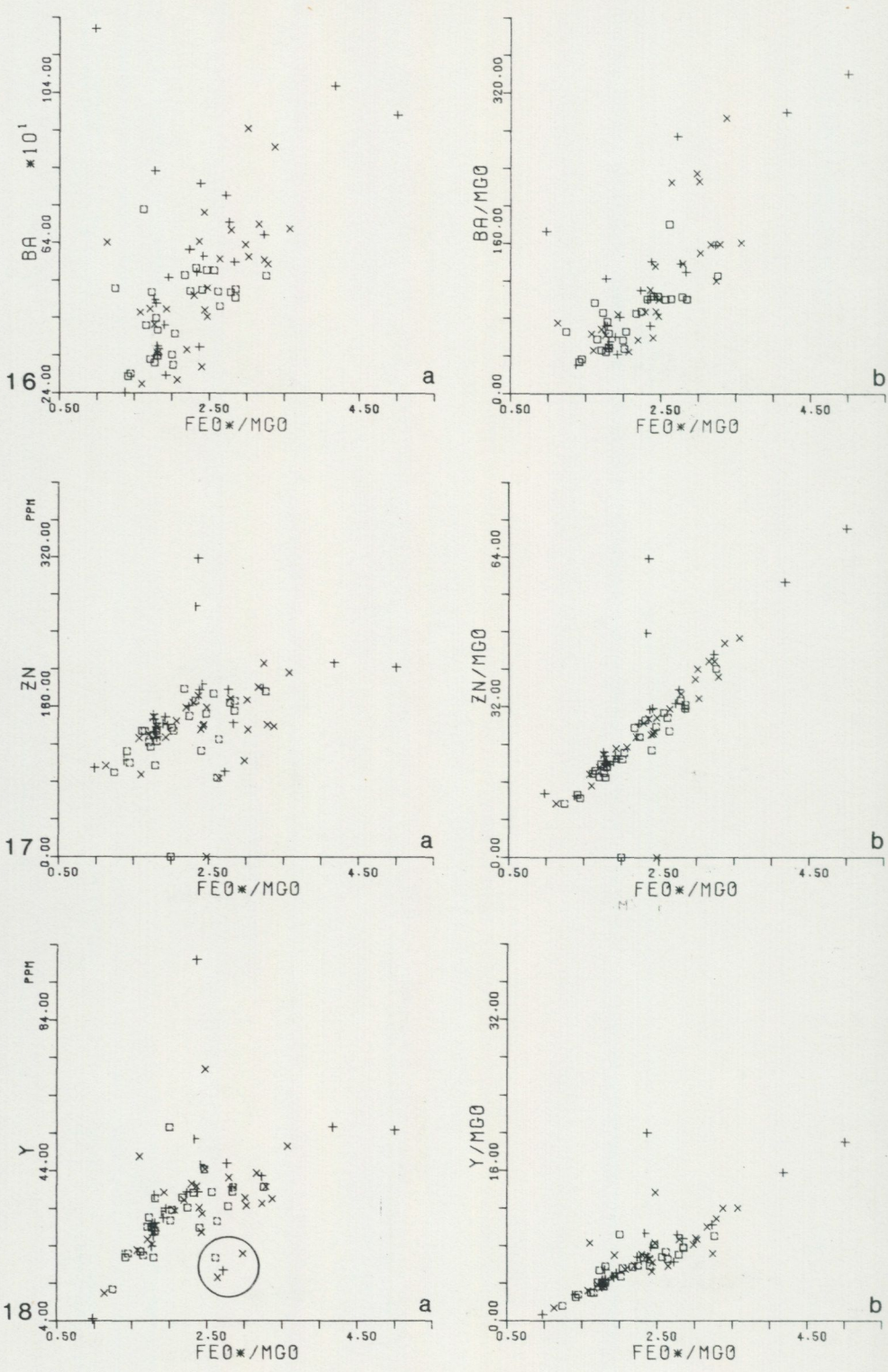

Fig. 45, continued.

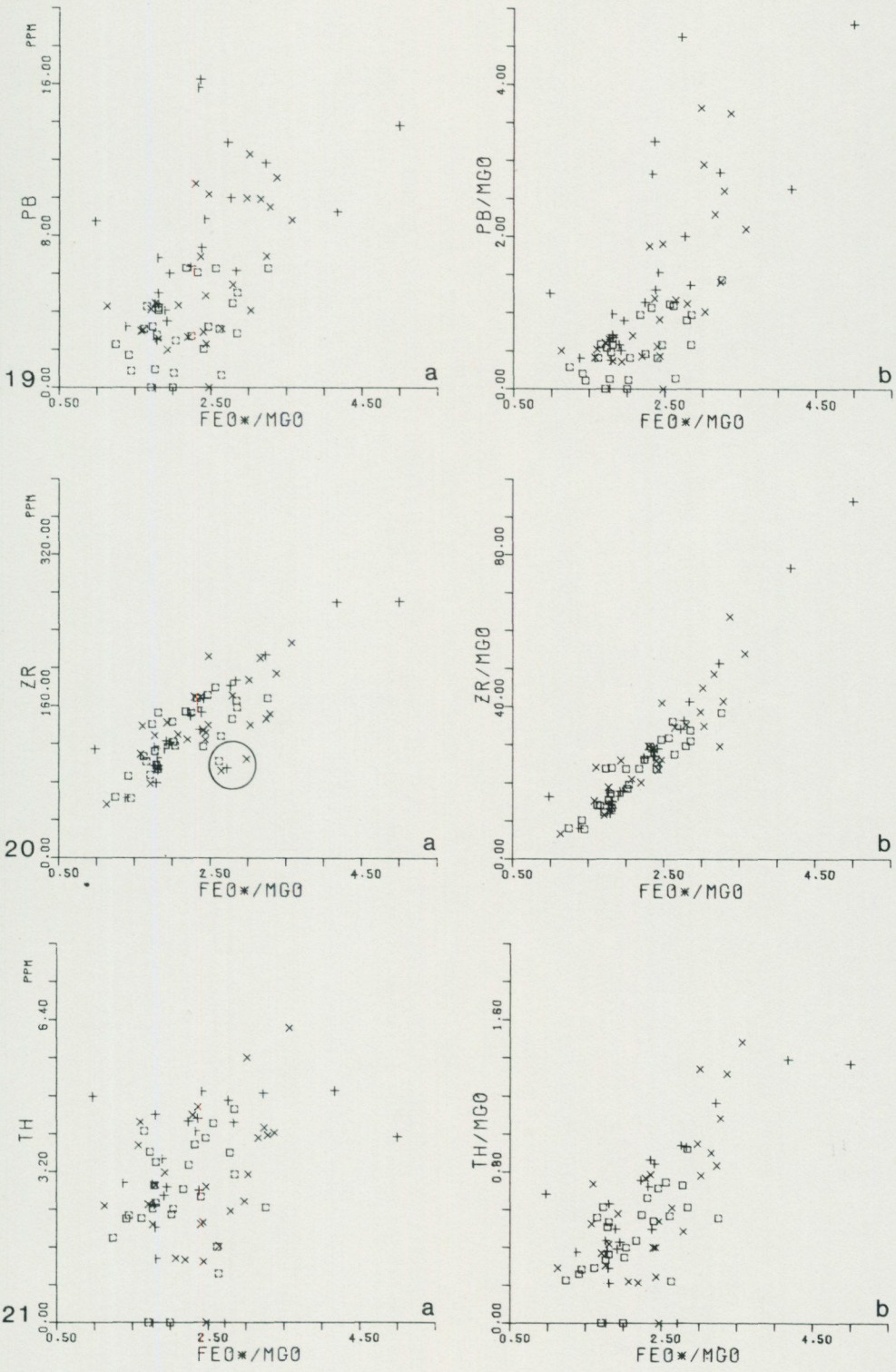

Fig. 45, continued.

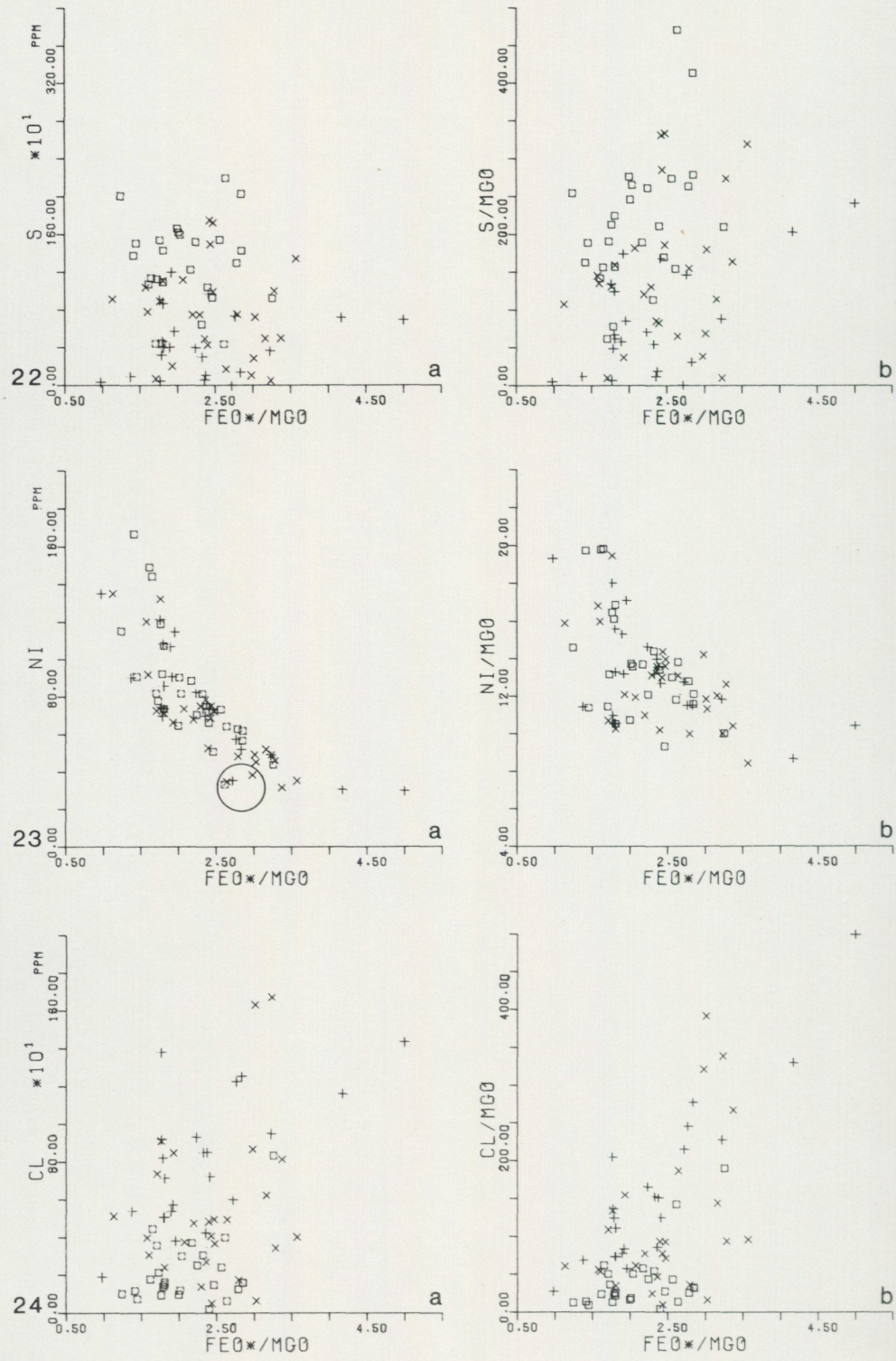

Fig. 45, continued.

DISCUSSION OF THE METASOMATIC EFFECT OF THE METAMORPHISM

The results of the statistical evaluation of the metasomatic effect of the metamorphic transition given in Table 6 will be supplied with some short comments for each component.

SiO_2 (Figs. 43:1 and 45:1). The statistical tests fail to indicate a statistically significant difference of the SiO_2 contents between the two rock groups. The large difference in plot pattern between the SiO_2 diagrams and the SiO_2/MgO diagrams illustrates the danger of making raw percentage comparisons.

TiO_2 (Figs. 43:2 and 45:2). No (statistically significant) differences could be shown here. The small difference between the TiO_2 and TiO_2/MgO diagrams, especially when compared with that for SiO_2, might be due in part to the low TiO_2 content as compared with the SiO_2 content.

Al_2O_3 (Figs. 43:3 and 45:3). No differences could be shown.

Fe_2O_3 (Fig. 43:4 and 45:4). The amphibolitic rocks have very significantly higher contents, as can be readily seen in the diagrams.

FeO (Figs. 43:5 and 45:5). The amphibolitic rocks are significantly lower in this component.

*FeO** (Fig. 43:6). As the FeO*/MgO diagram for obvious reasons cannot be employed, we have to rely on the fixed pair diagram. The tests here fail to show any difference. This result, together with those recorded for Fe_2O_3 and FeO, indicates that the amphibolitic rocks have been formed under oxidizing conditions.

MnO (Figs. 43:7 and 45:6). MnO is an example (together with Ba and Zn) where the two tests give different results. The fixed pair diagram fails to show any difference, whereas the FeO*/MgO diagram indicates a significantly higher content in the amphibolitic rocks.

MgO (Figs. 43:8 and 45:7). This component is not readily evaluated in the diagrams employed as they use MgO as a normalising factor. Its relation to TiO_2, FeO*, P_2O_5, Zr and Ni characterizes Mg as an immobile element.

CaO (Figs. 43:9 and 45:8). No differences could be shown. The striking difference in plot pattern between the CaO and CaO/MgO diagrams demonstrates the importance of working in ratio diagrams.

Na_2O (Figs. 43:10 and 45:9). Both diagrams indicate a higher Na_2O content in the amphibolitic rocks. In the fixed pair diagram this difference is significant, in the FeO*/MgO diagram less significant.

K_2O (Figs. 43:11 and 45:10). Both diagrams indicate a (very) significantly higher K_2O content in the amphibolitic rocks. Note also the smaller variation shown in the gabbroic rocks.

H_2O (Figs. 43:12 and 45:11). Not surprisingly, the tests indicate a very significantly higher H_2O content in the amphibolitic rocks.

P_2O_5 (Figs. 43:13 and 45:12). No differences could be shown.

Rb (Figs. 43:14 and 45:13). The tests indicate a (very) significantly higher Rb content and a larger variation in the amphibolitic rocks. The scores in the tests are very similar to those of K.

Cu (Figs. 43:15 and 45:14). No differences could be shown.

Sr (Figs. 43:16 and 45:15). No differences could be shown.

Ba (Figs. 43:17 and 45:16). The fixed pair diagram fails to show any difference. The FeO*/MgO diagram reveals a significantly higher Ba content in the amphibolitic rocks.

Zn (Figs. 43:18 and 45:17). As for Ba.

Y (Figs. 43:19 and 45:18). No differences could be shown.

Pb (Figs. 43:20 and 45:19). A very significantly higher Pb content characterizes the amphibolitic rocks.

Zr (Figs. 43:21 and 45:20). No differences could be shown.

Th (Figs. 43:22 and 45:21). A significantly higher Th content in the amphibolitic rocks is indicated by both tests.

S (Figs. 43:23 and 45:22). All tests indicate a very significantly lower S content in the amphibolitic rocks.

Ni (Figs. 43:24 and 45:23). No differences could be shown.

Cl (Figs. 43:25 and 45:24). The tests indicate a very significantly higher content in the amphibolitic rocks.

K/Rb (Fig. 43:26 a). Only the fixed pair diagram was used, and the tests applied there failed to show a difference.

Mg/Ni (Fig. 43:26 b). Also for this ratio only the fixed pair diagram was used. It failed to bring out any difference.

CONCLUDING REMARKS ON THE METASOMATIC EFFECT

The statistical evaluations explained above may be summarized as follows: the formation of the amphibolitic rocks from the gabbroic rocks resulted in addition of Na, K, H_2O, Rb, Pb, Th, Cl, (Mn, Ba, Zn) to the basic rocks, and a subtraction of S. Fe_2O_3/FeO became increased. Immobile elements are Si, Ti, Al, Fe*, Mg, Ca, P, Cu, Sr, Y, Zr and Ni. No changes could be shown for K/Rb and Mg/Ni. The status of Mn, Ba and Zn is uncertain; the fixed pair diagrams fail to demonstrate any difference, whereas the FeO*/MgO diagrams show a significant difference. It is not directly apparent how to explain this difference of evaluation. We therefore prefer to reserve our opinion on the bulk chemical effect for Mn, Ba and Zn. Further investigations will be carried out to solve this problem. Another question to be answered by closer studies is whether there are differences between the transition from gabbroic rocks to hornblende metagabbro and the change from gabbroic rock to amphibolite.

Comparing the results of the present study of the chemical effect of a metamorphic imprint on basic rocks with the results of similar studies, one has to take into consideration that the nature and the extent of the bulk chemical effect of an imprint of weathering or metamorphism on a rock will be dependent on the nature of the rocks involved as well as the intensity of the weathering or metamorphism and the conditions under which the process has taken place. The process is not only controlled by T, P and other intensive parameters, but also by a range of extensive and kinetic factors, *e.g.*, the amount of H_2O(-rich fluid) taking part in the process, further the texture, structure (porosity) and chemical composition of both the rock unit considered and its country rock as well as their relative amounts and mode of intercalation. Thus, different rocks developing in different environments may be expected to show different types of element migrations. Identical element migration patterns can only be expected in metamorphic transitions taking place under identical conditions, both as to intensive and extensive factors. The claim of universal immobility for a range of elements (Winchester and Floyd, 1977; Floyd and Winchester, 1978) is therefore somewhat problematic.

Investigations by Elliott (1973; major elements) and Field and Elliott (1974; trace elements) deal with the chemical effect of amphibolite facies metamorphism

of Hyperite (?) bodies from S Norway. The character of the rocks involved and their geological setting compare very well with those of the Hyperite suite of the present study. Like the Värmland Hyperites these bodies have been emplaced into amphibolite facies, mainly quartzo-feltspathic country rocks. The whole complex thereafter underwent a renewed amphibolite facies metamorphism. This was claimed to result in a migration into the basic rocks of O (increase in Fe_2O_3/FeO), K, P, H_2O, Rb, V, Cl and probably Zr, and a depletion in Fe*, Ca, S and Zn, probably also in Si and Co. Table 7 presents a comparison of the results of the two studies with our present results. Some of the differences, *e.g.*, the depletion of Si and Ca, and the "no difference" for Na in the amphibolitic rocks suggested by Elliott (1973), might be explained by the fact that these conclusions are based on comparisons of raw analytical percentages and not on element (oxide) ratio considerations (see above). The differences concerning Mn, Ba and Zn will not be commented on here because our results are not consistent for these elements. As mentioned above, the differences concerning P and Zr may be partly a closed array effect, but might also reflect real differences in petrological history between the two areas. For example, the amount and composition of the aqueous solutions involved in the metamorphic process might be different for the two complexes.

REFERENCES

GFF = Geologiska Föreningens i Stockholm Förhandlingar

SGU = Sveriges Geologiska Undersökning

American Commission on Stratigraphic Nomenclature, 1970: Code of stratigraphic nomenclature. — A.A.P.G., Tulsa, Oklahoma.

BAILEY, J., and SØRENSEN, I., 1976: X-ray fluorescence analysis. — Inst. for Petrol., Københavns Universitet, intern. report.

BEACH, A., 1973: Amphibolitization of Scourian granulites. — Scott. J. Geol. 10, 35–43.

ELLIOTT, R.B., 1973: The chemistry of gabbro/amphibolite transition in South Norway. — Contrib. Mineral. Petrol. 38, 71–79.

ERDMANN, A., 1855: Vägledning till bergarternas kännedom. — I Marcus,Stockholm.

FIELD, D., and ELLIOTT, R.B., 1974: The chemistry of gabbro/amphibolite transition in South Norway, II. Trace elements. — Contrib. Mineral. Petrol. 47, 63–76.

FLANAGAN, F.J., 1973: 1972 values for international geochemical reference samples. — Geochim. Cosmochim. Acta 37, 1189–1200.

FLANAGAN, F.J., 1974: Reference samples for the earth sciences. — Geochim. Cosmochim. Acta 38, 1731–1744.

FLOYD, P.A., and WINCHESTER, J.A., 1975: Magma type and tectonic setting discrimination using immobile elements. — Earth Planet. Sci. Lett. 27, 211–218.

GARY, M., MCAFEE, R., and WOLF, C.L., 1972: Glossary of geology. — Amer. Geol. Inst., Washington.

GJELSVIK, T., 1952: Metamorphosed dolerites in the gneiss area of Sunnmøre on the West coast of Southern Norway. — Norsk Geol. Tidsskr. 30, 31–134.

GORBATSCHEV, R., 1971: Aspects and problems of Precambrian geology in western Sweden. — SGU C 650.

GORBATSCHEV, R., 1975: Fundamental subdivisions of Precambrian granitoids in the Åmål mega-unit and the evolution of the south-western Baltic Shield, Sweden. — GFF 97, 107-114.

GORBATSCHEV, R., 1980: The Precambrian development of southern Sweden. — GFF 102, 129-136.

GRESENS, R.L., 1967: Composition-volume relationships of metasomatism. — Chem. Geol. 2, 47-65.

GRIFFIN, W.L., and HEIER, K.S., 1973: Petrological implications of some corona structures. — Lithos 6, 315-335.

HABER, A., and RUNYON, R.P., 1973: General statistics, 2nd Ed. — Addison-Wesley, London.

HAGESKOV, B., 1980: The Sveconorwegian structures of the Norwegian part of the Kongsberg-Bamble-Østfold segment. — GFF 102, 150-155.

HAGESKOV, B., and PEDERSEN, S., 1981: Rb/Sr whole rock age determinations from the western part of the Østfold basement complex, SE Norway. — Bull. Geol. Soc. Denmark 29, 119-128.

HAMBERG, A., 1929: Alfred Elis Törnebohm. Levnadsteckning. — Kungl. Svenska Vetenskapsakad. ledam. 101, Almqvist & Wiksell, Uppsala och Stockholm.

HJELMQVIST, S., 1950: The titaniferous iron-ore deposit of Taberg in the south of Sweden. — SGU C 512.

HOLMES, A., 1920: The nomenclature of petrology. — Thomas Murby, London.

HÖGBOM, A., 1922: Berggrunden. *In* Beskrivning till kartbladet Väse. — SGU Aa 151.

IRVINE, T.N., and BARAGAR, W.R.A. 1971: A guide to the chemical classification of the common volcanic rocks. — Can. J. Earth Sci. 8, 523-548.

JOHANSSON, H.E., 1927: Hyperiternas geografiska och petrologiska ställning. — GFF 49, 305-307.

LINDH, A., 1974: The mylonite zone in south-western Sweden (Värmland). — GFF 96, 205-228.

LINDH, A., and KÄHR, Å-M. 1977: K-Ar dating in the Mylonite Zone, south-western Sweden. — GFF 99, 289-291.

LINDH, A., and MALMSTRÖM, L., 1980: A possible break in the Mylonite Zone in Värmland, south-western Sweden. — GFF 102, 95-103.

LUNDEGÅRDH, P.H., 1977: The Gräsmark Formation in western central Sweden. — SGU C 732.

LUNDEGÅRDH,P.H., 1980a: The gneissic granites and allied rocks in central and northwestern Värmland, western Sweden. — SGU C 777, 3-23.

LUNDEGÅRDH, P.H., 1980b: The Östmark Formation and neighbouring rocks in the Proterozoic of Värmland, western Sweden. — GFF 102, 137-140.

LUNDEGÅRDH, P.H., GORBATSCHEV, R., and LINDH, A., 1982: Berggrundskarta över Värmlands län. — Statens industriverk, mineralbyrån. With an explicative note in Swedish.

MAGNUSSON, N.H., 1928: Aktuella problem från Värmlands gnejsurberg; with comments of Johansson, Holmquist, Sundius and Benedicks. — GFF, 810-816.

MAGNUSSON, N.H., 1929: Berggrunden. *In* Beskrivning till kartbladet Nyed. — SGU Aa 144.

MAGNUSSON, N.H., 1933: Berggrunden. *In* Beskrivning till kartbladet Karlstad. — SGU Aa 174.

MAGNUSSON, N.H., 1937: Den centralvärmländska mylonitzonen och dess fortsättning i Norge. — GFF 59, 205-228.

MAGNUSSON, N.H., 1960: The Swedish Precambrian outside the Caledonian mountain chain. *In* Description to accompany the map of the Pre-Quaternary rocks of Sweden. — SGU Ba 16.

MAGNUSSON, N.H., ASKLUND, B., KULLING, O., KAUTSKY, G., EKLUND, J., LARSSON, W., LUNDEGÅRDH, P.H., HJELMQVIST, S., GAVELIN, S., and ÖDMAN, O., 1958: Karta över Sveriges berggrund. — SGU Ba 16.

MALMSTRÖM, L., 1981: The relationship between some hyperites, granites and gneisses in southern Värmland. — SGU C 781, 24-30.

MULDER, F.G., 1971: Paleomagnetic research in some parts of central and southern Sweden. — SGU C 653.

NORRISH, K., and CHAPPEL, B., 1967: X-ray fluorescence spectrography. *In* Physical methods in determinative mineralogy, 161-214. — Academic Press, London, New York.

O'NIONS, R.K., and BAADSGAARD, H., 1971: A radiometric study of polymetamorphism in the Bamble region, Norway. — Contrib. Mineral. Petrol. 34, 1-21.

PEARCE, J.A., and CANN, J.R., 1973: Tectonic setting of basic volcanic rocks determined using trace element analysis. — Earth Planet. Sci. Pett. 19, 290-300.

PEARCE, T.H., 1968: A contribution to the theory of variation diagrams. — Contrib. Mineral. Petrol. 19, 142-157.

POLDERVAART, A., and GILKEY, A.K., 1954: On clouded plagioclase. — Amer. Mineral. 39, 75-91.

PRIEM,H.N.A., MULDER, F.C., BOELRIJK, N.A.I.M., HEBEDA, E.H., VERSCHURE, R.H., and VERDURMEN, E.A.T., 1968: Geochronological and paleomagnetic reconnaissance surveuy in parts of central and southern Sweden. — Phys. Earth Planet. Int. 1, 373-380.

SKALA, W., 1979: Some effects of the constant-sum problem in geochemistry. — Chem. Geol. 27, 1-9.

SKIÖLD, T., 1976: The interpretation of the Rb-Sr and K-Ar ages of late Precambrian rocks in south-western Sweden. — GFF 98, 3-29.

SØRENSEN, I., 1975: X-ray fluorescence spectrometry at GGU. — Grønlands Geol. Unders. Rapp. 75, 16-18.

SØRENSEN, I., 1976: Progress in calibrating an X-ray spectrometer. — Grønlands Geol. Unders. Rapp. 80, 149-159.

STRECKEISEN, A., 1976: To each plutonic rock its proper namne. — Earth Sci. Rev. 12, 1-33.

STRECKEISEN, A.L., 1967: Classification and nomenclature of igneous rocks. — N. Jb. Mineral. Abh. 107, 144-240.

TEALL, J.J.H., 1899: The Galloway granites and associated igneous rocks. Chapter 26 *in* PEACH, B.N., HORN, J., and TEALL, J.J.H.: The Silurian rocks of Britain, Vol. 1. Scotland, 607-632. — Mem. Geol. Survey United Kingdom, Glasgow.

TÖRNEBOHM, A.E., 1877: Om Sveriges vigtigare diabas- och gabbroarter. — Kongl. Svenska Vetenskapsakademiens handlingar 14:13, Stockholm.

UJIIE, H., and NAGASE, K., 1971: Cluster analysis of living planktonic formainifera from the southeastern Indian Ocean. — Proc. II Planktonic Conf. Roma, 1970, Ed. A. Ferinacci. Tecnoscienza, Roma.

WELIN, E., and GORBATSCHEV, R., 1976: Rb-Sr age of granitoid gneisses in the "Pregothian" area of South-Western Sweden. — GFF 98, 378-381.

WELIN, E., and KÄHR, A.-M., 1980: The Rb-Sr and U-Pb ages of a Proterozoic gneissic granite in central Värmland, western Sweden. — SGU C 777, 24-28.

WELIN, E., LUNDEGÅRDH, P.H., and KÄHR, A.-M., 1980: The radiometric age of a Proterozoic hyperite diabase in Värmland county, western Sweden. — GFF 102, 49-52.

WIMAN, E., 1961: Aspects of the Precambrian geology of south-eastern Värmland, Sweden. — Bull. Geol. Inst. Uppsala 39.

WINCHESTER, J.A., and FLOYD, P.A., 1977: Geochemical discrimination of different magma series, and their differentiation products using immobile elements. — Chem. Geol. 20, 325-343.

YODER, H.S., and TILLEY, C.E., 1962: Origin of basaltic magmas: An experimental study of natural and synthetic rock systems. — J. Petrol. 3, 342-532.

ZECK, H.P., and KALSBEEK, F., 1981: Geochemistry of amphibolite facies metamorphism of basic dykes, Precambrian basement, Greenland. — Chem. d. Erde 40, 1-22.

ZECK, H.P., and MALLING, S., 1974: The Gillberga synform (Precambrian basement, SW Värmland, Sweden); literature synopsis and preliminary notes on its re-interpretation. — Geol. Soc. Denmark Bull. 23, 159-174.

ZECK, H.P., and MORTHORST, J.R., 1982: Continental tholeiites in the Ti-Zr-Y discrimination diagram. — N. Jahrb. Min. Mh. 1982, 193-200.

ZECK, H.P., SHENOUDA, H.H., RØNSBO, J.G., and POORTER, R.P.E., 1982: Hypersthene-ilmenite (/magnetite) symplectites in coronitic olivine gabbronorites. — Lithos 15, 173-182.

ZECK, H.P., and WALLIN, B., 1980: A 1220±60 M.Y. Rb-Sr isochron age representing a Taylor-convection caused recrystallization event in a granitic rock suite. — Contrib. Mineral. Petrol. 74, 45-53.

TABLE 1. Chemical and normative composition of gneisses in the Ölme area. Coordinates refer to the Swedish national grid, topographic map 10 D Karlstad NO. Major elements in weight per cent, trace elements in ppm. Major element analyses by Geological Survey of Greenland; trace elements by the authors (JRM)

Sample nr.	31701	31722	31740	31763	31774	31795	32005	32023
Coordin.	87725/ 93305	87720/ 93275	87650/ 90016	88960/ 93950	87600/ 90105	89190/ 94365	89230/ 94730	76800/ 93502
SiO_2	70.96	73.35	72.77	69.19	72.17	71.24	72.40	73.29
TiO_2	0.40	0.31	0.25	0.29	0.29	0.31	0.28	0.36
Al_2O_3	14.84	14.42	14.31	15.41	14.07	14.79	14.09	12.62
Fe_2O_3	0.01	0.10	0.59	0.32	0.41	0.37	0.55	1.98
FeO	1.87	0.96	0.92	1.59	1.27	1.75	1.22	0.84
MnO	0.07	0.04	0.07	0.14	0.11	0.10	0.15	0.07
MgO	0.60	0.25	0.29	0.68	0.29	0.61	0.62	0.15
CaO	2.43	0.82	0.67	1.87	0.75	1.66	1.40	0.64
Na_2O	5.40	5.20	4.76	5.57	4.00	4.50	4.17	3.68
K_2O	0.96	3.55	4.63	2.72	5.13	2.98	4.37	5.25
P_2O_5	0.10	0.04	0.10	0.15	0.11	0.12	0.10	0.11
H_2O^+	0.51		0.30	0.31	0.34	0.26	0.25	0.34
l.o.i.[1]	0.71	0.40	0.40	0.59	0.74	0.60	0.29	
Total	98.35	99.44	99.76	98.52	99.34	99.03	99.64	98.99
Rb	34	77	160	71	155	69	102	187
Ba	890	1440	375	894	462	1450	1240	270
Sr	377	128	58	262	63	304	236	39
Y	51	43	138	35	56	27	27	151
Zr	260	274	306	169	259	121	139	435
Cu	32	27		39		31	22	
S	83	32	6	49	17	33	4	4
Cl	270	96	70	114	101	360	101	47
CIPW norm								
Q	29.28		25.63	21.44	27.85	29.28	27.05	30.51
or	5.67		27.36	16.07	30.32	17.61	25.83	31.03
ab	45.70		40.28	47.13	33.85	38.08	35.29	31.14
an	10.14		2.04	6.53	0.47	5.30	6.29	2.41
ac								
ns								
di								0.04
hy	4.39		1.64	4.13	2.44	4.10	3.15	0.36
he								0.67
mt	0.01		0.86	0.46	0.59	0.54	0.80	1.89
il	0.76		0.47	0.55	0.55	0.59	0.53	0.68
ap	0.23		0.23	0.35	0.25	0.28	0.23	0.25
cc	0.45		0.23	0.64	0.91	0.77		
C	1.20		0.72	0.91	1.76	2.22	0.19	

[1] inclusive H_2O^+

TABLE 1 continued

Sample nr.	32034	32046	35130	35133	35144	35145	35147	35148
Coordin.	76554/ 93540	83790/ 97775	89220/ 93240	90350/ 82200	82510/ 98040	87230/ 90020	87430/ 90690	90350/ 82200
SiO_2	72.79	74.70	67.34	75.49	75.63	67.85	72.14	66.84
TiO_2	0.24	0.22	0.41	0.16	0.19	0.54	0.31	0.71
Al_2O_3	13.94	11.56	16.49	12.21	11.52	16.57	13.30	14.81
Fe_2O_3	0.42	1.08	0.86		1.01	1.01	0.88	1.56
FeO	1.15	1.27	1.73	0.72	0.83	1.00	1.80	2.10
MnO	0.07	0.09	0.12	0.03	0.09	0.17	0.13	0.12
MgO	0.17	0.15	0.89	0.19	0.11	0.38	0.10	0.90
CaO	0.57	0.35	2.26	0.72	0.35	0.82		2.01
Na_2O	3.23	3.97	5.72	3.01	2.87	4.58	3.92	3.77
K_2O	6.38	5.12	2.92	5.53	5.51	6.40	5.47	5.22
P_2O_5	0.11	0.08	0.18	0.04	0.03	0.14	0.09	0.19
H_2O^+	0.31	0.33	0.30			0.55	0.28	
l.o.i.[1]	0.38	0.66	0.52	0.36	0.29	0.55	1.20	0.65
Total	99.45	99.30	99.44	98.40	98.43	100.01	99.34	98.88
Rb	191	154	79	151	204	104	202	146
Ba	403	110	1010	446	111	480	448	1520
Sr	51	12.0	422	102	16.8	48	32	235
Y	121	136	46	56	111	67	158	54
Zr	398	451	204	70	381	484	451	402
Cu	2.5		25	3.1				28
S	68	17	10	55	11	36	16	187
Cl	69	41	124	98	62	53	95	174
CIPW norm								
Q	27.73	31.52	16.91	34.59	36.77	14.59	27.20	19.22
or	37.70	30.26	17.26	32.68	32.56	37.82	32.33	30.85
ab	27.33	30.96	48.40	25.47	24.29	38.76	33.17	31.90
an	2.11		8.65	3.31	1.54	3.15		8.07
ac		2.32						
ns								
di								0.54
hy	1.92	2.28	4.23	1.59	0.82	1.37	2.56	3.59
he								
mt	0.61	0.40	1.25		1.46	1.46	1.28	2.26
il	0.46	0.42	0.78	0.30	0.36	1.03	0.59	1.35
ap	0.25	0.19	0.42	0.09	0.07	0.32		0.44
cc		0.44	0.50					
C	0.95		0.75	0.06	0.27	0.95	0.93	

TABLE 1 continued

Sample nr.	35151	35158	35160	35173	35175	35176	35189	35190
Coordin.	90350/ 82200	90350/ 82200	90350/ 82200	79100/ 93890	79020/ 93960	79310/ 94735	76690/ 93715	76555/ 93555
SiO_2	64.89	65.39	75.47	71.64	75.28	76.02	75.19	78.40
TiO_2	0.80	0.51	0.15	0.36	0.15	0.14	0.16	0.19
Al_2O_3	14.67	16.57	12.18	12.47	11.62	12.09	11.99	9.27
Fe_2O_3	1.70	1.15		1.45	0.75	0.67	1.31	0.67
FeO	2.78	1.88	0.93	1.70	0.96	1.02	0.83	1.76
MnO	0.15		0.03	0.16	0.08	0.08	0.08	0.54
MgO	1.36	0.87	0.21	0.20	0.13			0.15
CaO	2.61	2.84	0.50	0.78	0.41	0.42	0.36	0.54
Na_2O	3.94	4.65	2.76	3.87	3.63	3.55	3.71	1.02
K_2O	4.66	3.61	5.86	5.42	5.12	5.06	5.26	5.43
P_2O_5	0.22	0.13	0.04	0.05	0.02	0.04	0.05	0.08
H_2O^+						0.24	0.32	0.39
l.o.i.[1]	0.73	0.73	0.38	0.53	0.39	0.47	0.57	0.71
Total	98.51	98.32	98.46	98.63	98.54	99.56	99.51	98.76
Rb	134	92	134	179	247	243	211	141
Ba	1480	1810	668	265	24	22	32	302
Sr	267	440	152	30	4.8	3.9	6.5	34
Y	56	44	34	172	213	195	215	341
Zr	370	281	89	447	501	390	420	601
Cu	33	41	12.1					
S	240	100	15	14	24	13	8	92
Cl	188	216	54	96	40	48	45	41
CIPW norm								
Q	16.56	16.75	35.02	26.44	33.42		33.33	49.87
or	27.54	21.33	34.63	32.03	30.26		31.09	32.09
ab	33.34	39.35	23.36	32.75	30.72		31.39	8.63
an	8.58	13.24	2.22	0.65	0.29			0.13
ac								
ns								
di	2.41			2.49	1.38			
hy	4.86	3.83	2.04	0.85	0.66		0.33	3.74
he								
mt	2.46	1.67		2.10	1.09		1.90	0.97
il	1.52	0.97	0.28	0.68	0.28		0.30	0.36
ap	0.51	0.30	0.09	0.12	0.05		0.12	0.19
cc							0.53	0.73
C		0.16	0.48				0.19	1.67

TABLE 1 continued

Sample nr.	35197	35202	35203	35206	35207	35212	35216	35221
Coordin.	86755/ 90270	87270/ 93100	87040/ 93195	86950/ 93200	86955/ 93260	87445/ 95660	87300/ 96450	82445/ 98065
SiO_2	71.75	69.51	70.61	70.24	72.07	74.76	74.80	70.59
TiO_2	0.29	0.54	0.47	0.39	0.32	0.25	0.24	0.41
Al_2O_3	14.99	14.64	14.53	14.65	13.92	12.15	12.06	15.02
Fe_2O_3	0.44	1.11	0.83	0.77	1.45	0.93	1.22	0.68
FeO	0.94	1.62	1.50	1.01	0.14	1.47	1.15	1.31
MnO	0.15	0.11	0.10	0.14	0.17	0.14	0.11	0.13
MgO	0.20	0.65	0.55	0.45	0.24	0.12	0.16	1.36
CaO	0.61	1.44	1.35	1.18	0.50	0.50	0.34	2.81
Na_2O	4.69	3.69	3.62	4.11	4.05	3.61	3.57	3.52
K_2O	5.21	5.59	5.53	4.84	5.07	5.20	5.27	2.35
P_2O_5	0.09	0.18	0.19	0.06	0.05	0.06	0.07	0.12
H_2O^+	0.41	0.36	0.97			0.43	0.28	0.73
l.o.i.[1]		0.50		0.47	0.24	0.59	0.41	1.01
Total	99.77	99.58	100.25	98.31	98.22	99.78	99.40	99.31
Rb	101	176	158	126	140	231	186	94
Ba	467	1180	1100	1410	1410	77	119	744
Sr	59	179	173	255	113	8.3	12.6	557
Y	91	74	62	46	36	174	145	58
Zr	338	319	281	261	274	409	400	270
Cu	1.6	24	15.7	22	18.4			23
S	23	61	36	16		30	17	
Cl	58	62	78	68	36	69	43	42
CIPW norm								
Q	23.57	22.86	24.54	24.40	27.82	32.40	33.03	33.53
or	30.79	33.04	32.68	28.60	29.96	30.73	31.14	13.89
ab	39.69	31.23	30.63	34.78	34.27	30.55	30.21	29.79
an	0.29	5.08	5.46	5.46	2.15	1.08	0.41	11.39
ac								
ns								
di								
hy	1.66	2.99	2.85	1.96	0.60	2.08	1.31	4.80
he					1.40			
mt	0.64	1.61	1.20	1.12	0.08	1.35	1.77	0.99
il	0.55	1.03	0.89	0.74	0.61	0.47	0.46	0.78
ap	0.21	0.42	0.44	0.14	0.12	0.14	0.16	0.28
cc	0.77	0.32				0.36	0.30	0.64
C	1.53	0.66	0.59	0.65	0.98	0.19	0.33	2.51

TABLE 1 continued

Sample nr.	35223
Coordin.	76565/ 93575
SiO_2	71.78
TiO_2	0.01
Al_2O_3	15.95
Fe_2O_3	
FeO	0.52
MnO	0.03
MgO	0.05
CaO	1.20
Na_2O	5.30
K_2O	4.33
P_2O_5	0.03
H_2O^+	0.24
l.o.i.[1]	0.73
Total	99.93

Rb	97
Ba	383
Sr	85
Y	22
Zr	50
Cu	4.7
S	11
Cl	124

CIPW norm

Q	22.70
or	25.59
ab	44.85
an	2.66
ac	
ns	
di	
hy	1.12
he	
mt	
il	0.02
ap	0.07
cc	1.11
C	1.57

TABLE 2. Strike measurements on (sub-)vertical joint planes at 11 Hyperite localities (Figs. 3 and 7-14)

(1)	Brattåshöjden:	4x65°, 105°, 132°, 2x135°, 6x155°, 5x172°
(2)	Träfors:	2°, 3x66°, 7x160°, 172°, 2x174°, 177°, 178°
(3)	Haghöjden:	4x105°, 106°, 113°, 3x160°, 176°
(4)	Högeberg:	0°, 5°, 8°, 2x10°, 3x13°, 32°, 33°, 35°, 2x43°, 45°, 48°, 60°, 63°, 156°, 162°, 2x172°, 2x177°
(5)	Ölme:	60°, 118°, 160°, 168°, 2x174°
(6)	Nore:	160°, 170°, 174°
(7)	Sjöstad:	5°, 33°, 44°, 52°, 55°, 70°, 2x173°, 2x174°, 175°
(8)	Gäslösa:	17°, 75°, 3x176°
(9)	Skanum:	2x63°, 70°, 73°, 178°, 2x179°
(10)	Tållerud:	4x8°, 12°, 52°
(11)	Västkärr:	3x0°, 6°, 8°, 13°, 23°, 169°, 174°, 178°

Distribution of all 117 measurements (see the rose diagram of Fig. 18)

Interval	Number of measurements
01° - 20°	19
21° - 40°	5
41° - 60°	10
61° - 80°	14
81° - 100°	0
101° - 120°	8
121° - 140°	3
141° - 160°	19
161° - 180°	39

TABLE 3. Range of mineralogical composition in Hyperite rocks. Based on estimated compositions of 12 gabbroic rocks, 16 hornblende metagabbros and 16 amphibolites

	Gabbroic rock	Hornblende metagabbro	Amphibolite
Olivine	0-20	-	-
Ca-rich pyroxene	10-40	0-10	-
Ca-poor pyroxene	0- 5	-	-
Plagioclase	35-80	20-65	14-60
Magnetite	2- 5	1-10	0- 2
Ilmenite	0- 1	0- 1	-
Hornblende	1-10	8-55	20-67
K-feldspar	0- 1	-	-
Biotite	1-10	1-15	1-20
Apatite	0- 2	0- 1	0- 1
Quartz	0- 1	1-15	1-15
Garnet	0-10	1-10	0- 8
Rutile	0- 1	0- 1	-
Pyrite	0- 1	0- 1	0- 1
Epidote	-	0- 1	0- 7
Titanite	-	0- 2	0- 3
Zircon	0- 1	0- 1	0- 1
Scapolite	-	0- 2	0- 1
Saussurite	-	0- 1	0- 1
Sericite	0- 1	0- 1	0- 1
Chlorite	0- 1	0- 1	0- 8
Calcite	0- 1	0- 1	0- 2

TABLE 4. Chemical and normative composition of Hyperites in the Ölme area: amphibolites (nr.1-22), hornblende meta-gabbros (nr.23-48) and gabbroic rocks (nr.49-74). Coordinates refer to the Swedish national grid, topographic map 10 D Karlstad NO. Major elements in weight per cent, trace elements in ppm. Major element analyses by Geological Survey of Greenland; trace element by the authors (JRM)

Sample nr.	31702	31714	31724	31749	31751	31765	31767	31776
	1	2	3	4	5	6	7	8
Coordin.	87725/ 93305	87723/ 93305	87720/ 93275	87600/ 90125	87602/ 90125	88960/ 93950	88965/ 93950	87600/ 90105
SiO_2	48.00	48.18	48.46	48.97	48.63	49.24	48.28	47.60
TiO_2	1.20	1.24	1.41	1.65	1.89	1.15	1.97	1.55
Al_2O_3	15.50	15.73	15.53	15.49	15.08	21.10	16.41	15.15
Fe_2O_3	2.51	2.40	2.89	2.62	3.79	2.09	2.71	2.76
FeO	9.75	9.68	10.01	10.24	10.01	5.70	10.39	9.31
MnO	0.24	0.22	0.21	0.21	0.21	0.14	0.23	0.37
MgO	6.79	6.63	6.99	5.64	5.65	2.79	4.53	5.00
CaO	8.26	8.74	8.85	7.53	7.69	9.44	8.09	5.12
Na_2O	2.67	2.94	2.96	2.99	2.51	4.26	3.19	3.41
K_2O	1.98	1.24	0.92	1.46	1.81	1.43	1.44	4.35
P_2O_5	0.18	0.15	0.17	0.31	0.36	0.20	0.34	0.41
H_2O^+	1.10	1.03	0.96	1.00		0.78	0.62	1.36
l.o.i.[1]	2.56	2.29	1.66	2.16	1.77	1.53	1.64	4.56
Total	99.64	99.44	100.06	99.27	99.40	99.07	99.22	99.59
Rb	64	30	122	40	51	34	33	305
Ba	832	479	341	622	798	766	589	362
Pb		2.5	5.0	6.4	7.4	13	6.2	16
Sr	175	235	1320	242	235	391	258	101
Y	29	27	30	38	38	17.5	40	100
Th		2.5	4.4	4.3	2.8		4.2	4.3
Zr	64	79	93	150	153	95	187	135
Ni	74	70	74	82	77	36	52	70
Cu	24	59	77	57	42	39	37	
Zn	146	133	138	161	178	91	143	319
S	46	320	870	400	107	1	139	59
Cl	920	820	510	930	850	600	1260	430
CIPW norm								
Q								
or	11.70	7.33	5.44	8.63	10.70	8.45	8.51	25.71
ab	22.59	24.88	25.05	25.30	21.24	32.51	26.99	28.09
an	24.46	26.06	26.37	24.53	24.54	34.23	26.21	11.09
ne						1.91		0.41
di	5.03	6.88	9.86	2.87	9.28	5.43	4.39	
hy	15.12	15.79	15.08	25.87	21.81		17.80	
ol	9.98	8.43	8.45	0.78	0.15	8.37	3.93	18.72
mt	3.64	3.48	4.19	3.80	5.50	3.03	3.93	4.00
il	2.28	2.36	2.68	3.13	3.59	2.18	3.74	2.94
ap	0.42	0.35	0.39	0.72	0.83	0.46	0.79	0.95
cc	3.32	2.87	1.59	2.64		1.71	2.32	4.18
C								0.77

[1] inclusive H_2O^+

TABLE 4 continued

Sample nr.	31778	31780	31797	32001	32007	32027	32040	35111
	9	10	11	12	13	14	15	16
Coordin.	87601/ 90105	87615/ 90105	89190/ 94365	89193/ 94365	89230/ 94730	76586/ 93572	83935/ 97820	84920/ 98000
SiO_2	48.60	47.60	50.21	48.65	50.08	46.05	46.06	46.43
TiO_2	2.13	1.85	2.58	2.15	2.60	2.14	1.56	1.85
Al_2O_3	14.60	15.38	14.20	15.93	13.86	16.42	17.03	16.73
Fe_2O_3	4.20	3.38	3.50	3.25	3.74	3.08	2.13	3.02
FeO	10.03	9.99	11.24	10.52	11.36	10.35	10.59	10.51
MnO	0.24	0.25	0.24	0.20	0.25	0.20	0.24	0.20
MgO	5.00	5.60	2.88	4.17	3.53	6.72	6.96	6.99
CaO	7.67	7.43	7.28	7.97	7.21	7.74	8.82	7.90
Na_2O	2.86	3.47	2.24	3.16	2.51	3.27	3.00	2.73
K_2O	1.67	2.21	1.97	1.53	2.25	1.57	1.46	1.37
P_2O_5	0.39	0.46	0.78	0.44	0.76	0.46	0.26	0.29
H_2O^+		1.09	0.98	0.72	1.48	1.51	0.98	
l.o.i.[1]	1.82	1.91	2.25	1.95	1.63	2.22	1.96	2.22
Total	99.21	99.53	99.37	99.92	99.78	100.22	100.07	100.25
Rb	49	93	42	36	54	45	64	38
Ba	695	562	981	661	1060	547	365	421
Pb	10	16	14	12	9.3	6.0	6.9	4.1
Sr	199	189	208	222	199	246	250	221
Y	46	53	55	43	56	34	38	33
Th	4.7	4.1	3.9	4.8	4.9	2.9	2.0	3.5
Zr	182	158	271	214	270	120	106	115
Ni	58	74	30	49	31	115	108	107
Cu	74	51	69	87	57	39	43	65
Zn	178	267	202	180	207	141	142	142
S	730	300	690	370	720	570	470	400
Cl	1230	850	1440	950	1170	380	510	540
CIPW norm								
Q	0.28		7.38	0.48	4.51			
or	9.87	13.06	11.64	9.04	13.30	9.28	8.63	8.10
ab	24.20	29.36	18.96	26.74	21.24	27.67	24.46	23.10
an	22.07	19.86	22.87	24.76	19.91	25.49	28.69	29.35
ne							0.50	
di	11.10	7.27	0.05	3.45	8.37	4.45	5.91	6.53
hy	18.84	1.50	24.88	22.12	18.52	0.81		6.09
ol		16.04				19.80	22.02	16.29
mt	6.09	4.90	5.07	4.71	5.42	4.47	3.09	4.38
il	4.05	3.51	0.53	4.08	4.94	4.06	2.96	3.51
ap	0.90	1.07	1.83	1.02	1.76	1.07	0.60	0.67
cc		1.86	2.89	2.80	0.34	1.61	2.23	
C								

TABLE 4 continued

Sample nr.	35119	35125	35132	35146	35204	35213	31713	31726
	17	18	19	20	21	22	23	24
Coordin.	88615/ 95795	88500/ 97000	83460/ 98090	87200/ 90050	87125/ 93185	87445/ 95700	87722/ 93305	87717/ 93275
SiO_2	47.64	48.28	46.83	54.22	48.35	47.06	48.23	48.70
TiO_2	2.00	1.32	1.73	0.62	1.01	1.32	1.23	1.41
Al_2O_3	14.45	16.82	16.31	15.87	16.67	17.67	15.88	15.58
Fe_2O_3	3.37	3.25	2.51	1.93	2.10	2.40	2.27	2.74
FeO	10.95	8.95	10.95	5.08	8.94	9.52	9.56	10.12
MnO				0.18	0.20		0.22	0.20
MgO	5.80	6.75	6.89	7.00	7.89	6.46	6.78	6.96
CaO	7.57	7.98	8.76	6.68	9.26	8.83	8.83	9.08
Na_2O	2.53	2.82	2.78	3.41	2.81	3.25	3.10	2.50
K_2O	1.90	1.15	0.89	2.77	0.53	0.77	1.05	0.84
P_2O_5	0.36	0.21	0.23	0.32	0.16	0.19	0.15	0.19
H_2O^+				0.96	0.97		0.87	0.74
l.o.i.[1]	2.47	1.77	1.68	1.74	1.92	1.80	1.89	1.52
Total	99.03	99.30	99.56	99.82	99.84	99.26	99.19	99.84
Rb	74	24	20	67	7.2	15.7	25	107
Ba	604	488	287	1210	241	357	463	345
Pb	8.9	4.4	3.5	8.8	3.2	4.4	4.1	2.6
Sr	205	256	230	763	256	263	242	1330
Y	46	24	32	4.6	22	28	26	29
Th	4.9	3.0	2.7	4.8	3.0	1.4	3.3	2.9
Zr	168	117	123	115	64	97	78	95
Ni	74	122	91	135	90	86	73	71
Cu	66	67	68	96	109	54	50	77
Zn	184	152	149	95	103	128	130	138
S	970	910	1200	34	94	400	68	1110
Cl	720	1380	570	190	540	720	740	240
CIPW norm								
Q				0.22				
or	11.23	6.80	5.26	16.37	3.13	4.55	6.21	4.96
ab	21.41	23.86	23.52	28.86	23.78	27.50	26.23	21.16
an	22.46	29.84	29.40	19.82	31.31	31.35	26.32	28.81
ne								
di	10.53	6.85	10.35	5.08	6.20	9.22	8.28	8.28
hy	16.31	15.57	7.13	22.03	18.75	0.69	12.36	25.41
ol	5.11	6.90	14.76		8.21	17.73	10.64	1.62
mt	4.89	4.71	3.64	2.80	3.04	3.48	3.29	3.97
il	3.80	2.51	3.29	1.18	1.92	2.51	2.34	2.68
ap	0.83	0.49	0.53	0.74	0.37	0.44	0.35	0.44
cc				1.77	2.16		2.32	1.77
C								

TABLE 4 continued

Sample nr.	31741	31753	31769	31782	31799	32003	32009	32011
	25	26	27	28	29	30	31	32
Coordin.	87647/ 90017	87609/ 90125	88975/ 93960	87620/ 90105	89192/ 94365	89195/ 94365	89232/ 94732	89235/ 94732
SiO_2	47.96	49.69	46.51	47.74	49.98	48.92	51.00	48.99
TiO_2	1.88	2.01	3.16	1.95	1.25	2.11	1.73	2.00
Al_2O_3	15.58	14.66	13.11	15.34	21.69	15.95	18.37	16.74
Fe_2O_3	4.45	2.86	3.82	3.81	1.85	3.69	2.67	2.87
FeO	9.14	10.98	12.56	10.28	6.39	10.38	7.89	9.99
MnO	0.19	0.25	0.24	0.22	0.15	0.22	0.19	0.19
MgO	5.72	4.85	4.94	5.80	2.70	4.33	3.05	4.17
CaO	7.56	8.23	8.40	7.56	9.50	7.94	7.91	7.71
Na_2O	3.58	2.36	2.84	2.87	3.44	2.96	3.46	3.56
K_2O	1.44	1.52	1.46	1.59	1.20	1.61	1.89	1.82
P_2O_5	0.46	0.37	0.28	0.44	0.31	0.42	0.40	0.39
H_2O^+	1.31	0.75	0.84	1.32	0.65	0.82	1.26	0.79
l.o.i.[1]	2.02	1.71	2.75	2.30	1.53	1.39	1.54	1.76
Total	99.98	99.49	100.07	99.90	99.99	99.92	100.10	100.19
Rb	41	40	36	44	25	38	49	46
Ba	499	674	595	643	635	689	897	846
Pb	11	5.4	6.9	6.9	10	9.9	11	12
Sr	195	222	213	195	322	212	312	244
Y	41	42	35	40	22	43	37	37
Th	4.4	2.4	4.1	4.6	2.6	3.9	4.0	5.6
Zr	170	171	146	169	104	210	194	187
Ni	75	48	49	79	38	52	32	49
Cu	60	94	28	51	37	77	61	47
Zn	163	168	207	171	102	181	139	167
S	750	750	50	490	104	490	500	290
Cl	140	175	1670	270	870	620	820	1630
CIPW norm								
Q		3.74	0.11		0.44	0.55	0.84	
or	8.51	8.98	8.63	9.40	7.09	9.51	11.17	10.76
ab	30.29	19.97	24.03	24.29	29.11	25.05	29.28	30.13
an	22.19	24.92	18.71	24.28	39.54	25.48	29.01	24.32
ne								
di	6.41	6.19	7.55	3.43		6.30	4.88	4.38
hy	10.71	23.94	23.67	22.08	15.14	20.58	14.94	11.70
ol	7.86			2.64				7.05
mt	6.45	4.15	5.54	5.52	2.68	5.35	3.87	4.16
il	3.57	3.82	6.00	3.70	2.37	4.01	3.29	3.80
ap	1.07	0.86	0.65	1.02	0.72	0.97	0.93	0.90
cc	1.61	2.18	4.34	2.23	2.00	1.30	0.64	2.21
C					0.24			

TABLE 4 continued

Sample nr.	32019 33	32021 34	32022 35	32029 36	32032 37	32038 38	35115 39	35116 40
Coordin.	76831/ 93508	76835/ 93507	76827/ 93507	76595/ 93572	76597/ 93570	83950/ 97835	83680/ 97945	83865/ 97850
SiO_2	47.09	45.88	46.68	47.85	47.94	46.77	46.78	47.26
TiO_2	2.32	2.38	2.27	2.56	2.76	1.84	2.21	1.83
Al_2O_3	16.98	16.00	16.24	17.80	17.46	16.07	17.62	16.68
Fe_2O_3	3.33	4.37	2.58	2.53	3.42	2.88	2.51	3.59
FeO	9.81	9.28	10.49	9.76	9.07	11.03	10.20	9.55
MnO	0.21	0.24	0.22	0.18	0.18	0.27	0.13	0.22
MgO	5.25	5.34	5.17	3.66	4.01	6.19	5.19	6.16
CaO	8.52	7.80	8.10	7.70	8.44	8.43	9.24	8.68
Na_2O	2.99	4.01	3.42	3.70	3.27	2.89	3.53	2.70
K_2O	1.02	1.66	1.16	1.74	1.28	0.93	0.77	0.87
P_2O_5	0.49	0.50	0.40	0.52	0.46	0.28	0.33	0.29
H_2O^+			1.28	1.16	0.63	1.28		
l.o.i.[1]	1.49	1.86	2.24	1.97	1.51	2.09	1.44	1.74
Total	99.50	99.32	98.97	99.97	99.80	99.67	99.93	99.57
Rb	23	60	29	53	37	37	8.7	17.1
Ba	460	442	519	584	605	355	309	275
Pb	2.3	10		9.5	4.1	2.7	2.9	4.3
Sr	312	280	372	293	280	227	317	249
Y	33	44	71	40	35	36	34	33
Th	1.3	2.9		4.0	3.1	1.3	2.1	1.4
Zr	132	140	212	152	140	125	134	130
Ni	75	73	72	46	45	68	53	74
Cu	46	51	54	68	55	71	40	66
Zn	141	159		140	135	158	135	144
S	1500	990	1720	1000	720	750	430	1120
Cl	52	500	370	340	65	480	480	380
CIPW norm								
Q					0.17			
or	6.03	9.81	6.86	10.28	7.56	5.50	4.55	5.14
ab	25.30	25.72	28.94	31.31	27.67	24.46	27.75	22.85
an	29.90	20.76	25.54	26.82	29.18	28.13	29.96	30.83
ne		4.45					1.15	
di	7.56	12.03	4.68	2.39	3.41	5.58	11.37	8.49
hy	12.45		9.51	6.60	17.91	15.02		15.84
ol	6.40	12.69	10.95	9.83		9.56	15.14	5.33
mt	4.83	6.34	3.74	3.67	4.96	4.18	3.64	5.21
il	4.41	4.52	4.31	4.86	5.24	3.49	4.20	3.48
ap	1.14	1.16	1.00	1.20	1.07	0.65	0.76	0.67
cc			2.23	1.84	2.00	1.84		
C								

TABLE 4 continued

Sample nr.	35129	35162	35168	35183	35191	35198	35200	35214
	41	42	43	44	45	46	47	48
Coordin.	89500/ 96075	90350/ 82200	78525/ 95960	78150/ 94050	76515/ 93560	86755/ 90270	87165/ 93970	87495/ 95700
SiO_2	50.31	47.75	51.16	49.31	46.99	48.62	47.36	50.35
TiO_2	1.05	0.86	1.99	1.36	2.32	2.53	1.43	1.66
Al_2O_3	21.81	15.87	15.46	16.98	16.58	13.92	17.57	15.16
Fe_2O_3	1.96	2.83	1.89	1.41	3.28	4.15	3.17	2.40
FeO	5.25	7.08	7.52	10.03	9.90	11.28	9.17	8.44
MnO				0.17		0.26	0.20	
MgO	2.65	8.50	5.75	7.15	5.29	4.20	6.80	5.49
CaO	9.64	10.02	10.38	8.18	7.95	7.66	8.37	9.54
Na_2O	3.72	2.82	2.72	2.86	3.18	2.96	2.88	2.85
K_2O	1.40	1.17	0.69	1.02	1.47	1.75	0.97	1.06
P_2O_5	0.18	0.26	0.33	0.29	0.41	0.53	0.33	0.24
H_2O^+						0.97	0.79	
l.o.i.[1]	1.12	2.22	1.50	1.40	2.10	2.17	1.92	2.02
Total	99.09	99.37	99.37	100.15	99.47	100.03	100.17	99.21
Rb	28	33	16.7	21	36	40	22	23
Ba	598	640	265	454	720	677	422	462
Pb	3.1	4.3	3.0	3.0	4.8	8.8	4.4	2.0
Sr	372	475	251	252	346	201	275	220
Y	15.4	11.3	48	23	28	51	25	38
Th	1.6	2.5	4.3	3.8	2.1	6.2	2.1	3.2
Zr	92	56	139	109	124	226	129	142
Ni	35	135	92	120	69	35	132	66
Cu	47	112	35	55	68	75	52	83
Zn	84	97	87	126	139	196	149	127
S	173	910	780	1040	1750	1340	890	200
Cl	500	510	310	400	410	400	910	850
CIPW norm								
Q			3.35			2.21		1.25
or	8.27	6.91	4.08	6.03	8.69	10.34	5.73	6.26
ab	31.48	23.73	23.02	24.20	26.91	25.05	24.37	24.12
an	38.68	27.19	27.94	30.48	26.63	19.53	32.15	25.44
ne		0.07						
di	6.58	16.80	17.44	6.76	8.35	6.20	0.06	16.68
hy	2.33		14.77	15.50	5.60	20.95	19.05	16.25
ol	5.37	16.12		10.49	11.08		7.37	
mt	2.84	4.10	2.74	2.04	4.76	6.02	4.60	3.48
il	1.99	1.63	3.78	2.58	4.41	4.81	2.72	3.15
ap	0.42	0.60	0.76	0.67	0.95	1.23	0.76	0.56
cc						2.73	2.57	
C								

TABLE 4 continued

Sample nr.	31715 49	31728 50	31742 51	31755 52	31771 53	31784 54	32013 55	32030 56
Coordin.	87720/ 93305	87715/ 93275	87650/ 90020	87613/ 90125	88990/ 93950	87622/ 90105	89350/ 94650	76595/ 93572
SiO_2	48.27	48.70	48.44	48.57	48.31	48.07	49.40	48.74
TiO_2	1.24	1.43	1.86	2.16	2.79	1.83	1.04	1.84
Al_2O_3	15.63	15.61	15.73	14.56	14.58	15.16	19.30	18.33
Fe_2O_3	1.68	2.34	2.97	2.71	3.25	3.34	1.81	3.03
FeO	10.69	10.53	10.51	12.15	11.38	11.07	8.61	9.14
MnO	0.21	0.21	0.21	0.24	0.22	0.21	0.15	0.19
MgO	7.15	6.99	5.68	5.12	4.39	6.48	5.73	4.94
CaO	9.01	8.99	8.20	8.62	8.62	7.96	8.45	7.64
Na_2O	2.79	2.71	2.86	2.81	3.03	2.68	3.27	3.66
K_2O	0.78	0.82	1.28	1.30	1.34	1.19	1.02	1.17
P_2O_5	0.12	0.25	0.46	0.37	0.28	0.42	0.19	0.41
H_2O^+	0.69	1.01	0.59	0.47	0.80	0.52	0.46	0.46
l.o.i.[1]	1.61	1.36	1.57	1.41	1.75	1.54	1.26	1.02
Total	99.18	99.94	99.77	100.02	99.94	99.95	100.23	100.11
Rb	17.2	102	31	31	34	29	23	26
Ba	330	338	573	516	553	554	439	513
Pb		4.1	6.1	5.0	6.3	6.3	2.8	2.0
Sr	228	1330	204	217	234	197	263	314
Y	29	28	38	40	40	37	21	29
Th		2.5	3.8	3.1	2.4	2.8	2.9	2.7
Zr	87	94	168	158	168	154	98	117
Ni	82	74	82	62	44	89	92	66
Cu	67	67	49	112	53	74	56	49
Zn	122	134	166	166	176	179	97	113
S	440	1100	640	1430	920	1230	450	1040
Cl	360	151	310	161	840	370	139	22
CIPW norm								
Q					0.29			
or	4.61	4.85	7.56	7.68	7.92	7.03	6.03	6.91
ab	23.61	22.93	24.20	23.78	25.64	22.68	27.67	30.97
an	27.82	28.01	26.30	23.28	22.23	25.82	34.97	30.13
ne								
di	8.48	10.51	4.29	9.30	10.60	3.70	0.54	1.28
hy	17.38	18.24	24.32	22.88	19.65	26.77	14.91	11.83
ol	9.42	6.91	1.38	1.61		1.82	8.80	8.41
mt	2.44	3.39	4.31	3.93	4.71	4.84	2.62	4.39
il	2.36	2.72	3.53	4.10	5.30	3.48	1.98	3.49
ap	0.28	0.58	1.07	0.86	0.65	0.97	0.44	0.95
cc	2.09	0.80	2.23	2.14	2.16	2.32	1.82	1.27
C								

TABLE 4 continued

Sample nr.	32042	32044	35110	35112	35113	35114	35118	35124
	57	58	59	60	61	62	63	64
	84000/ 97860	83930/ 97880	84170/ 97950	84860/ 98000	83800/ 97915	83760/ 97955	88620/ 95795	88500/ 97000
SiO_2	49.04	50.19	47.96	47.40	49.85	49.96	48.96	48.16
TiO_2	1.78	2.07	1.22	1.71	2.52	1.93	2.16	1.22
Al_2O_3	15.57	14.22	16.66	16.84	14.00	14.84	14.94	17.18
Fe_2O_3	2.46	2.27	1.87	1.78	3.27	2.92	2.12	3.23
FeO	9.83	11.41	10.26	11.16	11.00	10.45	12.56	9.11
MnO	0.22	0.24	0.18	0.19	0.20	0.20	0.21	0.16
MgO	6.03	5.46	8.44	7.23	4.90	5.83	5.64	7.27
CaO	9.27	8.46	8.85	8.99	8.71	8.57	8.14	8.07
Na_2O	3.00	2.78	2.38	2.62	2.75	2.55	2.69	2.87
K_2O	0.78	1.38	0.66	0.70	1.24	1.19	1.31	0.92
P_2O_5	0.22	0.29	0.22	0.28	0.33	0.32	0.43	0.25
H_2O^+	0.37	0.45						
l.o.i.[1]	0.99	0.84	0.91	0.98	0.94	1.02	0.90	1.60
Total	99.19	99.61	99.62	99.99	99.70	99.78	100.06	100.04
Rb	16.4	37	14.0	14.1	28	28	29	19.4
Ba	341	567	284	320	494	510	567	420
Pb		3.2	1.7	1.0	2.9	2.7	6.3	4.3
Sr	258	212	230	240	205	207	217	262
Y	56	41	21	29	38	34	38	21
Th		3.9	2.2	2.4	4.5	3.3	4.2	4.1
Zr	143	171	86	112	165	152	179	102
Ni	65	51	167	119	57	70	73	144
Cu	87	44	73	62	82	61	68	58
Zn		152	112	130	155	150	173	134
S	1660	930	1370	1540	2030	1520	1540	1140
Cl	97	149	118	95	159	250	240	450
CIPW norm								
Q		0.34			1.90	1.28		
or	4.61	8.16	3.90	4.14	7.33	7.03	7.74	5.44
ab	25.39	23.52	20.14	22.17	23.27	21.58	22.76	24.29
an	26.72	22.25	32.83	32.12	22.20	25.53	24.82	31.28
ne								
di	11.48	12.79	7.90	8.79	15.67	12.31	10.64	5.82
hy	18.80	23.33	16.52	11.31	18.12	22.39	19.74	14.42
ol	2.97		11.87	13.90			5.28	9.62
mt	3.57	3.29	2.71	2.58	4.74	4.23	3.07	4.68
il	3.38	3.93	2.32	3.25	4.79	3.67	4.10	2.32
ap	0.51	0.67	0.51	0.65	0.76	0.74	1.00	0.58
cc	1.41	0.89						
C								

TABLE 4 continued

Sample nr.	35128	35131	35163	35167	35184	35192	35199	35201
	65	66	67	68	69	70	71	72
Coordin.	89500/ 96075	83425/ 98130	90350/ 82200	78525/ 95960	78150/ 94050	76512/ 93560	86755/ 90270	87170/ 93975
SiO_2	50.52	46.98	49.22	49.57	50.25	47.93	48.79	47.50
TiO_2	1.13	1.82	0.96	1.83	1.54	2.26	2.20	1.27
Al_2O_3	21.37	16.53	16.36	15.73	17.37	17.76	15.83	17.29
Fe_2O_3	1.85	2.51	2.29	2.16	1.18	3.53	3.50	1.92
FeO	5.71	11.01	7.73	9.56	9.16	9.12	10.55	10.47
MnO		0.19	0.18	0.17	0.15	0.17	0.22	0.20
MgO	2.82	6.59	7.88	6.36	5.91	4.66	4.92	7.54
CaO	9.18	8.94	10.49	9.14	8.39	8.91	9.02	8.31
Na_2O	3.41	2.75	2.52	2.80	3.04	3.30	2.75	2.59
K_2O	1.37	0.70	0.71	1.07	1.20	0.96	1.21	0.96
P_2O_5	0.22	0.29	0.33	0.33	0.31	0.48	0.37	0.31
H_2O^+							0.49	0.94
l.o.i.[1]	1.52	1.35	1.16	1.02	1.12	0.72	1.09	1.75
Total	99.09	99.66	99.88	99.74	99.63	99.80	100.45	100.11

Rb	33	13	14.9	24	27	20	27	18.9
Ba	510	314	518	406	508	471	508	429
Pb	3.1	0.8	2.3	4.2	3.2	0.7	4.4	3.1
Sr	358	235	506	220	260	369	224	273
Y	21	31	12.4	37	32	31	35	22
Th	1.6	2.3	1.8	3.4	3.6	1.0	3.6	2.2
Zr	102	122	64	153	141	128	146	107
Ni	33	90	115	107	78	64	63	149
Cu	51	64	117	63	50	49	89	53
Zn	84	137	90	123	117	125	164	134
S	430	1620	2000	1430	1130	2190	1300	1070
Cl	400	120	101	163	210	64	125	178

CIPW norm

Q	0.07						0.58	
or	8.10	4.14	4.20	6.32	7.09	5.67	7.15	5.67
ab	28.86	23.27	21.32	23.69	25.72	27.92	23.27	21.92
an	38.96	30.69	31.23	27.19	30.21	30.81	27.28	32.72
ne								
di	4.26	9.72	15.16	13.15	7.75	8.46	9.34	1.12
hy	12.00	10.57	14.33	17.02	16.55	9.73	20.87	18.55
ol		12.16	6.52	3.96	5.82	5.96		11.44
mt	2.68	3.64	3.32	3.13	1.71	5.12	5.07	2.78
il	2.15	3.46	1.82	3.48	2.92	4.29	4.18	2.41
ap	0.51	0.67	0.76	0.76	0.72	1.11	0.86	0.72
cc							1.36	1.84
C								

TABLE 4 continued

Sample nr.	35205 73	35215 74
Coordin.	87040/ 93195	87497/ 95700
SiO_2	48.88	50.37
TiO_2	0.99	1.59
Al_2O_3	16.94	15.41
Fe_2O_3	1.67	2.24
FeO	10.05	10.24
MnO	0.21	0.19
MgO	7.97	6.02
CaO	9.47	8.52
Na_2O	2.61	2.82
K_2O	0.60	1.01
P_2O_5	0.20	0.26
H_2O^+	0.43	
l.o.i.[1]	0.91	1.24
Total	100.50	99.91
Rb	11.5	25
Ba	292	397
Pb	0.9	2.5
Sr	235	214
Y	22	34
Th	2.3	2.4
Zr	63	118
Ni	91	82
Cu	92	74
Zn	100	134
S	1510	1600
Cl	74	300
CIPW norm		
Q		
or	3.55	5.97
ab	22.09	23.86
an	32.74	26.41
ne		
di	8.14	11.71
hy	16.85	23.78
ol	10.86	0.07
mt	2.42	3.25
il	1.88	3.02
ap	0.46	0.60
cc	1.09	
C		

TABLE 5. Average chemical composition of the rock types within the Hyperite bodies: gabbroic rocks, hornblende meta-gabbros and amphibolites. $\bar{x}$: mean; s: standard deviation. The composition of the individual samples are given in Table 4

	gabbroic rocks		hornblende metagabbros		amphibolites	
	$\bar{x}$	s	$\bar{x}$	s	$\bar{x}$	s
SiO_2 (%)	48.85	0.96	48.30	1.46	48.34	1.72
TiO_2	1.71	0.49	1.93	0.55	1.68	0.50
Al_2O_3	16.30	1.66	16.58	1.93	16.00	1.49
Fe_2O_3	2.46	0.66	2.97	0.79	2.89	0.62
FeO	10.13	1.41	9.43	1.58	9.73	1.55
FeO*	12.34	1.63	12.10	2.01	12.33	1.91
MnO	0.20	0.02	0.21	0.04	0.22	0.05
MgO	6.08	1.28	5.23	1.41	5.76	1.44
CaO	8.73	0.57	8.51	0.80	7.95	0.95
Na_2O	2.85	0.29	3.12	0.41	2.99	0.43
K_2O	1.03	0.25	1.28	0.35	1.67	0.80
P_2O_5	0.31	0.09	0.36	0.11	0.34	0.17
H_2O^+	0.59	0.21	0.97	0.26	1.04	0.25
l.o.i.[1]	1.21	0.30	1.82	0.37	2.07	0.63
Rb ppm	27	17	36	19	59	61
Ba	449	95	541	165	603	257
Pb	3.3	1.8	6.0	3.3	8	4.2
Sr	297	221	316	217	303	259
Y	31	9.1	35	12	38	18.6
Th	2.9	0.9	3.2	1.3	3.7	1.1
Zr	127	34	143	42	140	58
Ni	85	32	68	28	78	29
Cu	68	19	60	19	61	21
Zn	135	27	143	31	163	53
S	1280	470	770	480	450	350
Cl	220	170	540	400	800	340

[1] Inclusive H_2O^+

TABLE 6. Results of the statistical tests (Haber & Runyon, 1973, two-tailed tests),
(a) in fixed pair diagrams, X/MgO - X/MgO, (Figs. 42, 43), t-test and Wilcoxon matched-pairs signed-rank test,
(b) in X/MgO - FeO*/MgO diagrams (Figs. 44, 45), t-test.
-: not significant, $\alpha > 0.10$; x: less significant, $0.10 > \alpha > 0.05$; xx: significant, $0.05 > \alpha > 0.01$; xxx: strongly significant, $\alpha < 0.01$

	(a)		(b)
	t-test	rank test	t-test
SiO_2	-	-	-
TiO_2	-	-	-
Al_2O_3	-	-	-
Fe_2O_3	xxx	xx	xxx
FeO	x	x	xxx
FeO*	-	-	
MnO	-	-	xx
MgO	-	-	
CaO	-	-	-
Na_2O	xx	xx	x
K_2O	xx	xx	xxx
H_2O	xxx	xxx	xxx
P_2O_5	-	-	-
Rb	xx	xx	xxx
Ba	-	--	xx
Pb	xxx	xxx	xxx
Sr	-	--	-
Y	-	-	-
Th	xx	xx	xx
Zr	-	-	-
Ni	-	-	-
Cu	-	-	-
Zn	-	-	xxx
S	xxx	xxx	xxx
Cl	xxx	xxx	xxx
K/Rb	-	-	
Mg/Ni	-	-	

TABLE 7. The metasomatic effect of amphibolite facies metamorphism of gabbroic rocks. Results of studies of Elliott (1973) and Field & Elliott (1974) on Hyperites (?) from S Norway compared with the results of the present study on Swedish Hyperites from Värmland

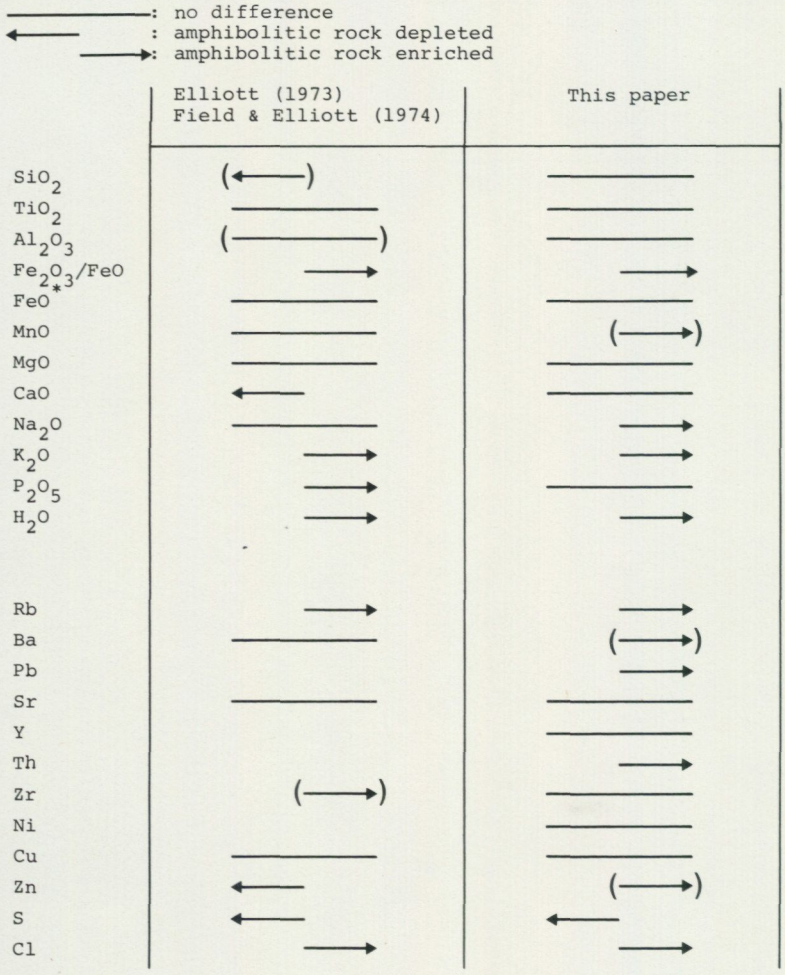

Fig. 1. Geological map of the Ölme area, SW Sweden. Surveyed by J.R. Morthorst in the period 1975—1977.

Fig. 1

GEOLOGICAL MAP OF THE ÖLME AREA, SW SWEDEN

SURVEYED BY J.R.MORTHORST
in
1975 - 1977

HYPERITE
GNEISS

SHARP CONTACT
CONSTRUCTED CONTACT
ESTIMATED CONTACT
FOLIATION
JOINT
FAULT
SAMPLE LOCALITY
CONTOUR INTERVAL 5 m

0 500 1000 1500 m

PRISKLASS F

Distribution
Liber Kartor
162 89 STOCKHOLM
Sveriges geologiska undersökning
Box 670, 751 28 UPPSALA

Schmidts Boktryckeri AB
Helsingborg 1983

ISBN 91-7158-284-3
ISSN 0373-2657